Master thesis

Uplift Prevention Analysis of a Water Retaining System Subjected to a Large and Rapid Drawdown

Mònica Relats Martínez

October 20, 2023
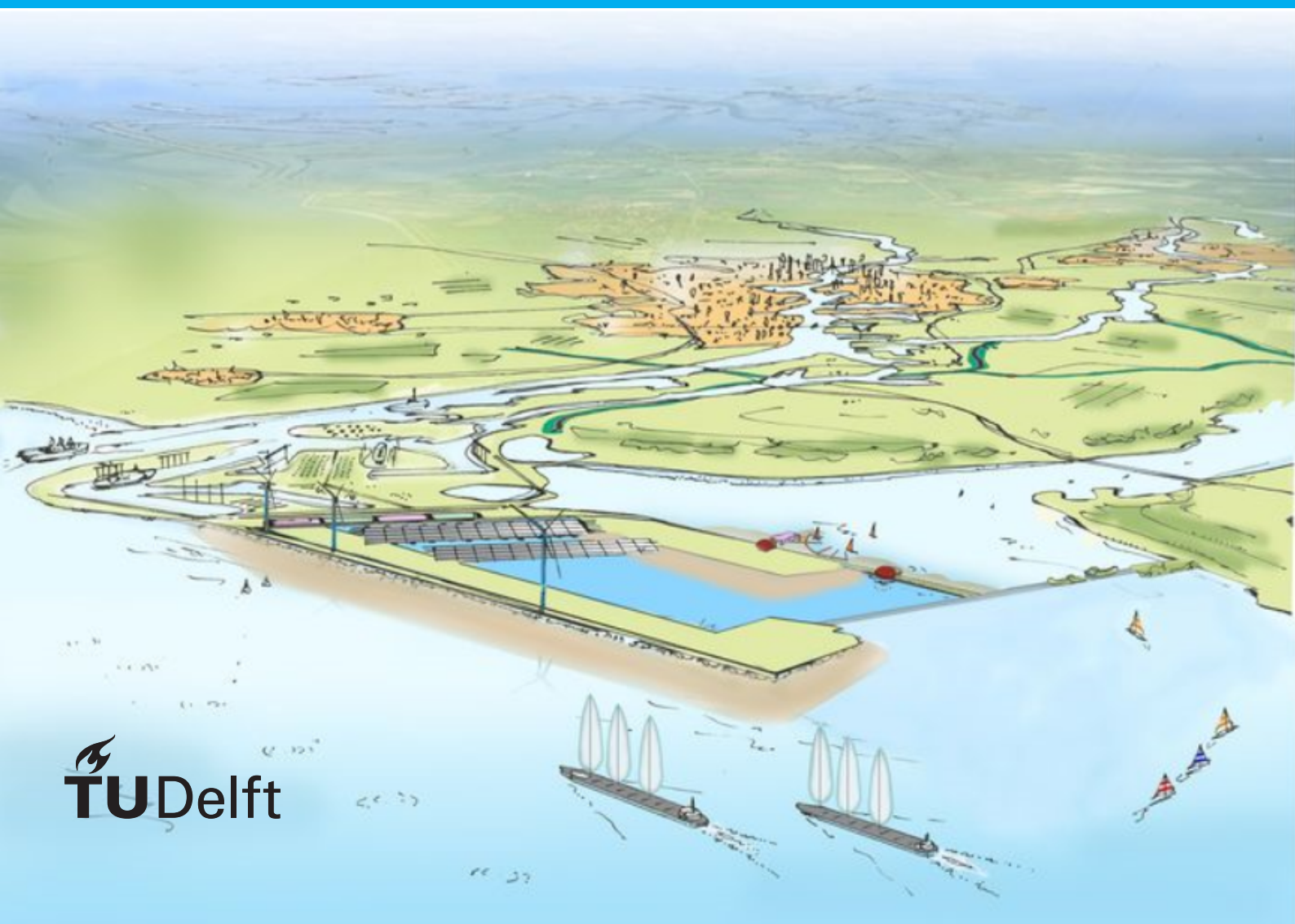
TUDelft

Master thesis

Uplift Prevention Analysis of a Water Retaining System Subjected to a Large and Rapid Drawdown

by

Mònica Relats Martínez

to obtain the degree of Master of Science
at the Delft University of Technology,
to be defended publicly on Friday October 20, 2023 at 9:00 AM.

Student number:	5133408	
Thesis committee:	Ir. R. E. P. (Richard) de Nijs,	TU Delft, supervisor
	Prof. dr. W. (Wout) Broere,	TU Delft
	Dr. ing. M. Z. (Mark) Voorendt,	TU Delft
Thesis advisors:	Ir. M. (Marga) Hoogvliet,	Ballast Nedam
	Ir. H.A. (Huub) Lavooij,	DELTA21

An electronic version of this thesis is available at http://repository.tudelft.nl/.

Preface

This thesis signifies the end of a wild ride through my Master's in Geotechnical Engineering. As I stand here, looking back, I can't help but see the twists and turns that have brought me to this point—and the people who made it all possible.

This journey wasn't an easy walk. Sometimes, I felt like I bit off more than I could chew with the research and deadlines. Let's say they had a way of sneaking up on me. But amidst the chaos, I learned that resilience is key, and having a support system is even more crucial.

To begin, I express my heartfelt gratitude to all my supervisors for their invaluable support throughout this journey. I also thank Huub and Leen from DELTA21 for their trust in including me in this groundbreaking project. Last but certainly not least, I appreciate Marga for her unwavering assistance and for continuously broadening my perspectives.

Secondly, my family and friends deserve a huge shoutout. They've been my cheering section, keeping me going when I hit roadblocks. Their encouragement and faith have been my secret weapons throughout this academic adventure.

And then there's Gwen. She´s been a rock. Her patience, belief in me, and willingness to lend an ear (even during my research rants) have been lifesavers. This journey wouldn't have been the same without her.

This thesis isn't the holy grail of Geotechnical Engineering, but rather a glimpse of where I'm at right now. Knowledge keeps evolving, and that's the exciting part. I hope this work adds a little splash to the ever-expanding pool of knowledge and motivates others to tackle future challenges head-on.

Mònica Relats Martínez
Delft, October 2023

Abstract

This research addresses the complex challenge of mitigating uplift within a water-retaining system, specifically focusing on the Valmeer Energy Storage Lake (ESL), an integral part of the DELTA21 project. The need for rapid emptying of the ESL during storm surges, often within a tight 12-hour window, has raised concerns about potential seabed uplift and associated volume loss. The central objective of this research is to ensure the stability and integrity of the ESL under these drawdown conditions, particularly by investigating how the soil at the lake's bottom can achieve equilibrium.

This study explores the Delta21 plan and the energy storage lake concept. Subsequently, it investigates the geological characterisation of the ESL site, providing data for subsequent analyses. Furthermore, a possible solution for using anchor piles is proposed; for that, a review of the Eurocode is done to understand the mechanisms of anchor piles and anchor pile groups. This research study employs Finite Element Method (FEM) calculations to assess bottom stability, both with and without incorporating anchor piles.

Throughout the research, a combination of hand calculations and Finite Element Method (FEM) analysis was employed to understand the subject matter comprehensively. The optimal centre-to-centre distance of 1.2m emerged as the key to effectively preventing uplift. The study also explores the interchangeability of volume elements and embedded piles within the FEM analysis, highlighting their comparable functionality.

Furthermore, an investigation into complete collapse scenarios suggests that tension piles´ contribution to soil stability might be closely related to their weight rather than their spacing. Nevertheless, the spacing implementation presents challenges, emphasising the necessity for innovative solutions.

Additional soil investigations are recommended to understand the impermeable layer´s exact location further. With its potential for uplift due to backpressure, this impermeable layer adds complexity to the interaction between soil layers. Recognising the constraints of the research scope, it is evident that further field investigations and research endeavours are indispensable for a comprehensive understanding of the site conditions and the impermeable layer's behaviour.

In the final stages, the research concludes with a discussion and recommendations for the DELTA 21 plan specifically and presents the results obtained during this research.

Contents

1

Introduction

1.1. Motivation for the research

Climate change is already causing more extreme weather events, including intense storms and floods. This threatens flood protection in the Netherlands, which is essential for safeguarding people, property and infrastructure. To reduce the risk of climate change-related flooding, it is important to improve the resilience of the flood protection system and reduce greenhouse gas emissions. Improving flood protection resilience will help to reduce the intensity and frequency of extreme weather events. (European Commission and European Environment Agency, 2021)

However, using more clean energy also requires buffers to protect the energy system from fluctuations in supply and demand. For example, wind and solar power are intermittent energy sources, which can cause problems if not properly managed. Therefore, it is important to invest in energy storage and other technologies that can help to smooth out these fluctuations. This will help ensure that we can continue to use more clean energy while protecting against the risks of climate change.

Delta21 wants to future-proof the southwestern delta, combining a solution for flood protection, energy storage and nature restoration. The main principle of DELTA21 is to build a 30-square-kilometre storage basin (Energy Storage Lake, also known as Valmeer) where energy is temporarily stored and then generated again using pumps and turbines. Large pumping capacities can be employed as super pumping stations to push excess river water to the sea during floods, storms and heavy river discharges. In this research, the Valmeer construction's feasibility will be analysed.

1.2. Problem analysis

1.2.1. Main Problem

The main problem that will be tackled in this research is the buoyancy prevention analysis of a water-retaining system subjected to a large and rapid drawdown. This water retaining system is also known as an energy storage lake (or Valmeer in Dutch). During storm surges, the energy storage lake has to be emptied to store the new water volume generated by the storm. As the lake is emptied at rapid velocities, it uplifts its seabed, possibly resulting in a loss of volume or a bottom outburst.

1.2.2. Introduction to the DELTA21 concept

DELTA21 (Figure 1.1) is a unique and visionary concept that combines hydraulic and geotechnical engineering. With this concept, three combined ambitions are achieved simultaneously: Flood risk management, Energy storage and Nature restoration. Flood risk management is achieved by realising a water discharge system and a new water storage lake surrounded by dunes (Lavooij et al., 2018).
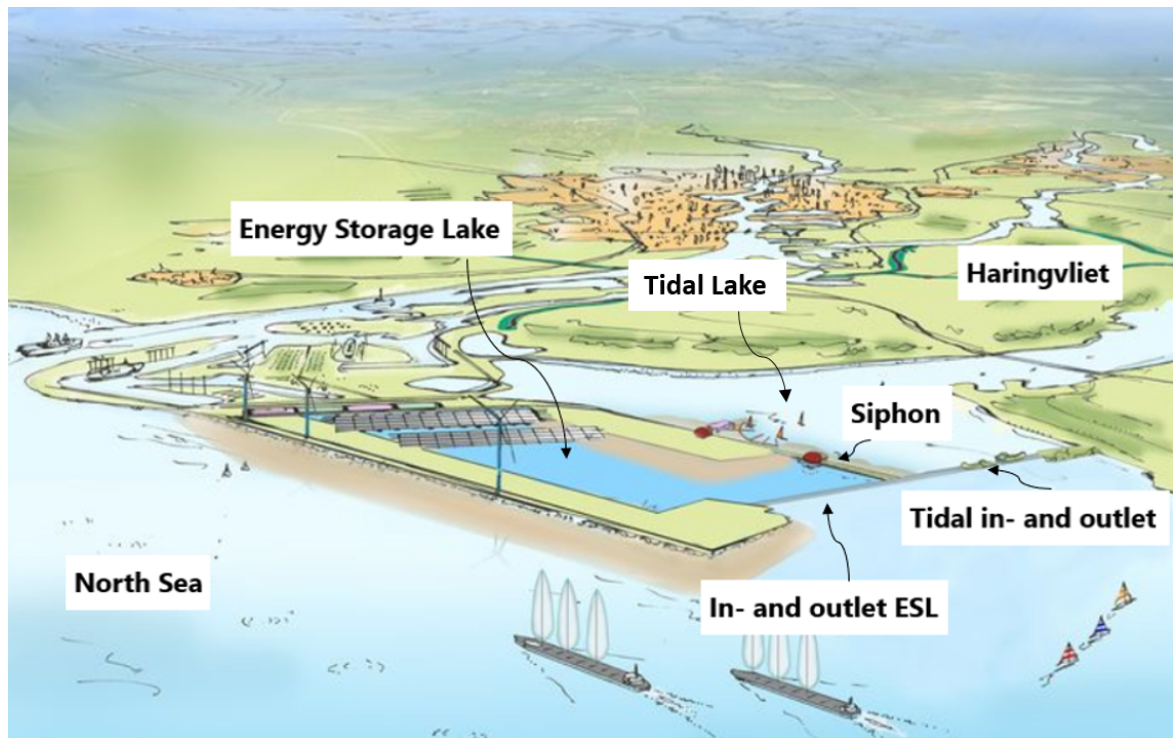
Figure 1.1: DELTA21 components in normal and extreme circumstances (Lavooij et al., 2018)

During extreme circumstances at a storm surge in combination with high river water discharges, water is pumped to the North Sea to achieve higher flood protection (Lavooij et al., 2018). In an Energy Storage Lake (water storage basin surrounded by dunes), turbines and the same pumps store and generate energy under normal circumstances. This is an addition to the dyke improvement program of the Delta Program Commissioner.

According to Meehl et al., 2000, the number of extreme events will increase as well as a rise of the sea level, which will lead to the flooding of some now protected areas. This and the rapid drawdown during the emptying of the energy storage lake, according to Lavooij et al., 2018, could lead to a potential uplift of the impermeable clay layer and, consequently, a reduction in the volume of the water storage capacity of the lake. Therefore, a better understanding of the effect of the clay uplift due to the rapid drawdown is necessary.

1.2.3. The Valmeer subsoil
The subsoil of the Valmeer consists of the seabed to approx. NAP -50 m of fine sand with occasional lenses of sand and silt. From NAP- 50 m to NAP - 60 m an approx. a 10 m thick clay layer is supposed to appear in the Maasvlakte area. It is assumed that this same subsurface extends to the area where the Valmeer is planned (Lavooij et al., 2018).

The average water level in the Valmeer, during operation, is from NAP - 5 to NAP - 20 m, although in storm cases, the water level can be lowered to NAP -22.5 m. The water pressure under the clay layer is estimated to be, if it is found to be at a depth of NAP - 60 m, of ~ 600 kPa (Lavooij et al., 2018). Since the position of the natural underseal (clay layer at depths from NAP- 50 m to NAP - 60 m) shows variations, during the large and rapid drawdowns, the bottom of the storage lake experiences an uplift. This reduces the volume that the energy storage lake can store and thus reduces the flood prevention capacity of the DELTA21 project.

1.3. Research Questions
The main research question is *How to ensure the equilibrium of the bottom of the Energy Storage Lake of the proposed Delta21 plan in the Netherlands?*

From this main question, multiple sub-questions can be drawn and are the following:

RQ 1: Is there a clay layer under the Energy Storage Lake (Valmeer)?

 • *If so, at what depth?*

RQ 2: Can this clay layer and the sand layer(s) above it withstand the backpressure of the groundwater at the bottom of the clay layer? Is that resistance stable enough?

 • *If not, what can be done to obtain the necessary safety?*

RQ 3: If the stability of the clay layer is not ensured, can tension piles be used to prevent uplift instability of the clay layer?

1.4. Scope

In this master thesis, the exact location of the impermeable clay layer will be investigated. Although there has not been a lot of relevant soil investigation in the area, the best estimation possible will be carried out with the data available.

Furthermore, the ecology or environmental aspects are not treated since that is part of the wider Delta21 plan. The outcome of this master's thesis is a practical design; thus, not all relevant aspects can be treated.

1.5. Methodology and thesis outline

A study of the subsoil is going to be carried out, as well as preliminary hand calculations to determine the stability of the problem, a finite element analysis is later needed to determine the possible uplift of the impermeable clay layer and to model possible solutions. For this, the commercial program PLAXIS will be used later. Figure 1.2 illustrates how each chapter corresponds to the specific methodological steps undertaken in the research. This graphical representation provides a visual roadmap of how each research phase contributes to the overall investigation.
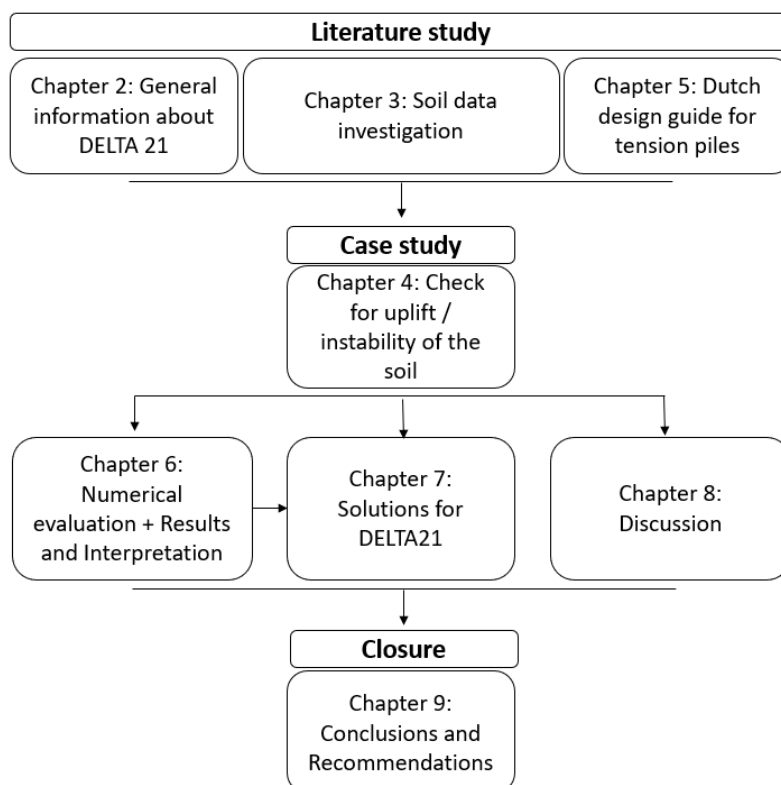
Figure 1.2: Steps to follow along with this thesis.

The research is structured into chapters corresponding to specific methodological steps. In chapter 2, the Delta21 plan and the energy storage lake concept will be elaborated upon to set the context for the study. Chapter 3 will delve into a detailed geological description of the ESL site, providing vital data for subsequent analyses. Chapter 4 will perform FEM calculations to assess bottom stability with and without anchor piles. In chapter 5, the literature review of anchor piles will be made to understand their use and possible implications in this project. Chapter 7, will explore potential solutions that align with Delta21's objectives. In chapter 8 the research findings are interpreted, addresses limitations, suggest avenues for further research, and offer a reflective analysis of the research process. Finally, chapter 9 will synthesize conclusions drawn from the research.

This research employs a structured approach involving literature study, subsoil analysis, hand calculations, and Finite Element Analysis (FEM). And are the following:

1. **Literature Study:** The literature study aims to gather a comprehensive understanding of relevant concepts, methods, and theories related to geotechnical engineering, water-retaining systems, buoyancy prevention, and stability analysis. This collected knowledge will provide the foundation for informed decision-making throughout the research. It will aid in identifying factors that influence soil behaviour, uplift phenomena, and potential solutions. The insights gained from the literature study will inform the subsequent steps of the research.

2. **Soil data investigation Study:** Conducting a thorough subsoil study involves detailed investigations into the geological characteristics and properties of the Energy Storage Lake (ESL) site. This step aims to ascertain the soil composition, permeability, layering, and any other relevant factors that could influence stability, uplift, and other phenomena. The subsoil study will provide essential data to inform subsequent calculations and simulations.

3. **Preliminary Hand Calculations:** Preliminary hand calculations will be employed to assess the initial stability of the energy storage lake. These calculations will involve applying engineering principles and equations to determine if the system can resist potential buoyancy and uplift effects. This step will provide a basic understanding of the problem's magnitude and help guide further analysis.

4. **Finite Element Analysis (FEM):** FEM analysis is a pivotal step to simulate and model the complex behaviour of the energy storage lake under varying conditions. This includes assessing the potential for uplift of the impermeable clay layer due to rapid drawdown. Commercial software like PLAXIS will create numerical models that accurately represent real-world conditions. FEM analysis allows a deeper understanding of how factors affect system stability.

The research is structured into chapters corresponding to specific methodological steps:

- **Chapter 2:** The Delta21 plan and the energy storage lake concept will be elaborated upon to set the context for the study.

- **Chapter 3:** will delve into a detailed geological description of the ESL site, providing vital data for subsequent analyses.

- **Chapter 4:** will perform FEM calculations to assess bottom stability with and without anchor piles.

- **Chapter 5:** The literature review of anchor piles will be conducted to understand their application and implications in this context.

- **Chapter 7:** will explore potential solutions that align with Delta21's objectives.

- **Chapter 8:** a discussion of the results and the whole project will be carried out.

- **Chapter 9:** will synthesize conclusions drawn from the research.

2

DELTA21 plan

This chapter aims to introduce the DELTA21 plan and its components in more detail. For this, Delta Works need to be mentioned, as the DELTA21 plan wants to be a crucial part against flooding, support and add effectiveness to the existing flood protection in the Netherlands (Delta Works). Therefore, this chapter will consist mainly of a literature study of Delta Works and the DELTA21 plan.

2.1. Delta Works

The Rijkswaterstaat built the Delta Works to protect the country against flooding from the North Sea. Three locks, six dams and four storm surge barriers form the Delta Works. Storm surge barriers are movable flood barriers that close automatically or manually when water levels are (very) high near river mouths, tidal inlets, and estuaries. They make up the Netherlands' most extensive flood defence system.

The Delta Works were started to get built in the year after the Great Flood of 1953. The 1953 flood was the worst natural disaster to strike the Netherlands in the twentieth century. A solid north-westerly storm and a spring tide in many country areas triggered flooding. The calamity killed 1,836 people and tens of thousands of animals and destroyed many homes. This project consisted of three locks, six dams and five storm surge barriers, completed in 1997. Since 2018, the number of storm surge barriers has increased to six, making the Haringvliet Barrier also functioning (Rijkswaterstraat, 2013a). One of the last structures that were added to the Delta Works was the Maeslantkering; this 210 m wide, 22 m high and 15 m deep movable storm surge barrier is the largest in the world and can withstand a storm tide of 5m above NAP. It is situated in the Nieuwe Waterweg near Hook of Holland, protecting the residents of the province of Zuid-Holland (Rijkswaterstraat, 2013b). In figure 2.1 an overview of the delta works can be found.

Figure 2.1: Overview of the Delta Works (Zegwaard and Wester, 2014)

In summary, Delta Works is a valuable case study for this research and a source of inspiration for researching combating flooding in the Netherlands. Their legacy, innovative solutions, and the lessons learned can inform and guide modern flood control (like DELTA 21) and water management strategies, helping to protect vulnerable regions and communities.

2.2. What is DELTA21?

The principal aspect of the DELTA21 plan is an Energy Storage Lake (ESL), where the water can be temporarily stored and produced with the assistance of pump turbines into hydropower. Within the ESL, the pump/turbine capacity will allow the lake to be emptied in 12 hours, and 400 million m^3 of seawater will be traded once a day. The pumps discharge excessive water from the river due to high river discharges during heavy storms at sea (return period of 10 years), during which the new storm surge barrier is closed, blocking the river discharge. A new form of protective barrier, following the Haringvliet locks, will be constructed. With the expected sea-level rise, the DELTA21 plan will increase its use for surge security. For this plan to succeed, a functioning Maeslantkering is vital. Although with DELTA21, the work of the Maeslantkering will be simplified (Lavooij et al., 2018).

The DELTA21 plan will influence flood protection in the densely populated area of Rijnmond-Drechtsteden, with cities like Rotterdam and Dordrecht. In this area, water comes from two sides; the sea and rivers. Among other areas, due to subsidence and anticipated climate change, the expectation is that, without action, in 2050, 30% of all dykes will be too low and in 2100, even the 50%. (Lavooij et al., 2018)

The Delta Works protect the Dutch coast against flooding from the sea. But when these barriers are closed for a more extended period, the river discharge will lead to higher water levels in the hinterland, and as a consequence, it will increase the risk of river flooding. The DELTA21 plan aims to increase the flood protection of the downstream area and prevent the water level from surpassing NAP + 2,5 m in the Dordrecht area. Allowing the surrounding dunes on the seaside in the Delta21 plan to become part of the primary flood defence system and thus, it will not be the need to raise the current dikes in the Dordrecht area. (Lavooij et al., 2018)

2.3. Main components

Water needs to be pumped out of the system to avoid flooding the upstream areas during the closure of the inlet/outlet structure due to a storm surge. The great capacity of the pumps will allow them to get rid of the excess river discharge during extreme storm events (maximum discharge of 10.000 m^3/s). Additionally, during regular sea conditions, water can be turbined into the Valmeer to obtain electrical

energy. The exterior part of the Energy Storage Lake will be composed of sprayed sandy dunes, which sand will come from the dredged material extracted from the Energy Storage Lake. (Lavooij et al., 2018)
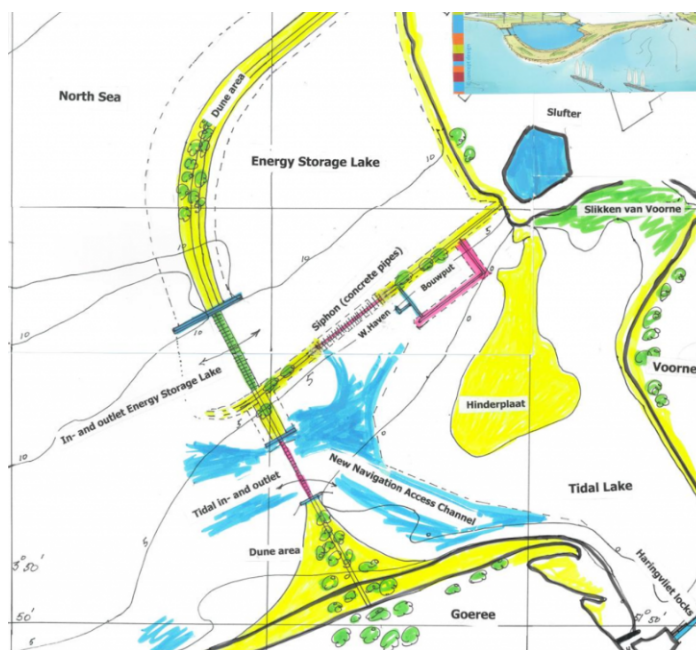
Figure 2.2: Representation of the DELTA21 plan parts (Lavooij et al., 2018)

The tidal lake (Getijmeer) will have a barrier open during normal conditions and closed during storm surge conditions. During the latter conditions, the water level upstream of the Haringvliet is controlled by lowering the water level at the Getijmeer by letting water through Valmeer's spillway. The Getijmeer's gates will remain open during regular conditions, allowing saltwater to come within the Haringvliet.

In principle, the flood defence function will be carried out by the combination of the exterior dunes of both Valmeer and Getijmeer, by the inlet/outlet of both Valmeer and Getijmeer, by the ship lock of the Getijmeer and storm surge barrier (Figure 2.2). DELTA21 will allow leaving the dike levels as they currently are even in the event of a large (1 m) sea-level rise (Lavooij et al., 2018) and will cut by half the probability of closing the Maeslant barrier with respect to the present configuration, reducing it to 1/2 years for the worst sea-level scenario (Lavooij et al., 2018).

DELTA21 will generate hydroelectricity at the Energy Storage Lake from the beginning of its use, and eventually, windmills and solar panels can also be installed in the system. The project will also bring ecological improvement. Since the existing Haringvlietdam will lose its storm surge barrier function, its gates can be opened entirely to allow saltwater intrusion back into the Haringvliet and restore fish migration.

2.4. Energy Storage Lake

The Valmeer (ESL) will be positioned on the north side against Maasvlakte 2. The long side of the ESL by the sea runs as parallel as possible to the Dutch coast, and it will be surrounded on three sides by sand dunes, which are sprayed with sand dredged from the Valmeer. The top of the dunes on the seaside will have NAP +10 m and will be 250 m wide (from NAP +5 m), and the ones on the Tidal Lakeside will have NAP +5 m and will be 100 m wide. The total volume will be 400 million m^3 (Lavooij et al., 2018). Sea dunes surround the energy storage lake, with a gentle inner slope of 1:10 with a safety factor higher than 3 (van Adrichem, 2021).

The inlet and outlet structures (Figure 2.2) of the energy storage lake will be located on the south side, and the spillway on the southeast end distinguishes it from the tidal lake. The in- and outlet structures

consist of caissons with several pump turbines needed to provide a total discharge of 10.000 m³/s within 12 hours and a siphon spillway. The bottom level of the energy storage lake will be between NAP -25 m and NAP -27,5 m, and the ESL's lower and upper 5 m will not be used due to pump requirements (Ansorena Ruiz, 2020). This means that the water level within the energy storage lake can rise or fall with a maximum of 17,5 m. It can be illustrated in Figure 2.3 that the water level of the ESL will have a maximum level of NAP -5 m and a minimum of NAP -22,5 m. Therefore, the water level rises or falls by a maximum of 17,5 m in 12 hours; thus, it will significantly influence its bottom stability.
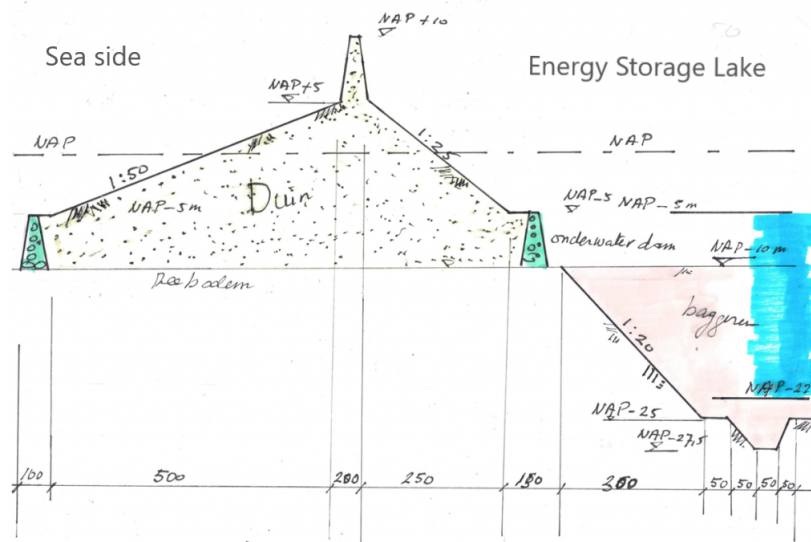
Figure 2.3: DELTA21's dune and Energy Storage Lake cross-section (Lavooij et al., 2018)

The dimensions of the inside of the ESL are the following and can be seen in Figure 2.4 and are of about 30 km². As can be seen, the primary flood defences surround the whole of Valmeer and Getijmeer. They are situated North (outer dunes/dike of the Valmeer) and the West (outer dunes/dike of the Valmeer and Getijmeer, inlet/outlet of both Valmeer and Getijmeer and the ship lock of the Getijmeer).
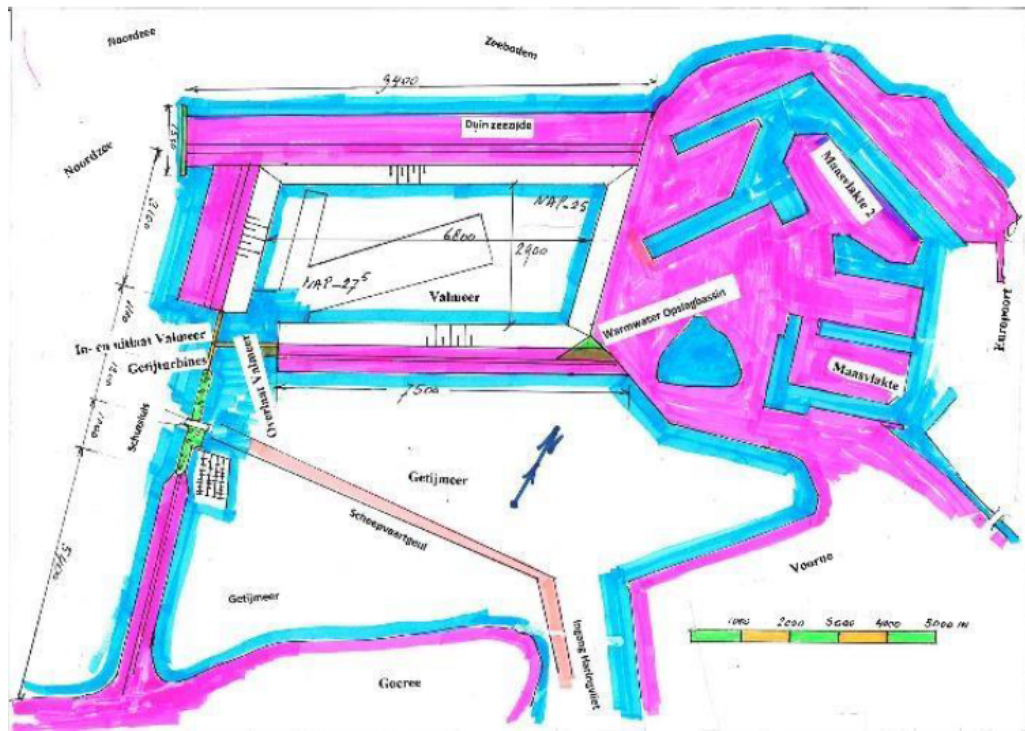
Figure 2.4: Top view of the DELTA21 plan (Lavooij et al., 2018)

<div style="text-align: right">

3

</div>

Soil data investigation

In order to proceed with the design of the energy storage lake, some soil investigation of the zone has to be carried out to determine the location of the expected impermeable clay layer. No specific soil investigation was made for the DELTA21 plan; thus, it is necessary to find soil information online (e.g. DINOloket). In this chapter, the soil data online information will be investigated, the soil parameters needed for later calculation will be retrieved, and some recommendations will be drawn.

3.1. Soil data online information

From the information available in DINOloket, 5 relevant CPTs and 2 Boreholes were found relevant for the problem at hand. It can be seen in Figure 3.1 the location of these CPTs, Boreholes and inland crosssections. The red dots limit the inside of the Energy Storage Lake from A to E.

Figure 3.1: CPT and borehole locations (Source: Google Earth)

Borehole BS031271 (Figure 3.3) is located in the middle of the North Sea. Looking into the bathymetry, it can be estimated that the seawater level is around 13.2 m deep. Thus, it can be seen that a 10m

thick clay layer appears at a depth of NAP -66.4m to NAP -75.9m. This confirms the prediction made by Lavooij et al., 2018.

To determine if the clay layer is continuous, borehole BS031272 and CPT000144101 (Figures 3.4 and 3.5), which are situated on land, are analysed. From borehole BS031272 (Figure 3.4), it can be seen that a 10 m thick clay layer appears at NAP -52.3m to NAP - 62.3m.

On the other hand, from the CPT S36H00033_00 (Appendix A), it can be seen that the supposed clay layer is at NAP -60m to NAP -75.15m. This CPT makes it unclear that the impermeable layer is indeed a clay layer; the friction ratio for the lowest qc value corresponds to 3.6%. This qc value of 3 MPa with the friction ratio value is plotted into the Robertson soil type classification chart (Figure 3.2). In 3.2 it can be seen that the soil described corresponds to zone 3, and it is clay - silty clay to clay. Although the soil corresponds to a clayey silt/silty clay, from the previous CPT (S36H00033_00), it can be seen that it is not continuous and has sand intercalations.
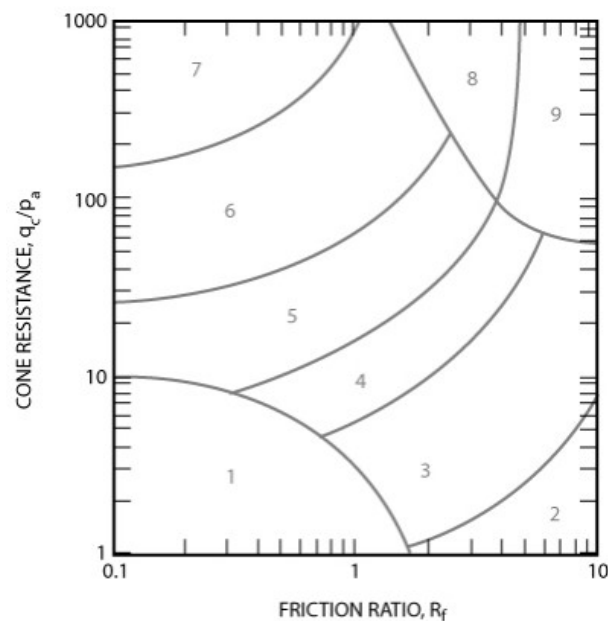
Zone	Soil Behavior Type
1	Sensitive, fine grained
2	Organic soils - clay
3	Clay – silty clay to clay
4	Silt mixtures – clayey silt to silty clay
5	Sand mixtures – silty sand to sandy silt
6	Sands – clean sand to silty sand
7	Gravelly sand to dense sand
8	Very stiff sand to clayey sand*
9	Very stiff fine grained*

Heavily overconsolidated or cemented

P_a = atmospheric pressure = 100 kPa ~ 1 tsf

Figure 3.2: Soil type classification chart proposed by Robertson et al., updated by Robertson, 2010

From the following boreholes (Figures 3.3 and 3.4) it can be seen that at least two locations of the clay layer need to be investigated, depths from - NAP 66.4m to - NAP 75.9m and from - NAP 52.3m to - NAP 62.3m. It is the first depth interval the most favourable to maintain equilibrium and the last the most unfavourable one.

As there is no more information about the location of the impermeable layer, a subgroup analysis is proposed in the following chapters to investigate the uncertainty at hand.
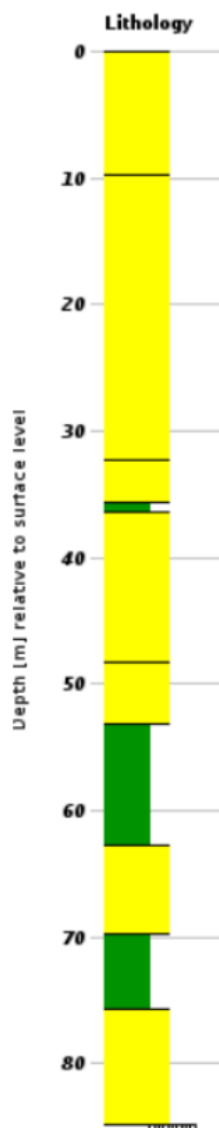
Figure 3.3: Borehole BS031271 (Source: DINOloket)
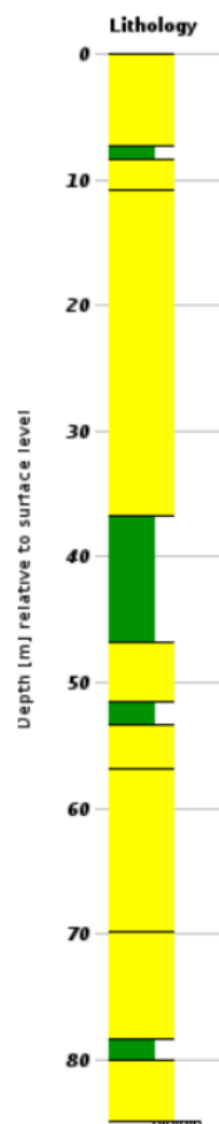
Figure 3.4: Borehole BS031272 (Source: DINOloket)
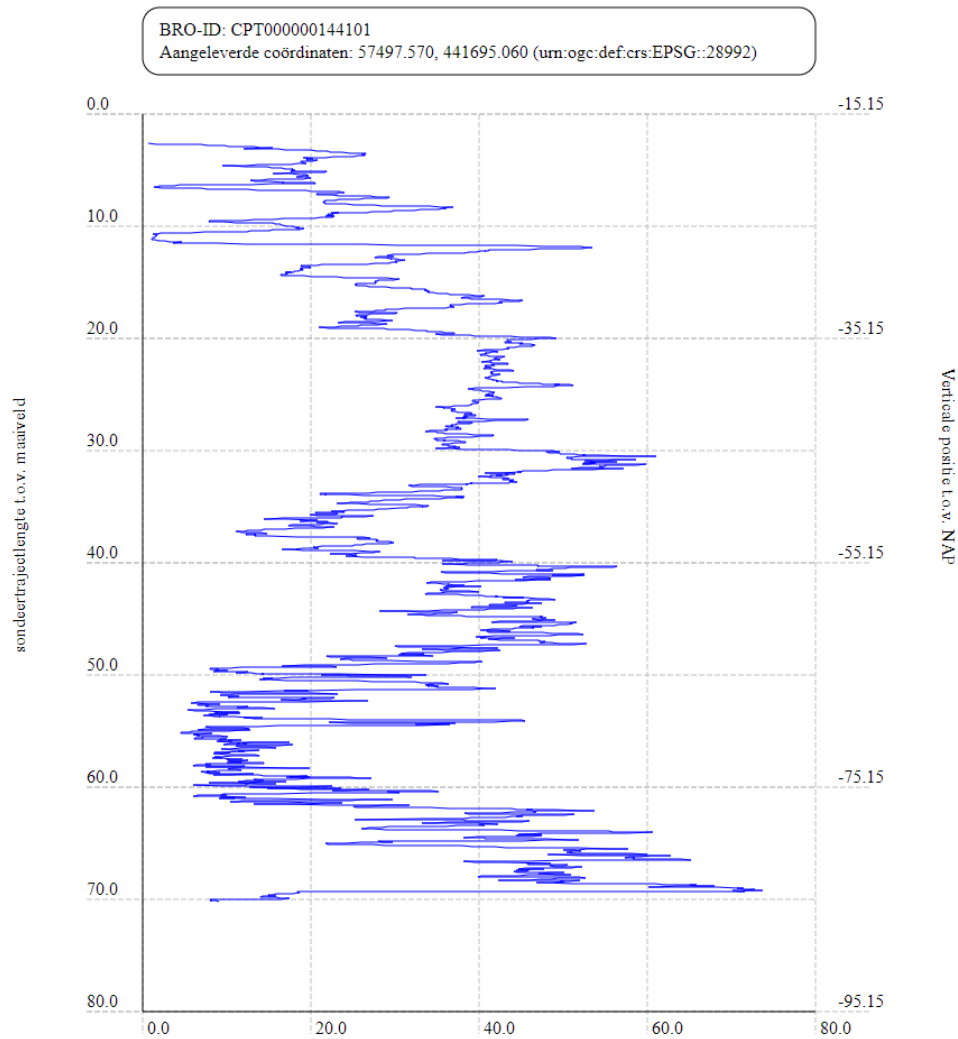
Figure 3.5: CPT000144101 data (Source: DINOloket)

3.2. Soil parameter determination

To carry out all the calculations to investigate the validity of the research questions, the soil parameters have to be determined using the soil data previously discussed together with the NEN9997, 2016. For the determination of the sand layer, equation 3.1 is used to convert the q_{cpt} to a standardized parameter on effective vertical stress of 100 kPa (q_{ref}), to use table 2b from the NEN9997, 2016.

Equations 3.1 and 3.4 are found in table 2b of the NEN9997, 2016 to get the conversion done to a standardized 100 kPa. Equation 3.4 is used to convert q_{cpt} to a q_{ref}. Both equations are used to determine the parameters for the sand layer. In equation 3.2, the effective vertical stress of the sand is calculated, where it is assumed to be a γ_{sand} of 21 kN/m³.

$$C_{qc} = \left(\frac{100}{\sigma_v}\right)^{0,67} \tag{3.1}$$

$$\sigma'_v = \frac{(52,3m - 27,5m) \cdot 21kN/m^3}{2} = 260,5kPa \tag{3.2}$$

$$C_{qc} = \left(\frac{100}{260,5kPa}\right)^{0,67} = 0,526 \tag{3.3}$$

$$q_{ref} = C_{qc} \cdot q_{cpt} \tag{3.4}$$

$$q_{ref} = 0,526 \cdot 25 MPa = 13,15 MPa \tag{3.5}$$

For the clay layer, equation 3.7 is used to standardize the parameters to use table 2b of the NEN9997, 2016.

$$C_u = \frac{q_{cpt}}{N_{kt}} \tag{3.6}$$

$$C_u = \frac{5000 kPa}{25} = 200 kPa \tag{3.7}$$

where:

q_{cpt}:   is the cone resistance retrieved from CPT000144101 (figure 3.5), in kPa;
N_{kt}:   cone factor used 25 for clay soils, in m;
C_u: is the undrained shear strength, in kPa;

Finally, the parameters obtained from these calculations are put in table 2.b from the NEN9997, 2016. It can be seen that the sand layer corresponds to medium-dense sand; thus, γ_{sand} is defined as 19 or 20 kN/m^3. Additionally, the clay layer corresponds to a stiff layer, with γ_{clay} being 20 or 21 kN/m^3. As various γ values are considered for each layer, a subgroup analysis will be conducted in subsection 4.5 to report this uncertainty. The same parameters are assumed for the sand under the clay layer.

3.3. Recommendations

To better understand the exact location of the impermeable layer, more soil investigation needs to be carried out in the middle of the ESL. More boreholes and CPTs need to be performed in that location, and remote sensing to determine the continuity of the layer and check to double-check the clay location. The boreholes will help determine if the impermeable layer is a clay or water-resistant layer. These measures are out of this project's scope; thus, they won't be carried out for this graduation project or investigated further.

The presence of the clay layer in a specific location generates an impermeable layer that, if applied back-pressure, would experience an uplift if not enough pressure above the clay layer is present.

<div style="text-align: right; font-size: 4em;">4</div>
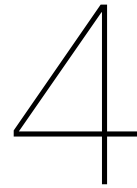
Bottom stability

In this chapter, the bottom stability equilibrium of the Energy Storage lake will be investigated. To do that, the use of the NEN9997, 2016 is necessary to implement each equation part's correspondent parameter partial factor. Later, hand calculations are carried out to perform a subgroup analysis of the soil parameters and the location of the clay layer.

4.1. General

Failure by uplift is checked by comparing the sum, $G_{dst,d}$ and $Q_{dst,d}$, of the design values of the destabilising permanent and variable vertical actions, i.e. the sum of the water pressures under the structure (permanent and variable parts) and any other upwards forces, with the sum, $G_{stb,d}$ and R_d, of the design values of the stabilising permanent vertical actions and the design value of any additional resistance to uplift provided, for example, by tension piles.

$$G_{dst,d} + Q_{dst,d} \leq G_{stb,d} + R_d \tag{4.1}$$

where:

$V_{dst,d}$:   design value of the destabilising variable vertical actions, i.e. the sum of the water pressures under the structure, in kPa;

$G_{stb,d}$:   design value of the stabilising permanent vertical actions, in kPa;

R_d: design value of any additional resistance to uplift,in kPa.

This inequality is commonly used to assess the stability of submerged structures against uplift failure, as well as impermeable layers in excavations.

Clause 2.4.7.4(2) of the NEN9997, 2016 permits the treatment of the additional resistance to uplift resulting from tension piles, ground anchors, or friction forces as a stabilizing permanent vertical action. Consequently, the design value is obtained by applying the partial factor on permanent favourable actions (recommended at 0.9). If the partial factor values on actions recommended in Table A.15 (Table 4.1) of the NEN9997, 2016 are applied, the resulting uplift (UPL) design is less conservative than if the partial soil parameter values in Table A.16 (Table 4.2) of the NEN9997, 2016 is used. This is because applying the partial factor in Table A.16 to the additional tensile pile resistance is equivalent to multiplying the resistance by 0.71 (or multiplying the ground strength parameters by 0.8 in the case of friction forces). Therefore, verifying the GEO ultimate limit state is crucial, which refers to the failure or excessive deformation of the ground, where the strength of soil or rock is essential in providing resistance. Examples include overall stability, bearing resistance of spread foundations or pile foundations if clause 2.4.7.4(2) is applied to the resistance from tension piles, ground anchors, or friction.

Table 4.1: Partial factors on actions (γ_f). **Table A.15** from the NEN9997, 2016.

Action	Symbol	Value
Permanent		
Unfavourable [a]	$\gamma_{G;dst}$	1,0
Favourable [b]	$\gamma_{G;stb}$	0,9
Variable	$\gamma_{G;stb}$	1,5
Unfavourable [a]		
[a] Destabilizing;		
[b] Stabilising		

Table 4.2: Partial factors for soil parameters and resistances. **Table A.16** from the NEN9997, 2016

Soil Parameter	Symbol	Value
Angle of shearing resistance [a]	$\gamma_{\varphi'}$	1,25
Effective cohesion	$\gamma_{c'}$	1,25
Undrained shear strength	γ_{CU}	1,40
Tensile pile resistance	$\gamma_{s;t}$	1,40
Anchorage resistance	γ_a	1,40
[a] This factor is applied to tan φ'		

Where applicable, it must be shown that the following limit states are not exceeded:

- failure or exceptional deformation of the substrate, affecting the strength of the soil or the rock makes a significant contribution to resistance (GEO);

- loss of balance of the construction or the subsoil as a result of buoyancy due to water pressure(buoyancy) or other vertical loads (UPL).

4.2. Uplift failure mechanism (UPL)

If the friction forces are neglected, the design against uplift of an impermeable layer where there is no seepage through the layer, e.g. at the bottom of, or below, an excavated building pit (Figure 4.1), can use stresses instead of forces. In this case, the design value of the destabilising total water pressure u_d acting at the interface between the two layers must be less than or equal to the stabilising total vertical stress $\sigma_{stb,d}$ due to the total weight of the soil above the interface.

$$u_d \leq \sigma_{stb,d} \tag{4.2}$$
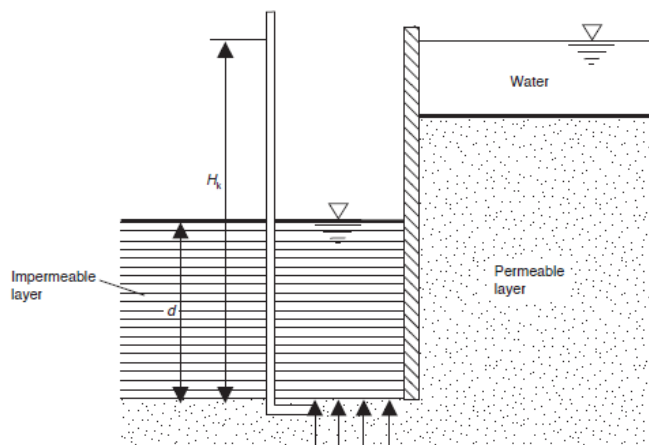
Figure 4.1: Uplift of an impermeable layer. (Source: NEN9997, 2016)

Using the values for the partial factors given in *Annex A.4* from the NEN9997, 2016 is equivalent to an overall factor of safety (FS) against uplift given by:

$$FS = \gamma_{G,dst}/\gamma_{G,stb} = 1.00/0.90 = 1.11 \qquad (4.3)$$

where:

$\gamma_{G,dst}$:　permanent destabilising action factor;
$\gamma_{G,stb}$:　permanent stabilising action factor.

4.3. Uplift failure mechanism with a structure (GEO)

The occurrence of ground failure or excessive deformation, wherein the strength of the soil or rock plays a vital role in offering resistance, is a prominent consideration in geotechnical engineering (GEO). The limit state in GEO frequently holds significance in determining the dimensions of structural components engaged in foundations or retaining structures. Moreover, it occasionally affects the strength evaluation of the structural elements themselves.

4.3.1. Design approach used

For limit states type STR and GEO for permanent and temporary situations, the NEN9997, 2016 describes 3 design approaches. The three approaches differ in how the partial factors are divided among the loads, load effects, material properties, and resistances. Different methods of how uncertainties are considered in modelling load effects and resistances are partly to blame for these disparities.

The design approach for this calculation is design approach 3 from the NEN9997, 2016, which states that a single combination of the sets of partial factors (4.4) is applied to the calculations for checking each relevant ultimate limit state in the ground and in the structure. It is important to note that in this approach, the partial factors are applied to load effects and to strength parameters of the soil.

$$(A1 \quad \text{or} \quad A2)" + "M2" + "R3 \qquad (4.4)$$

where they are the partial factors applied:

$A1$:　for loads or load effects on structural loads;
$A2$:　for loads or load effects on geotechnical loads;
$M2$:　for the ground parameters;
$R3$:　for the resistances.

4.4. Preliminary Uplift force calculation

For the case studied, the following figure (figure 4.2) has been made to visualize the mechanism in hand. A subgroup analysis for different depths of the soil layers and their different soil weight parameters will be carried out in the following chapters to account for the soil investigation uncertainty. To

calculate the preliminary uplift force in the initial stage of the construction, the uplift failure mechanism (UPL) from the NEN9997, 2016 will be used.
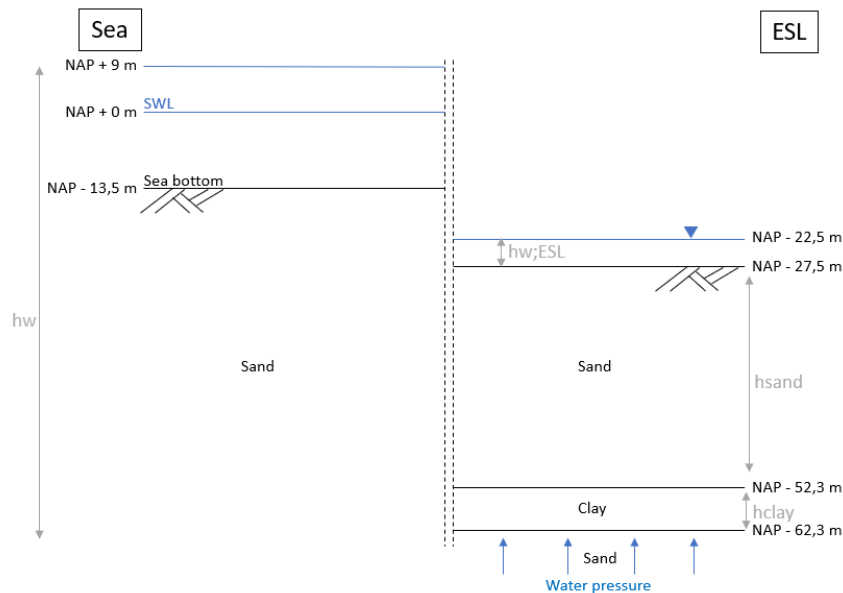
Figure 4.2: Actual situation of the case study.

According to a study made by the RIZA (Rijksinstituut voor Integraal Zoetwaterbeheer en Afvalwater-behandeling), the average sea level at Hoek van Holland in the next 50 to 100 years will vary from approx. + NAP 1.9 m (Low sea water level) to + NAP 3.7 m (High sea water level) (Lavooij et al., 2018). The sea-level rise is based on a conservative starting point and on the expectation that sea-level rise will not accelerate until after 2050. The design criteria for the Delta21 sea defence structure are established based on the design wave conditions with a return period of 18,565 years (Versteeg, 2023). Furthermore, as shown in 4.3, the wave heights and the storm surge levels corresponding to a return period of 18,656 years are considered for different levels of sea level rise. It's important to note that this specific return period is selected for designing the sea defence against the overtopping failure mechanism.

The analysis incorporates sea level rise scenarios of up to five meters, accounting for the substantial uncertainties associated with such changes. This consideration aligns with the potential sea level rise projections for the 100-year lifespan of the Delta21 sea defence (Arias et al., 2021).

Water depth at toe [m]	Storm surge level [NAP+m]	Amount of sea level rise [m]	Significant wave height [m]
20.52	6.52	1 (base scenario)	7.87
21.52	7.52	2	8.17
22.52	8.52	3	8.47
23.52	9.52	4	8.73
24.52	10.52	5	8.97

Figure 4.3: Significant wave heights/storm surge levels with a return period of 18656 years for different amounts of sea level rise. (Versteeg, 2023)

The total water level used for this project will be the one used for the high sea level rise of + 3.7m (≈4m). This is equivalent to storm surge levels of NAP + 9m. This will be considered for the water column calculation outside the ESL and backpressure under the clay layer.

The preliminary calculation was carried out to determine the current uplift situation with no measures applied. The soil properties are estimated using Table 2b of the Eurocode (as explained before in section 3); for the time being, the density of the sand is defined as 20 kN/m^3 and the clay density as 21

kN/m^3. With the use of the Eurocode, a partial factor is applied for each of the uplift equilibrium actions. For the permanent destabilising action (in this case, the uplift force generated by the water pressure) it is used a factor of 1 and for the permanent stabilising action it is used a factor of 0.9.

The depths at which the sand and clay are situated are defined in section 3 and can be seen in figure 4.2. The sand layer appears from the bottom of the energy storage lake at - NAP 27.5 m to - NAP 52.3 m. The clay layer is found at depths from - NAP 52.3 m to - NAP 62.3 m.

For this preliminary calculation, the equilibrium from equation 4.5 has to be satisfied. The design requirements to prevent uplift failure are checked according to the following inequality in Clause 2.4.7.4 of the NEN9997, 2016.

$$V_{dst,d} \leq G_{stb,d} + R_d \tag{4.5}$$

where:

$V_{dst,d}$: design value of the destabilising variable vertical actions, i.e. the sum of the water pressures under the structure, in kPa;

$G_{stb,d}$: design value of the stabilising permanent vertical actions, in kPa;

R_d: design value of any additional resistance to uplift, in this case, 0 as there is no additional resistance, i.e. piles.

Analysing the problem situation, it can be seen that the water pressure from the seaside is the destabilising variable vertical action ($V_{dst,d}$). Once this is defined, the water pressure underneath the clay layer is calculated with the following equation (note that the water pressure distribution is assumed to be hydrostatic):

$$P_w = \gamma_w \cdot h_w \cdot PartialFactor \tag{4.6}$$
$$P_w = 10kN/m^3 \cdot (62.3m + 9m) \cdot 1 = 713kPa \tag{4.7}$$

After retrieving the destabilising variable, the design value of the stabilising permanent vertical action is calculated. This action corresponds to the side of the energy storage lake (G_{stb}), soil and water parts. Equation 4.8 and 4.10 correspond to the sand and clay pressures, multiplied by their partial factor, 0.9. As we work in saturated conditions (total stresses), the water pressure acting with the soil is also considered when calculating G_{stb} by using the saturated soil weight properties of each one of the soils. Equation 4.14 calculates the total soil pressure on the lakeside, G_{stb}.

$$P_{sand} = (\gamma_{sand} \cdot h_{sand}) \cdot PartialFactor \tag{4.8}$$
$$P_{sand} = 20kN/m^3 \cdot (52.3m - 27.5m) \cdot 0.9 = 446.4kPa \tag{4.9}$$

$$P_{clay} = \gamma_{clay} \cdot h_{clay} \cdot PartialFactor \tag{4.10}$$
$$P_{clay} = 21kN/m^3 \cdot (62.3m - 52.3m) \cdot 0.9 = 189kPa \tag{4.11}$$

$$P_{w;ESL} = \gamma_w \cdot h_w \cdot PartialFactor \tag{4.12}$$
$$P_{w;ESL} = 10kN/m^3 \cdot 5m \cdot 0.9 = 45kPa \tag{4.13}$$

$$G_{stb} = P_{sand} + P_{clay} + P_{w;ESL} \tag{4.14}$$
$$G_{stb} = 446.4kPa + 189kPa + 45kPa = 680.4kPa \tag{4.15}$$

$$713kPa \nleq 680.4kPa + 0 \tag{4.16}$$

After carrying out all the calculations, it can be seen in equation 4.7 and 4.15 respectively, $V_{dst,d} \nleq G_{stb}$. Thus, it can be confirmed that the previous inequality ($V_{dst,d} \nleq G_{stb}$) is not satisfied. For that reason, uplift will occur, and measures will have to be taken into account.

If measures were not going to be used to reach equilibrium ($V_{dst,d}$ = G_{stb}), the Energy Storage Lake would need to be shallower, in this case, making the lake less deep, given that $\gamma_{sand} = 20kPa$ and $\gamma_{clay} = 21kPa$. This means that the thickness of the sand layer within the lake would increase (up to a minimum of 26.6m); thus, the pressure in the clay layer is the same as previously calculated.

$$P_{sand} = 20kN/m^3 \cdot (52.3m - 25.7m) \cdot 0.9 = 478.8kPa \tag{4.17}$$

$$G_{stb} = 478.8kPa + 189kPa + 45kPa = 712.8kPa \tag{4.18}$$

In this case, we find that,

$$713kPa = 712.8kPa + 0 \tag{4.19}$$

To ensure equilibrium without taking any measures into account, the Energy Storage Lake bottom depth will have to be maximum until -25.7m NAP. Even though equilibrium is reached, the soil parameter uncertainties and depth of the clay layer uncertainty must be investigated further to conclude. If the soil parameters were to be smaller, the equilibrium would not be satisfied at this depth and if the clay layer was to be at less depth.

For these reasons, a FEM analysis will be carried out to confirm these movements, and the modelling of anchor piles will be studied to prevent the uplift from happening in the events when equilibrium is not reached.

In the case of soil calculations, FEM analysis can provide more accurate results than other methods due to the following reasons:

1. **Soil is a complex material:** Soil is a highly heterogeneous and complex material that can exhibit non-linear behaviour, anisotropy, and variability in properties. FEM analysis can consider these complexities and accurately model soil behaviour under different loading conditions.

2. **FEM can simulate complex geometries:** FEM can simulate complex geometries, such as irregularly shaped excavations or foundations, which may be difficult to model using other methods. This allows for a more accurate representation of the soil structure and behaviour.

3. **FEM can model soil-structure interaction:** FEM can also simulate the interaction between the soil and structures, such as foundations or retaining walls. This is particularly important in geotechnical engineering, where the behaviour of the soil-structure system is critical to the safety and stability of the structure.

4. **FEM allows for parameter subgroup analysis:** FEM analysis can perform subgroup analysis to determine the effects of different input parameters on the output results. This helps to identify the most critical parameters and quantify their impact on the overall behaviour of the soil.

Overall, FEM analysis provides a powerful tool for accurately modelling the complex behaviour of soil under different loading conditions. It allows for a more detailed understanding of the soil-structure interaction and can provide more accurate results than hand calculations, making it an essential tool in geotechnical engineering.

4.5. Hand calculation subgroup analysis

In this section, a subgroup analysis will be performed to estimate the pressures the project site will likely experience due to soil uncertainties. The two main uncertainties that can contribute to the outcome of the initial equilibrium of the energy storage lake are each layer's soil weight (γ) and the soil depth at which the clay layer is to be found.

Equations previously used in section 4.4 will be used to achieve this subgroup analysis. The depth of the clay layer itself will be fixed at 10 m, as in both of the most unfavourable and favourable locations at which the clay layer is found, it is found to be 10 m and 9.5 m. Thus, it is assumed 10 m for the rest of the calculations.

4.5.1. Variation of the soil weight parameter

In this section, employing an uplift check at the bottom of the ESL, four different parameters will be used in four different combinations to determine which is the most favourable combination, which is the most unfavourable and how their influence is in case of uplift. For this check, the soil depth will be fixed at the most unfavourable clay layer depth (found in the previous section) from - NAP 52.3 m to - NAP 62.3 m. Thus, as before, the water pressure ($V_{dst,d}$) generated at the bottom of the clay layer will be constant and equal to 713kPa as well as the water pressure within the ESL (45kPa) (as calculated previously in section 4.4).

Sand 20kN/m^3 and clay 20kN/m^3

$$P_{sand} = 20kN/m^3 \cdot (52.3m - 27.5m) \cdot 0.9 = 446.4kPa \tag{4.20}$$

$$P_{clay} = 20kN/m^3 \cdot (62.3m - 52.3m) \cdot 0.9 = 180kPa \tag{4.21}$$

$$P_{soil} = G_{stb,d} = 446.4kPa + 180kPa + 45kPa = 671.4kPa \tag{4.22}$$

$$713kPa \nleq 671.4kPa + 0 \tag{4.23}$$

Sand 20kN/m^3 and clay 21kN/m^3

$$P_{sand} = 20kN/m^3 \cdot (52.3m - 27.5m) \cdot 0.9 = 446.4kPa \tag{4.24}$$

$$P_{clay} = 21kN/m^3 \cdot (62.3m - 52.3m) \cdot 0.9 = 189kPa \tag{4.25}$$

$$P_{soil} = G_{stb,d} = 446.4kPa + 189kPa + 45kPa = 680.4kPa \tag{4.26}$$

$$713kPa \nleq 680.4kPa + 0 \tag{4.27}$$

Sand 19kN/m^3 and clay 20kN/m^3

$$P_{sand} = 19kN/m^3 \cdot (52.3m - 27.5m) \cdot 0.9 = 424.08kPa \tag{4.28}$$

$$P_{clay} = 20kN/m^3 \cdot (62.3m - 52.3m) \cdot 0.9 = 180kPa \tag{4.29}$$

$$P_{soil} = G_{stb,d} = 424.08kPa + 180kPa + 45kPa = 649.08kPa \tag{4.30}$$

$$713kPa \nleq 649.08kPa + 0 \tag{4.31}$$

Sand 19kN/m^3 and clay 21kN/m^3

$$P_{sand} = 19kN/m^3 \cdot (52.3m - 27.5m) \cdot 0.9 = 424.08kPa \tag{4.32}$$

$$P_{clay} = 21kN/m^3 \cdot (62.3m - 52.3m) \cdot 0.9 = 189kPa \tag{4.33}$$

$$P_{soil} = G_{stb,d} = 424.08kPa + 189kPa + 45kPa = 658.08kPa \tag{4.34}$$

$$713kPa \nleq 658.08kPa + 0 \tag{4.35}$$

After checking all the combinations, it can be concluded that when the sand layer has a $\gamma_{sand} = 19kN/m^3$ and the clay layer has a $\gamma_{clay} = 20kN/m^3$, the pressure generated from the soil is the weakest.

Although, as it can be seen in figure 4.4, there is the weakest pressure within the combinations, all the combinations turned out to be not sufficient to maintain the uplift equilibrium. For that reason, further

Variation of the soil weight parameters
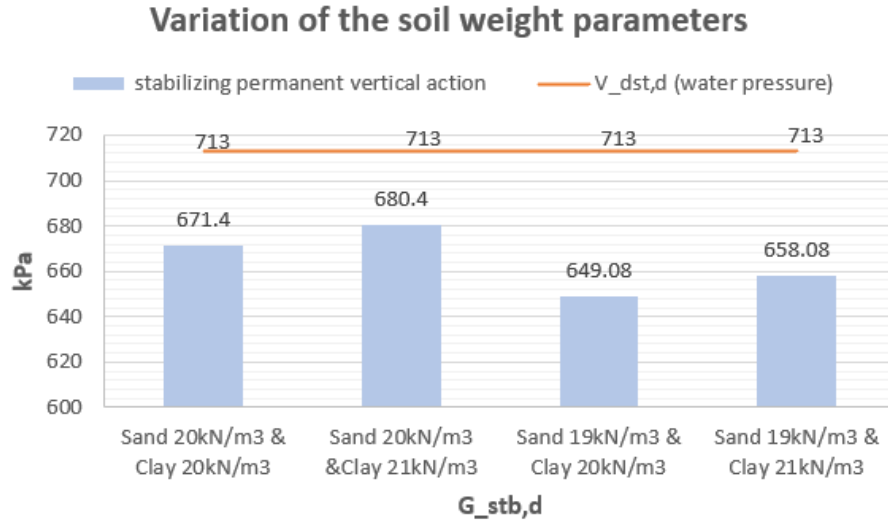
Figure 4.4: Overview of all the soil weight parameter combinations.

subgroup analysis investigation of the clay layer's location will be of greater influence in pressure generation.

From this analysis, the following parameters used as input for the FEM analysis will be $\gamma_{sand} = 19kN/m^3$ and $\gamma_{clay} = 20kN/m^3$. This will help achieve a more conservative design if tension piles are needed.

4.5.2. Variation of clay layer location

The most unfavourable depth of the clay layer found throughout the CPTs in chapter 3 is located from - NAP 52.3 m to - NAP 62.3 m. This calculation is already carried out in section 4.4. It can be seen that the equilibrium is not reached as the inequality is not satisfied.

The most favourable depth at which the clay layer is found in chapter 3 is at depths from - NAP 66.4 m to - NAP 75.9 m. The pressures generated if the clay layer is found at this depth are now calculated. The soil weight parameters (γ_{sand} and γ_{clay}) and the partial factors used for this calculation are the same as the ones we used in section 4.4 (γ_{sand}= 20kN/m³ and γ_{clay}= 21kN/m³).
In this case, the water pressure is not the same as before; thus, it needs to be calculated again.

$$P_w = \gamma_w \cdot h_w \cdot PartialFactor \tag{4.36}$$

$$P_w = 10kN/m^3 \cdot (75.9m + 9m) \cdot 1 = 849kPa \tag{4.37}$$

$$P_{w;ESL} = \gamma_w \cdot h_w \cdot PartialFactor \tag{4.38}$$

$$P_{w;ESL} = 10kN/m^3 \cdot 5m \cdot 0.9 = 45kPa \tag{4.39}$$

$$P_{sand} = (\gamma_{sand} \cdot h_{sand}) \cdot PartialFactor \tag{4.40}$$

$$P_{sand} = 20kN/m^3 \cdot (66.4m - 27.5m) \cdot 0.9 = 700.2kPa \tag{4.41}$$

$$P_{clay} = \gamma_{clay} \cdot h_{clay} \cdot PartialFactor \tag{4.42}$$

$$P_{clay} = 21kN/m^3 \cdot (75.9m - 66.4m) \cdot 0.9 = 179.55kPa \tag{4.43}$$

$$P_{soil} = P_{sand} + P_{clay} + P_{w;ESL} \tag{4.44}$$

$$P_{soil} = G_{stb,d} = 700.2kPa + 179.55kPa + 45kPa = 879.75kPa \tag{4.45}$$

$$849 kPa \leq 879.75 kPa + 0 \tag{4.46}$$

It can be concluded that the inequality is satisfied when the clay layer is from - NAP 66.4 m to - NAP 75.9 m. This means there is equilibrium, and uplift is not likely to occur.

At this time, knowing that the equilibrium is satisfied at the most favourable location of the clay layer, the exact location at which the equilibrium is just barely satisfied ($V_{dst,d} \cong G_{stb}$) is going to be found.
It is known that when the clay layer is from - NAP 52.3 m to - NAP 62.3 m, the inequality is not satisfied, and when it is from - NAP 66.4 m to - NAP 75.9 m, it is satisfied; thus, a depth between these two locations will be established. Using Excel and the iteration of the water and soil pressures, the exact location at which $V_{dst,d} = G_{stb}$ is found. The soil weight parameters to ensure a conservative result are γ_{sand}= 19kN/m^3 and γ_{clay}= 20kN/m^3.

When,

$$P_w = \gamma_w \cdot h_w \cdot PartialFactor \tag{4.47}$$
$$P_w = 10kN/m^3 \cdot (71.3m + 9m) \cdot 1 = 803kPa \tag{4.48}$$

$$P_{sand} = (\gamma_{sand} \cdot h_{sand}) \cdot PartialFactor \tag{4.49}$$
$$P_{sand} = 19kN/m^3 \cdot (61.3m - 27.5m) \cdot 0.9 = 577.98kPa \tag{4.50}$$

$$P_{clay} = \gamma_{clay} \cdot h_{clay} \cdot PartialFactor \tag{4.51}$$
$$P_{clay} = 20kN/m^3 \cdot (71.3m - 61.3m) \cdot 0.9 = 180kPa \tag{4.52}$$

$$P_{soil} = P_{sand} + P_{clay} + P_{w;ESL} \tag{4.53}$$
$$P_{soil} = G_{stb,d} = 577.98kPa + 180kPa + 45kPa = 802.98kPa \tag{4.54}$$
$$803kPa \approx 802.98kPa + 0 \tag{4.55}$$

It can be seen that when $V_{dst,d} \approx G_{stb}$, the clay layer is located from - NAP 61.3 m to - NAP 71.3 m. Knowing the three primary locations at which the clay layer can be found, a FEM analysis will be carried out, considering all of them.

4.6. Check against uplift failure

As shown before in chapter 4.4, the design requirements to prevent failure are checked according to the following inequality:

$$V_{dst,d} \leq G_{stb,d} + R_d \tag{4.5}$$

The recommended values of the partial factors for this UPL ULS in Table 4.1 are $\gamma_{G,dstb}$ = 1.0 on the permanent destabilising action and $\gamma_{G,stb}$ = 0.9 on the permanent stabilising action. Hence:

- the design value of the destabilising uplift force is:

$$V_{dst,d} = \gamma_{G,dst} \cdot \gamma_{water} \cdot H = 1.0 \cdot 10kN/m^3 \cdot (62.3m + 9m) = 713kPa \tag{4.56}$$

- the design value of stabilising weight is:

$$G_{stb,d} = \gamma_{G,stb} \cdot \gamma_{sand/clay} \cdot \gamma_{w;ESL} \cdot H \tag{4.57}$$

$$= 0.9 \cdot 19kN/m^3 \cdot (52.3 - 27.5m) = 424.08kPa \tag{4.58}$$

$$= 0.9 \cdot 20kN/m^3 \cdot (63.3 - 52.3m) = 180kPa \tag{4.59}$$

$$= 424.08kPa + 180kPa + 45kPa = 649.08kPa \tag{4.60}$$

As $V_{dst,d}$ = 668 kPa > $G_{stb,d}$ = 649.08 kPa, to prevent uplift failure, it is required a R_d ≥18.92 kPa. This could be provided by increasing the sand layer (reducing the depth of the ESL) or by tensile piles. For this project, tensile piles will be considered in the next chapter to solve the uplift failure.

5

Tension piles

In this chapter, the mechanisms of the tension piles will be introduced, and the Dutch Design Guide for its calculation. Later, the pile type and installation method will be discussed step by step to determine the shaft friction of the piles. Finally, an analytical analysis is carried out utilizing Excel.

5.1. Introduction to tension piles

The primary role in resisting loads, in contrast to compressing loading, the piles resist uplift force by shaft resistance only. This is so because soil's tensile strength is relatively small compared to its shear strength and can be safely neglected for a conservative estimate of load-carrying capacity. (Goel and Patra, 2007)

Tension piles are used in deep excavation pits to maintain vertical equilibrium and stabilize the surrounding soil. Unlike conventional designs with a rigid concrete floor, the piles that will be investigated in this report rely on frictional forces to transfer loads to a stable soil layer. Tension piles create additional weight by penetrating the clay layer and extending into the stable soil, counteracting uplift forces. The piles mobilize friction along their sides, resisting uplift by transferring forces to the soil through friction. This innovative approach eliminates the need for a concrete floor, offering a cost-effective and flexible solution for deep excavation projects.

5.2. Dutch Design Guide for Tension Piles

5.2.1. Introduction

In the Netherlands, the design methods can be divided into single and group piles methods. As CPTs and cone resistance determination are widely used for soil investigation in the Netherlands, the qc-method determines the maximum bearing capacity of single and group piles. With this method, the results obtained are better compared with reality.

In this chapter, a distinction is made between the calculation of the design bearing capacity of single and group piles. It is important to determine the value of the shaft friction coefficient and the root ball weight to calculate the pile's bearing capacity.

5.2.2. Single pile

For piles where the tensile resistance is largely derived from sand layers, the calculation method below can be used to determine the tensile resistance for certain situations from the results of a CPT. A distinction is made between the single pile and the pile group. Furthermore, a distinction was made between the different pile types, as with piles loaded under pressure. The validity of the calculation method is limited to the geometry and dimensions of which test load results were known when the method was derived. This calculation method does not apply to dynamic load changes. The calculation method is, therefore, only valid for:

- a length/diameter ratio of at least 13.5;

• a pile length of at least 7 m and at most 50 m.

For deviating piles or pile types, a new test load must be carried out or an extra one safety in the design method.

The design value of the tensile resistance of a pile must be determined with the following:

$$R_{t;d} = \int_0^L O_{s;av} \cdot q_{s;z;d} \cdot dz \tag{5.1}$$

where:

$R_{t;d}$:   design value of the resistance to the tension of the pile, in kN;
$O_{s;av}$:   average perimeter of the pile, in m;
L: length over which shaft friction is calculated, in m;
$q_{s;z;d}$:   design value of the shaft friction at depth z, in kPa;
z: indication of the depth, in m.

The design value of the shaft friction ($q_{s;z;d}$) is determined as follows:

$$q_{s;z;d} = \alpha_t \cdot q_{c;z;d} \tag{5.2}$$

where:

α_t: factor which takes the influence of the installation process into account;
$q_{c;z;d}$:   design value of the shaft friction at depth z, in kPa.

Table 5.1: Values for α_t in sand and gravely sand. Source: NEN9997, 2016.

Pile class/ type	α_t [1]
soil displacement insertion method:	
- driven smooth prefab concrete pile and steel tubular pile with closed point [2]	0,007
- pile made in the ground, where the concrete column presses directly against the ground and the pipe has been driven back from the ground [3]	0,012
- idem, the tube is removed vibrating	0,010
- driven-in MV pile	0,012
- screwed-in posts: with grout injection or mixing	0,009
profiles with little soil displacement:	
- driven steel profiles (including open steel tubular piles and sheet piles)	0,004
piles made with soil removal:	
- bored piles (and auger piles)	0,0045
[1] The values apply to very fine to coarse sand:105 μm <Mz <600 μm. With extremely coarse sand with Mz>600 μm and gravel with Mg>2mm, α_t must be reduced by 0.75 and 0.5 respectively.	
[2] The base plate of the tubular pile with closed base must not protrude more than 10 mm outside the pipe.	
[3] The diameter of the base plate may in principle be 30 - 50 mm larger than the outside diameter of the casing.	

For piles located in clay, loam or peat layers, the factors given in table 5.1 are irrelevant. Table 5.2 should be used in these cases.

Table 5.2: Values for α_t in clay, loam and peat. Source: NEN9997, 2016.

soil type	relative depth z / D_{eq}	α_t
clay / silt $q_c \leq 1$ MPa	0 < z / D_{eq} < 20	0,02
clay / silt $q_c \leq 1$ MPa	z / D_{eq} > 20	0,025
clay / silt $q_c \leq 1$ MPa	z / D_{eq} > 20	0,025
clay / silt $q_c > 1$ MPa	-	0,025
* The values for α_t are not based on test loads but on literature.		

5.2.3. Pile group

Two aspects play a role in the pile group, meaning that one of the single pile deviating calculation rules is used:

- the effect of compaction by installing the pile group;

- the relaxation due to the tensile load on the pile group.

These two effects are considered by the factors f_1 and f_2. The calculation value of the shaft friction of a pile in a pile group follows from the following:

$$p_{r;z;d} = f_1 \cdot f_2 \cdot \alpha_t \cdot q_{c;z;d} \qquad (5.3)$$

where:

$p_{r;z;d}$:   design value of the shaft friction at depth z, in kN/m^2;
α_t: factor, stated in tables 5.1 and 5.2, that takes into account the influence of the execution;
$q_{c;z;d}$:   design value of the cone friction at depth z, in kPa;
f_1:   factor for the effect of the compaction due to the tensile load of the pile group;
f_2:   factor for the effect of the relaxation due to the tensile load of the pile group.

The determination of $q_{c;z;d}$ and the factors f_1 and f_2 is described below step by step. It should be noted that the factors f_1 and f_2 are only applied for sands, and they should be set to $f_1 = f_2 = 1$ for clay applications.

The following steps are used to determine the necessary parameters:
Step 1: Determinate the starting points for the soil and piles;

- Soil: cone resistance, volumetric weights and soil layout (previously determined in chapter 3)

- Pile: type, dimensions, influence area of pile groups and spacing.

Step 2: Define the reduction value of cone resistance by excavation;

- if the piles are **installed non-vibration-free after excavation**, the reduction cone resistance following NEN 6743: 1991:

$$q_{c;z;exc} = q_{c;z} \cdot \frac{\sigma'_{v;z;exc}}{\sigma'_{v;z;0}} \quad \text{with} \quad q_{c;z;exc} \leq 12 \quad \text{or} \quad 15 MPa \qquad (5.4)$$

- if the piles have been **installed prior to excavation** or if this is the case demonstrably low-vibration inserted:

$$q_{c;z;exc} = q_{c;z} \cdot \sqrt{\frac{\sigma'_{v;z;exc}}{\sigma'_{v;z;0}}} \quad \text{with} \quad q_{c;z;exc} \leq 12 \quad \text{or} \quad 15 MPa \qquad (5.5)$$

where:
$q_{c;z;exc}$:   corrected, calculated cone resistance at depth z below the bottom of the excavation, in MPa, where the peaks in the CPT diagram at values of 15 MPa are marked as these values over a distance of at least 1 m and otherwise at values of 12 MPa;
$q_{c;z}$:   cone resistance measured before excavation at depth z, in MPa;
$\sigma'_{v;z;exc}$:   effective vertical stress at depth z below the bottom of the excavation, in kPa;
$\sigma'_{v;z;0}$:   initial effective vertical stress at depth z during probing, in kPa.

Step 3: Determination of the design value of the cone resistance;
The design value of the cone resistance for a pile in a pile group is generally determined by the following equations:

$$q_{c;z;d} = \frac{q_{c;z;a}}{\gamma_{s;t} \cdot \gamma_{m;var;qc} \cdot \xi} \qquad (5.6)$$

On the contrary, when excavating first, it is calculated as follows:

$$q_{c;d;rep;exc} = \xi \cdot q_{c;z;exc} \quad \text{and} \quad q_{c;d} = \frac{q_{c;z;rep;exc}}{\gamma_{m;b4} \cdot \gamma_{m;var;qc}} \tag{5.7}$$

where:

$q_{c;z;max}$:   cone resistance at depth z below ground level in MPa, where the peaks are in the CPT diagram at values of 15 MPa are rounded off as these values occur over a distance of at least 1 m, otherwise at values of 12 MPa;

$q_{c;z;exc}$:   cone resistance including effect excavation and cut at 12 resp. 15 MPa, see equation (5.4) and (5.5);

$q_{c;z;rep}$:   representative cone resistance without effect excavation;

$q_{c;z;rep;exc}$:   representative cone resistance including effect excavation;

ξ: factor for the number of probes and the redistribution capacity of the construction;

$\gamma_{m;b4}$:   material factor for tension loaded piles according to table 3 of NEN 6740: 1991; $\gamma_{m;b4} = 1.4$;

$\gamma_{m;var;qc}$:   factor that reflects the effect of changing loads. The tax variations in the determination of $\gamma_{m;var;qc}$ must be quasi-static. This one calculation rule does not apply to dynamic changes.

In order to determine factor ξ, table 5.1 from the NEN9997, 2016 is used. For non-rigid constructions, it must be maintained an M = 1. Only if a sufficiently high stiffness of the construction (or construction part) can be demonstrated may be deviated from this value (rigid structure, M> 1).

Correlatiefactoren ζ voor een niet-stijf bouwwerk							
ζ voor $n =$	1	2	3	4	5	7	10
ζ_1	1,39	1,32	1,30	1,28	1,28	1,27	1,25
ζ_2	1,39	1,32	1,30	1,03	1,03	1,01	1,00

Figure 5.1: Correlation factors ξ for determining characteristic values from static pile load tests (n = number of piles tested) for a non-rigid structure. (Source: CUR2001-4, 2011)

The factor ξ takes into account the structure's ability to transfer forces from a 'weak' foundation element to places with a 'strong' foundation element. It also considers a better knowledge of the variability and quality of the soil with the help of more CPTs.

For this research, a non-rigid construction is considered; thus, the ξ factor that will be used is $\xi = 1,39$.

Step 4: Determination of the effect of installation (factor f_1);
The sand layers in which the piles are driven are compacted and stretched by driving or vibrating piles. This effect, which may only be taken into account for earth-displacing piles, is expressed as a factor f_1, which is the increase of the cone resistance due to the pile installation displays:

$$f_1 = \frac{q_{c;z;1}}{q_{c;z;d}} \tag{5.8}$$

where:
$q_{c;z;1}$:   design value of the cone resistance after pile installation, in MPa;
$q_{c;z;d}$:   design value of the cone resistance for pile installation in MPa.

$$f_1 = e^{3 \cdot \Delta R_e} \quad \text{with} \quad \Delta R_e = \frac{\sum_1^n \Delta e}{(e_{max} - e_{min})} \tag{5.9}$$

$$\sum_1^n \Delta e = -\frac{(r-6)}{5.5} \cdot \frac{1 + e_0}{50} \tag{5.10}$$

where:

ΔR_e: increase in relative density due to pile installation and is calculated from the summation of the compaction effects Δ e of the surrounding piles, with which to distinguish is made between field posts, edge posts and corner posts;

e: void ratio;

Δe: decrease of the void ratio as a result of the insertion of a soil displacing pile within a distance of 6 × D_{eq};

e_{max}: maximum void ratio of the soil (most loose packing). The influence of this parameter is limited, so a global estimate will suffice. For normal consolidated sands in the Netherlands can be assumed in most cases of e_{max} = 0.80;

e_{min}: minimum void ratio of the soil (most tight packing). The influence of this parameter is limited, so a global estimate will suffice. For normal consolidated sands in the Netherlands can be assumed in most cases from e_{min} = 0.40;

n: number of posts within a distance of 6 × D_{eq};

r: centre-to-centre distance expressed in D_{eq} from a pile to the pile to be considered with a maximum of r = 6, if r > 6 no compaction effect is assumed;

e_0: initial pore number of the soil.

The factor f_1 applies to sands at ground displacement piles. For cohesive soil, f_1 = 1.0 must be used. According to report 236, 2017, this value equals 1.0 for micro piles.

Step 5: Determination of the effect of relaxation (factor f_2);
The grain tension in the layers from which the pile draws its tensile force decreases when the pile group is loaded under tension. A factor f_2 is applied to the cone resistance to account for this decrease:

$$f_{2;i} = \frac{-M_i + \sqrt{M_i^2 + \left(2 \cdot \sigma'_{v;j;0;d} + \gamma'_{i;d} \cdot d_i\right) \cdot \left(2 \cdot \sigma'_{v;j;0;d} + \gamma'_{i;d} \cdot d_i - 2 \cdot \sum_{n=0}^{i-1} q_{t;n;d}\right)}}{\left(2 \cdot \sigma'_{v;j;0;d} + \gamma'_{i;d} \cdot d_i\right)} \tag{5.11}$$

$$M_i = \frac{f_{1;i} \cdot O_{s;gem;i} \cdot \alpha_t \cdot q_{c;i;d} \cdot d_i}{A} \quad \text{with} \quad q_{t;i;d} = M_i \cdot f_{2;i} \tag{5.12}$$

where:
M_i: auxiliary factor of layer i, in kN/m^2;

$q_{t;i;d}$: design value of the contribution of the tensile resistance of layer i, in kN/m^2;

$\sigma'_{v;j;0;d}$: calculation value of the effective vertical grain stress after excavation (if applicable) in layer separation j, in kN/m^2;

$O_{s;gem;i}$: mean circumference of the pile in layer i, in m;

$q_{c;i;d}$: design value of the average cone resistance in layer i, in kPa;

d_i: thickness of layer i, in m;

A: surface of influence of the pile, that is, the area over which the stress spreads around a pile within a pile group, in m^2. The value of A is limited to the plane that covers half the centre-to-centre distance to the next foundation pile, see also figure 7.m;

$\gamma'_{i;d}$: calculation value of the effective volumetric weight of layer i, in kN/m^3.

For the calculation of f_2, the soil over the entire length of the pile is divided into layers with constant cone resistance $q_{c;z}$, each with a thickness not exceeding 1 m.

The value of A is limited to the plane half the centre-to-centre distance to the next foundation pile plates. For a regular pile pattern, A must be determined with (see figure 5.2):

$$A = \left(\frac{1}{2}Y_2 + \frac{1}{2}Y_1\right) \cdot X - A_{pile} \tag{5.13}$$

where:

Y_1:   centre-to-centre distance to the first adjacent pile row, in m;
Y_2:   centre-to-centre distance to the second adjacent pile row, in m;
X: centre-to-centre distance in the direction perpendicular to the pile rows, in m;
A_{pile}:   area of the pile cross-section, in m^2.
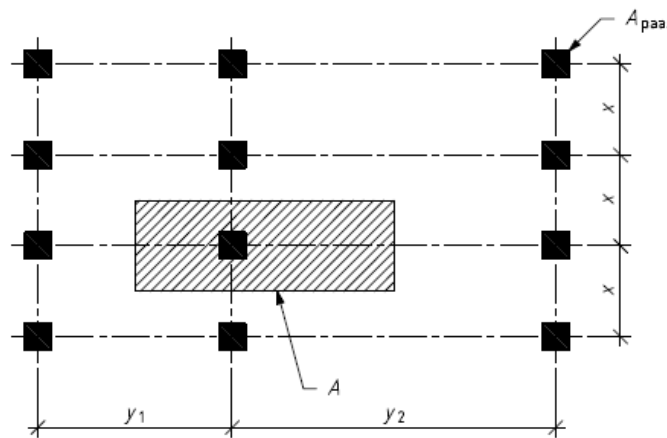
Figure 5.2: Influence area of a pile. (Source: NEN9997, 2016)

Step 6: Determination of tension resistance;
The total tensile strength for a pile in a pile group for m layers must be determined with the following equation:

$$R_{t;d} = A \cdot \sum_{i=1}^{m} q_{t;i;d} \quad \text{with} \quad R_{t;d} \leq R_{t;kluit;d} \tag{5.14}$$

where:
$R_{t;kluit;d}$:   root ball weight, excluding the pile weight, in kN, calculated in step 7.

When determining $R_{t;d}$, the shaft friction in the top meter of soil around the pile must be disregarded and equal to 0.

Step 7: Determination of root ball weight;
The root ball weight of a pile in a pile group can be calculated with the equation 5.15, and the soil volume around the pile will be mobilized. This criterion states that the tensile force on a pile can never be larger than the weight of the pile plus the conical-shaped ground around the pile.
It is reasonable to presume that the complete weight of the sand cannot be mobilized between the piles of a pile group to develop the pile's bearing capacity. Starting at the pile tip, a conical-shaped slide surface may form. The weight of the soil in the cone and cylinder shapes is compared to the predicted bearing capacity of the pile in the pile group using the:

$$R_{t;kluit;d} = \left(V_{cone} + V_{Cylinder}\right) \cdot \gamma'_d \tag{5.15}$$

where:
$R_{t;kluit;d}$:   root ball weight, excluding the weight of the pile, in kN;
V_{cone}:   volume of the conical soil volume at the bottom of the pile, excluding the volume of the pile, in m^3;
$V_{cylinder}$:   volume of the schematized 'cylindrical' soil volume around the rest of the pile, excluding the volume of the pile, in m^3;
γ'_d: design value of the effective volumetric weight of the soil, in kN/m^3. In layered soil structure, the weight per layer must be considered.

The half-top angle of the cone must be determined from table 5.3.

Paalsoort [a]	Halve tophoek binnen de paalgroep in °	Halve tophoek buiten de paalgroep in °
Grondverdringende palen	45	30
Weinig grondverdringende palen	$2/3 \times \varphi'$ [b]	$1/2 \times \varphi'$ [b]
Grondverwijderende palen	$2/3 \times \varphi'$ [b]	$1/2 \times \varphi'$ [b]
[a] Voor indeling van paalsoorten zie ook tabel 7.c.		
[b] φ' is de hoek van inwendige wrijving van de grond op de diepte van de kegel.		

Figure 5.3: Size of the top angle of the ground cone at the bottom of the pile. (Source: NEN9997, 2016)

The total calculated pull resistance may be increased by the effective, for soil-displacing piles, own weight of the pile, calculated according to:

$$G'_{stb;pile;d} = V_{pile} \cdot \gamma'_{pile;d} \quad \text{with} \quad \gamma'_{pile;d} = \frac{\gamma_{pile}}{\gamma_\gamma} - \gamma_{water} \tag{5.16}$$

where:
$R_{t;kluit;d}$:   root ball weight, excluding the weight of the pile, in kN;
V_{cone}:   volume of the conical soil volume at the bottom of the pile, excluding the volume of the pile, in m^3;
$V_{cylinder}$:   volume of the schematized 'cylindrical' soil volume around the rest of the pile, excluding the volume of the pile, in m^3;
γ'_d: design value of the effective volumetric weight of the soil, in kN/m^3. At layered soil structure, the weight per layer must be considered.

Finally, to determine the final pull-out capacity of the pile, the following equation is used:

$$F_{r;t;d} = MIN\left(R_{t;d}; R_{t;kluit;d}\right) + G'_{stb;pile;d} \tag{5.17}$$

5.3. Type of piles used

In the Netherlands, double-casing micropiles are commonly used to avoid excessive ground excavation. An outer and inner tube is drilled at depth during installation. The drill head of the rotating inner tube penetrates the ground by downward injection of drilling fluid. The used drilling fluid is water or occasionally a thin grout mixture with a w/c factor >=1.0. Upwards discharge of the drilled soil is possible between the inner and outer tubes. The outer tube acts as a casing, ensuring a stable borehole during the drilling. Consistently, the tip of the outer tube runs over the tip of the inner tube to prevent the injected drilling fluid from disturbing the soil layers around the borehole too much.
After reaching the desired depth, the inner tube gets pulled, the GEWI rod placed, and the bore fluid replaced with a w/c factor of 0.45 to 0.5 grout mixture.

To create a better attachment to the soil, an over-pressure is applied to the grout mixture, after which the outer tube gets pulled up approximately 0.5 meters. Due to the applied pressure, water is forced out of the grout, resulting in the hardening of the mixture.

After reaching a sufficient increase in pressure, the outer tube will get pulled another 0.5 meters, and the procedure repeats until approximately 4 meters below ground level or excavation level. The over-pressure is changed to hydrostatic pressure to prevent a blow-out, and finally, the outer tube is removed completely. This type of micropiles is called: **Double casing micro-pile with an inside spoil (Type A).**

5.4. Analytical evaluation of tension piles

Three centre-to-centre distances are evaluated 1, 2 and 3m. For the analytical evaluation, the input parameters chosen have been chosen for a cylindrical pile. The different centre-to-centre distances have been determined considering the diameter of the pile, so they won't overlap. The α_t, f_1, A, $O_{s;gem;i}$,

A_{paal} parameters are calculated in the previous subchapter 5.2. The excavation level and tension level are defined previously as the bottom of the ESL, and the bottom of the clay layer, respectively.

- centre to centre: 1/2/3 m

- A: 0,9 m^2

- α_t : 0,011

- f_1 : 1

- $O_{s;gem;i}$: 1,257 m

- A_{paal} : 0,126 m2

- Diameter pile (D_{eq}) : 0,4 m

- Pile weight: 2,24 kN/m (underwater)

- Excavation level: -27,5 m NAP

- Tension level: -52,5 m NAP

In Appendix C, the hand calculations of the tension piles for each centre-to-centre distance are shown.

From Appendix C, we can conclude various things. It is important to notice that the tension piles will only use 10 m under the clay layer; after that, they become less effective. Thus, the interpretation will be about those first 10 meters. In a group of tension piles, if the shaft friction or the root ball weight values are less than the other, then it is the value that governs the mechanism. It can be seen in the table for the 1m centre-to-centre distance that the first 1.5m after the clay layer, the shaft friction governs. After that, and for the rest of the 8.5m, the governing mechanism is the root ball weight. In the other two tables, 2m and 3m centre-to-centre distance, the shaft friction governs the full 10m under the clay layer.

The transition from shaft friction to root ball weight in the load-bearing behaviour of a pile occurs when the pile penetrates through various soil layers of different properties as it is driven or installed. This phenomenon is commonly encountered in deep foundation design, such as with driven piles or drilled shafts, and it is often associated with the soil conditions encountered at different depths.

As the pile penetrates deeper, it may encounter soil layers that are less competent or have lower frictional properties. In this transition zone, the shaft friction decreases because the soil can no longer provide sufficient friction to support the load. At this depth, the pile begins to rely more on the end-bearing capacity (root ball weight) to resist axial loads.

To obtain a more precise estimation of the shaft friction of the piles, an analytical evaluation is initially conducted. However, the FEM evaluation encounters difficulties in accurately approximating the pile's shaft friction. Consequently, the FEM analysis will focus on determining the load transfer between the piles, a factor that cannot be obtained through analytical evaluation. Therefore, the forthcoming chapter will employ a FEM analysis utilizing the commercial program PLAXIS.

The objective of these calculations is to ascertain the soil skin friction and incorporate it into the FEM analysis, allowing the soil to exhibit behaviour consistent with the original data derived from the CPT.

6

FEM Analysis

In this chapter, the finite element analysis will be carried out using PLAXIS 2D and 3D, as hand calculations are unreliable for this innovative design where no concrete floor is used to distribute the load along the whole ESL. Using the soil parameters from chapter 3 and the skin friction found in the previous chapter (Chapter 5), the best way to model the soil problem is going to be investigated.

6.1. Introduction

Engineers had to rely on hand calculations and physical testing before using FEM. While these methodologies adequately ensured that designs fulfilled performance requirements, they gave limited performance insight and frequently needed an assumption, test, and change design strategy. Because complicated designs were typically too difficult to examine by hand, hand calculations limited how an engineer could optimize a design. With FEM, we can get much more information about a design's performance.(Heibaum and Herten, 2009)

Engineers that utilize FEM should use it with manual computations. This provides a suitable starting point for a design that can be optimized using FEM. To assess the model's accuracy, hand computations should be utilized to validate FEM results. The hand calculations will keep you in check and tremendously improve your ability to think about the right way to set up the FEM and greatly improve the result.

To determine the most effective approach for modelling the soil problem, the following cases will be analyzed in PLAXIS:
In 2D, the following cases were analysed. It is essential to notice that the model types will be plain-strain and axisymmetric, where the axisymmetric provides a three dimension component that would be helpful to model piles.

- Soil without piles
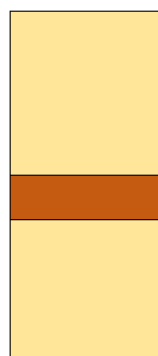
Figure 6.1: Soil without piles sketch in PLAXIS 2D.

- Axisymmetric model, to better represent the third dimension of the problem
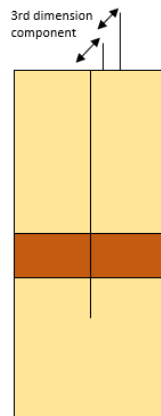
Figure 6.2: Axisymmetric model sketch in PLAXIS 2D.

As tension piles have three dimension components, the following cases will be analysed in 3D to assess better if it is possible to model tension piles correctly using PLAXIS axisymmetric model:

- Soil without piles
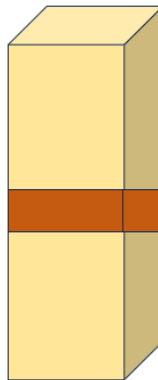
Figure 6.3: Soil model without piles sketch in PLAXIS 3D.

- Soil with just one volume pile
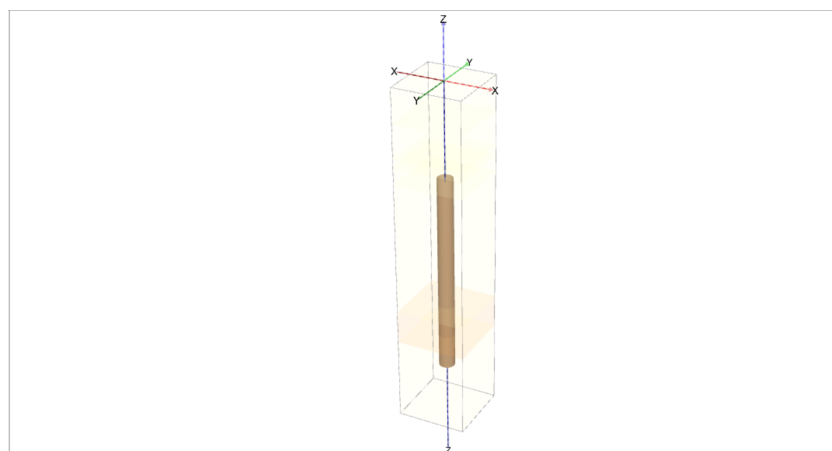
Figure 6.4: Soil model with one single volume pile sketch in PLAXIS 3D.

- Soil with just one embedded beam
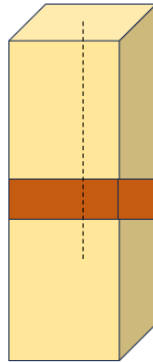
Figure 6.5: Soil model with one single embedded beam sketch in PLAXIS 3D.

- Embedded piles for different centre-to-centre distance
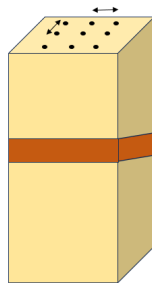
Figure 6.6: Soil model with a grid of embedded beams sketch in PLAXIS 3D.

- Volume piles for different centre-to-centre distances
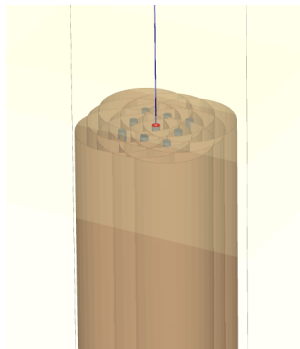
Figure 6.7: Soil model with a grid of volume piles sketch in PLAXIS 3D.

6.2. Determination of the best representative model

First of all, the model is divided into six construction stages, which are the following:

1. Initial Phase

2. Pile installation

3. Excavation 1 (until -10m NAP)

4. Excavation 2 (until -20m NAP)

5. Excavation 3 (until -27.5m NAP)

6. Dewatering (water level has been lowered to -22.5m NAP as it will be the lowest point when the ESL is functioning)

The excavation process is divided into three steps; due to the computational time of the program, by dividing it into three, fewer computational errors could be observed.
To develop an accurate soil model for determining the soil problem, the parameters identified in the previous chapter (Chapter 3) will be utilised and are determined in Appendix B.

The following cases will be modelled in PLAXIS 2D and 3D. Later the results of the surface settlement will be compared at excavation depth (-27.51m NAP) and assessed to determine the best model.
The settlement results from PLAXIS can be found in Appendix D.

No pile:

- Axisymmetric '2D' model of the soils and output the surface settlement profile at Y=-27.51m (NAP)

- '3D' model of the soils and output the surface settlement profile at Y=-27.51m (NAP)

Single pile:

- Axisymmetric '2D' model of the single pile and output the surface settlement profile at Y=-27.51m (NAP)

- Volume pile '3D' model of the single pile and output the surface settlement profile at Y=-27.51m (NAP)

- Embedded pile '3D' model of the single pile and output the surface settlement profile at Y=-27.51m (NAP)

3 by 3 grid of piles: This can only be done using PLAXIS 3D, as it is modelled in the three directions.

1. For 1m centre-to-centre (spacing is 2.5 times the diameter)

    - Volume pile '3D' model and output the surface settlement profile at Y=-27.51m (NAP)
    - Embedded pile '3D' model and output the surface settlement profile at Y=-27.51m (NAP)

2. For 1.2m centre-to-centre (spacing is 3 times the diameter)

    - Volume pile '3D' model and output the surface settlement profile at Y=-27.51m (NAP)
    - Embedded pile '3D' model and output the surface settlement profile at Y=-27.51m (NAP)

3. For 2m centre-to-centre

    - Volume pile '3D' model and output the surface settlement profile at Y=-27.51m (NAP)
    - Embedded pile '3D' model and output the surface settlement profile at Y=-27.51m (NAP)

4. For 3m centre-to-centre

    - Volume pile '3D' model and output the surface settlement profile at Y=-27.51m (NAP)
    - Embedded pile '3D' model and output the surface settlement profile at Y=-27.51m (NAP)

6.2.1. 2D vs 3D

In this sub-section, the location of which the clay layer was found to be at the most stable location (-66.4m to -75.9m NAP) is defined to find which of the previously discussed models is the best to perform the analysis. Looking at the models analysed in the previous sections, we can see that the deformed mesh for the volume piles and embedded piles in 3D give similar results. As the computational time for the volume piles is quite long, the best option will be using *the embedded piles' option*. Table 6.1 summarises the data analysis results of the deformed mesh at the top of the clay layer, comparing the 2D and 3D results.

Table 6.1: The following table presents summarised mesh during the dewatering phase, comparing the results obtained from the 2D and 3D analyses.

Deformed mesh	No pile [m]	1pile [m]	1m spacing [m]	1,2m spacing [m]	2m spacing [m]	3m spacing [m]
Volume piles 3D		0.03933	0.4098	0.03965	0.03957	0.03955
Embedded piles 3D	0.03892	0.04018	0.0405	0.04094	0.04026	0.03957
Axisymmetric	0.03892	-	0.03958	-	-	-
Embedded piles 2D	0.03892	-	0.03832	-	-	-

After conducting a thorough FEM analysis, it becomes apparent that the results obtained from the embedded beams exhibit a remarkable resemblance to those obtained from volume piles. This finding underscores the validity and reliability of employing embedded piles as an alternative solution.

A notable advantage arises regarding computational efficiency by opting for embedded piles and focusing on mesh refinement. The reduction in computational burden proves to be advantageous in several aspects. It enables faster processing and analysis of the data, allowing for quicker decision-making and potentially accelerating the overall project timeline.

Combining embedded piles and mesh refinement offers increased flexibility and adaptability in managing complex engineering scenarios. The refined mesh allows for a more detailed representation of the structural elements and their interactions, enhancing the analysis results' accuracy.

Furthermore, using embedded piles alongside mesh refinement demonstrates a commitment to incorporating realistic conditions and capturing intricate nuances in the analysis. This approach accounts for soil-structure interaction and varying material properties, leading to more precise and reliable results. Such accuracy is essential in ensuring the safety and stability of the structure under consideration.

6.3. Soil Parameter Setting and FEM Analysis Considerations

The soil parameters were obtained in previous chapters using the available CPTs around the ESL area. Thus, the following parameters were set for the different soil layers.

- The clay location depth used to know which was the better option for the FEM analysis goes from -66.4m to -75.9m NAP to ensure that no significant uplift will happen.

- Use the more accurate soil model to make a subgroup analysis of the different depths of the clay layer.

It is crucial to acknowledge that FEM analysis has limitations when simulating excavation effects. While the results obtained from the analysis provide valuable insights, it is important to recognize that they may not fully capture the intricacies and complexities associated with excavation processes.

Regarding realism, volume piles offer a more accurate representation of the actual conditions. Their inclusion in the analysis allows for a more comprehensive understanding of the structural behaviour under consideration. However, it is essential to note that using embedded piles can serve as a suitable approximation in situations where incorporating volume piles may be impractical or computationally intensive.

The use of embedded piles offers a pragmatic approach that balances accuracy and computational efficiency. While it may not provide a replica of the real-world scenario, it still provides valuable insights into the structural response and can guide engineering decisions effectively.

Therefore, when conducting FEM analysis, knowing the limitations and approximations associated with using embedded piles is important. While volume piles are considered more realistic, employing embedded piles can still yield meaningful results, facilitating informed decision-making within the constraints of computational resources and project requirements.

6.3.1. Subgroup Analysis of Clay Layer Depth

After checking which of the models is the most appropriate for the FEM analysis, the other clay locations will be investigated. To reach just the exact equilibrium, the location of the clay layer will be analysed from -61.3m to -71.3m NAP. For the most unfavourable case, the layer's background is from -52.3m to -62.3m NAP. As defined in the 2D vs 3D chapter, embedded piles in PLAXIS 3D will be used for these two subgroup analysis cases. The cases analysed are the following:

1. For 1m centre-to-centre

2. For 1.2m centre-to-centre

3. For 2m centre-to-centre

4. For 3m centre-to-centre

5. For 4m centre-to-centre

Please refer to Appendix E for the analysis results conducted using the embedded pile '3D' model and the surface settlement profile at Y=-27.51m (NAP). In Tables 6.2 and 6.3, you will find a summary of the deformed meshes for all the analysed cases.

Upon examination of the results, it becomes evident that the most effective centre-to-centre distance for each case is consistently 4m spacing. This finding highlights the importance of maintaining this distance between the embedded piles to achieve optimal results across the scenarios evaluated.

Table 6.2: Summary deformed mesh for the clay depth -61.3m to -71.3m NAP

Equilibrium (-61.3m to -71.3m NAP)					
Deformed mesh	1m spacing [m]	1,2m spacing [m]	2m spacing [m]	3m spacing [m]	4m spacing [m]
Embedded piles 3D	0.04927	0.04909	0.04854	0.04898	0.0485

Table 6.3: Summary deformed mesh for the clay depth -52.3m to -62.3m NAP

Most unfavourable (-52.3m to -62.3m NAP)					
Deformed mesh	1m spacing [m]	1,2m spacing [m]	2m spacing [m]	3m spacing [m]	4m spacing [m]
Embedded piles 3D	0.06969	0.06897	0.06832	0.0669	0.06648

6.3.2. Results and interpretation

It is of utmost significance to emphasize that a careful examination of the centrally embedded pile enables us to make insightful predictions regarding the movement of piles within the entirety of the ESL, particularly in the middle region of the lake. By closely observing the behaviour and response of this central pile, we gain valuable insights into the dynamic forces and environmental factors at play, allowing us to extrapolate and comprehend the potential pile movements across the entire expanse of the ESL.

Figure 6.8 illustrates the anticipated interchangeability between volume and embedded piles. This graph demonstrates that both types of piles can be utilized interchangeably, highlighting their comparable functionality and effectiveness. This visual evidence supports that similar outcomes and benefits can be achieved by employing volume or embedded piles, lending flexibility and adaptability to the overall design and implementation processes.
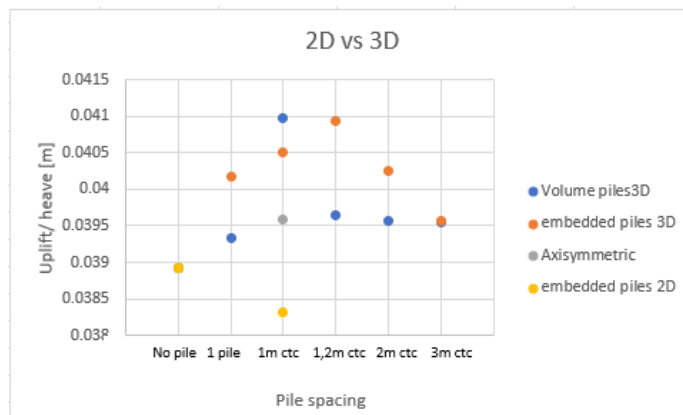
Figure 6.8: In the following figure, a cross-section at -66.41m NAP with the experienced total displacements can be seen.
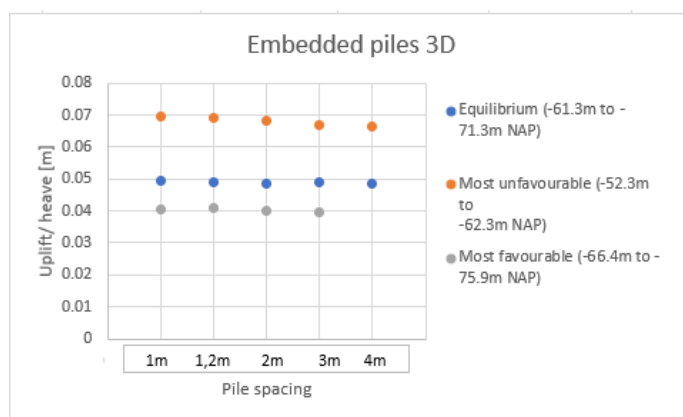
Figure 6.9: In the following figure, a cross-section at the different clay depths, where the experienced total displacements can be seen.

In the context of tension piles, the interpretation of normal and skin resistance forces is essential for understanding the behaviour and performance of the piles under tensile loading. Here's a breakdown of how these forces can be interpreted:

- **Normal Resistance Force:** The normal resistance force, also known as end-bearing or base resistance, is the resistance developed at the base of the pile due to the pile's interaction with the underlying soil or rock strata. It represents the load-carrying capacity of the pile through direct bearing on the soil or rock.

- **Skin Resistance Force:** The skin resistance force, also referred to as shaft resistance, is the resistance generated along the sides of the pile as it interacts with the surrounding soil. This resistance is predominantly a result of friction between the pile surface and the soil.

In the following figures (Figures 6.10 and 6.11), we can observe that skin resistance is crucial in tension piles as it contributes significantly to the overall load-carrying capacity of the pile. Higher skin resistance values indicate greater soil-pile interaction, resulting in increased load transfer and improved pile performance under tensile loading conditions.

As seen in the three figures in the 'hint box', the start of the clay layer, the T_{skin}, is in the same order of magnitude and negative resistances. In the least favourable case (Figure 6.11), the highest positive skin resistance is found at the top of the pile. When a positive skin resistance is observed at the top of a tension pile, it signifies the presence of an upward resistance force or uplift. This is somewhat unexpected for a tension pile, as its primary purpose is to withstand tensile loads and prevent uplift. Adhesion or cohesion between the soil and the pile surface, particularly in cohesive soils or soils with high clay content, can create positive skin resistance. Suction forces, resulting from pressure differentials between the soil pore water and the atmosphere, can also generate upward forces. Additionally, environmental factors like changes in groundwater levels or soil moisture content can induce positive skin resistance. Thus, further geotechnical investigations may be required to understand the pile´s behaviour and performance in such situations.
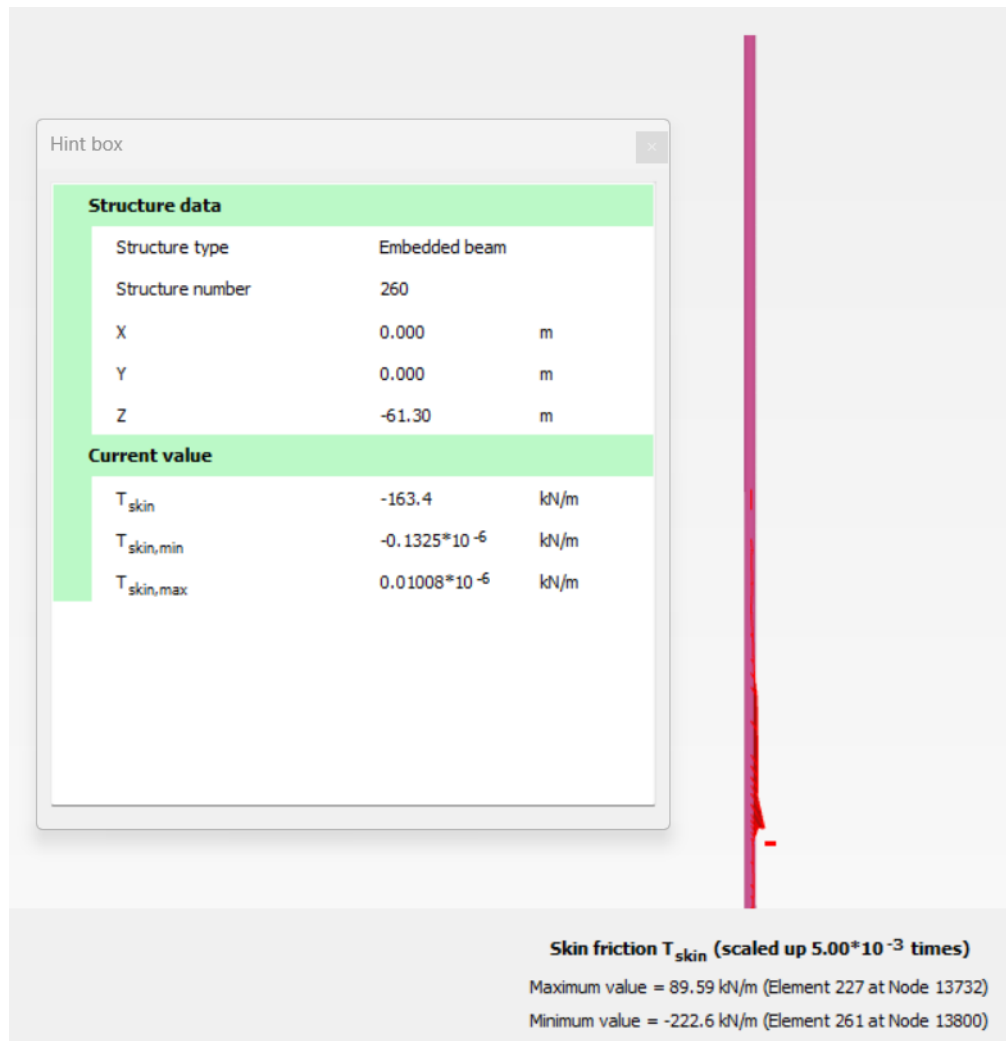
Figure 6.10: T_{skin}, at -61.3m to -71.3m NAP, 4m centre-to-centre embedded centre pile.

Structure data

Structure type	Embedded beam	
Structure number	217	
X	0.2257	m
Y	-0.2257	m
Z	-52.30	m

Current value

T_{skin}	-112.0	kN/m
$T_{skin,min}$	$-2.546*10^{-9}$	kN/m
$T_{skin,max}$	$4.982*10^{-9}$	kN/m

Skin friction T_{skin} (scaled up 0.0100 times)

Maximum value = 84.07 kN/m (Element 187 at Node 12627)

Minimum value = -153.4 kN/m (Element 217 at Node 12687)
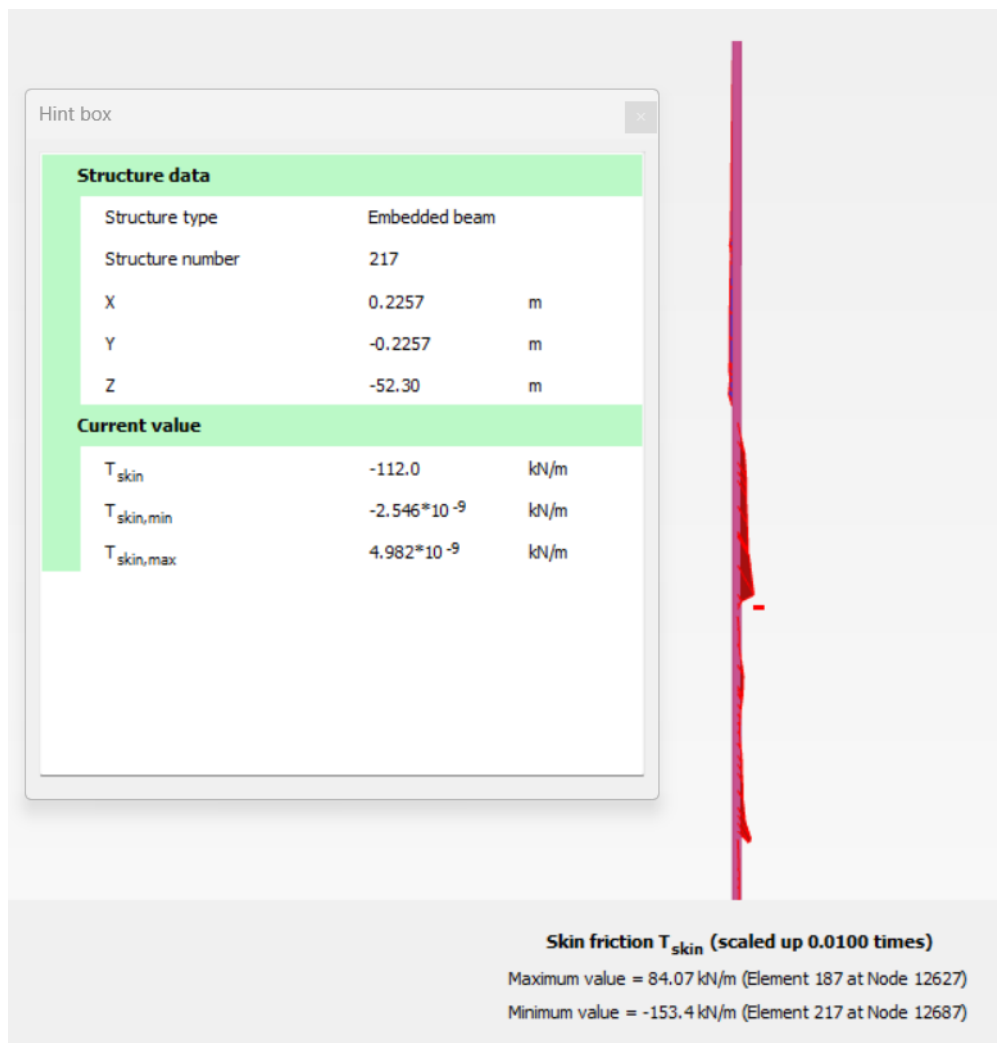
Figure 6.11: T_{skin}, at -52.3m to -62.3m NAP, 4m centre-to-centre embedded centre pile.

The magnitude of the normal resistance force (Figures 6.10 and 6.13) indicates the pile's ability to transfer tensile loads to the underlying soil or rock strata. Higher normal resistance values suggest that the pile effectively transmits tensile forces into the foundation material, ensuring stability and load-bearing capacity.

The minimal normal forces, with a negative value, suggest that there are sections along the same pile's length where the pile experiences a downward force. This negative force might be due to soil settlement, consolidation, or other mechanisms that induce a downward load on the pile. Comparing these values within the same tension pile highlights the variation in loading conditions along the pile's length.

Structure data

Structure type	Embedded beam	
Structure number	260	
X	0.000	m
Y	0.000	m
Z	-61.35	m

Current value

N	1106	kN
N_{min}	-4.996	kN
N_{max}	1135	kN

Axial forces N (scaled up 2.00*10^{-3} times)

Maximum value = 1642 kN (Element 249 at Node 13773)
Minimum value = 0.5589 kN (Element 281 at Node 13839)
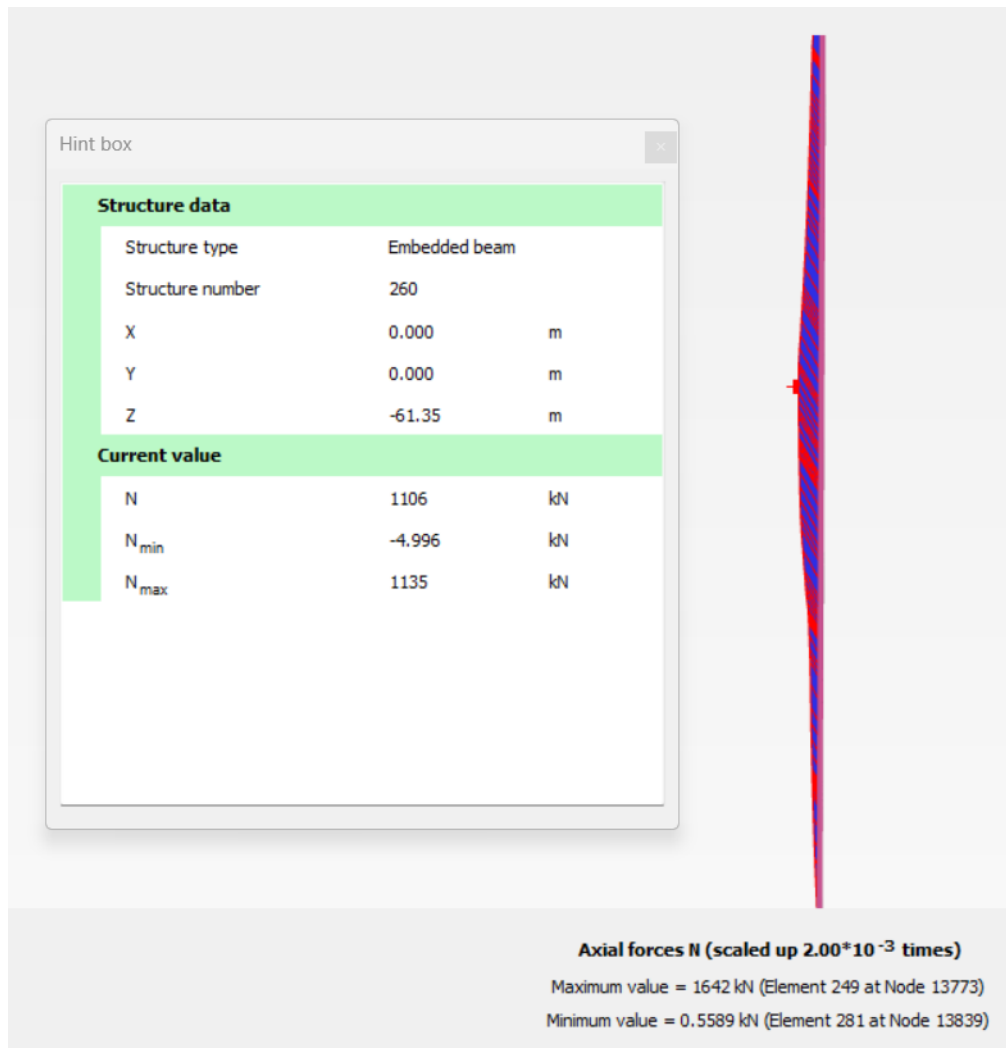
Figure 6.12: N force, at -61.3m to -71.3m NAP, 4m centre-to-centre embedded centre pile.
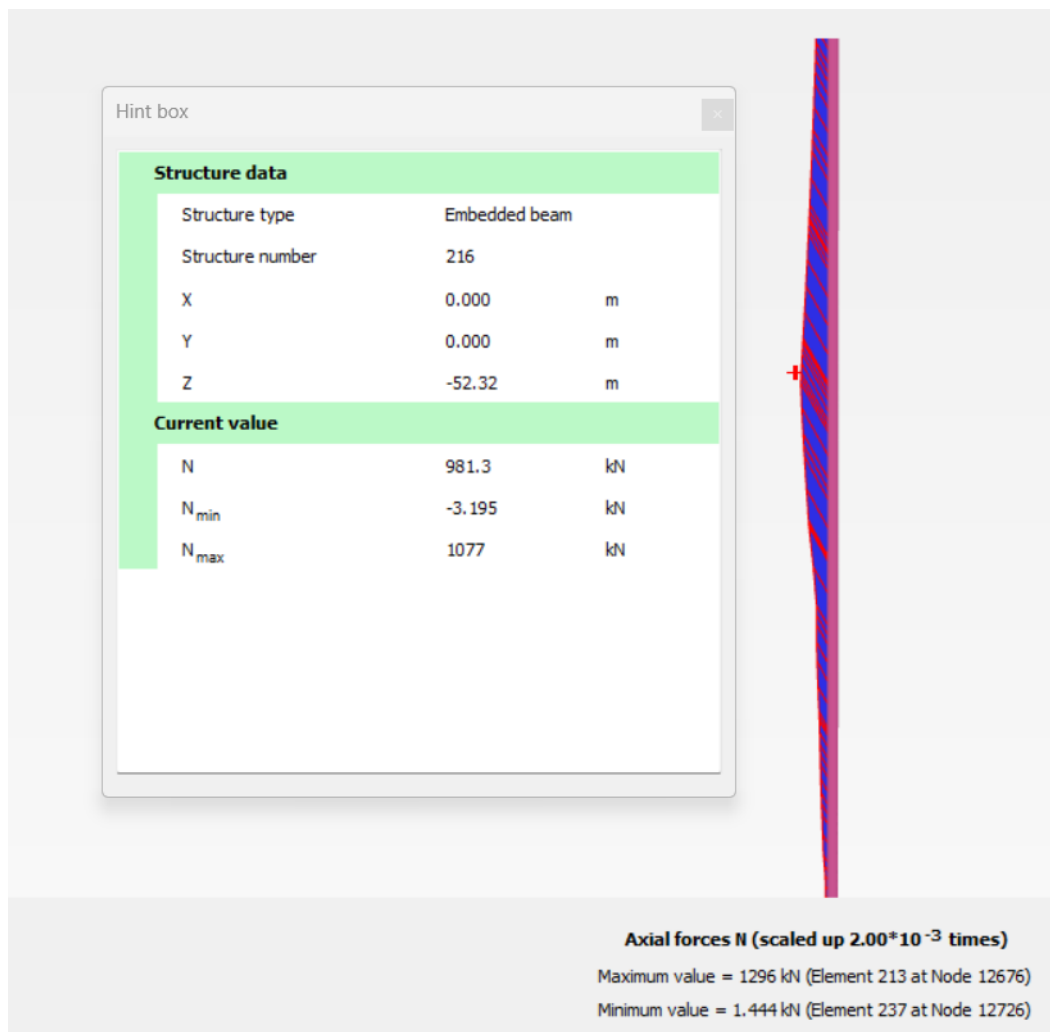
Figure 6.13: N force, at -52.3m to -62.3m NAP, 4m centre-to-centre embedded centre pile.

6.4. Results of a complete collapse

This section of the project investigates the critical point at which soil experiences complete collapse or failure. Our approach systematically increases centre-to-centre distances between embedded piles to analyze the soil's response under varying conditions. The primary focus is assessing the most unfavourable scenario, which involves investigating the clay layer within the depth range of -52.3m to -62.3m NAP while utilizing an embedded pile grid spaced at both 7 and 9m centre-to-centre.

The scenarios in Table 6.4 illustrate the correlation between increasing centre-to-centre distances and the resultant escalation in mesh deformation. Notably, these deformations reduce but do not lead to complete soil collapse. Instead, the deformations remain within a similar magnitude order as those observed with a 4m centre-to-centre distance between the embedded piles.

This intriguing observation raises critical questions about the role of tension piles in maintaining soil stability. Specifically, it prompts us to consider whether the tension piles contribute substantively to soil stability or if their weight alone is accountable for preventing soil collapse. To explore this further, additional research and investigations may be necessary.

Understanding the point of complete soil collapse is fundamental to the overall project, as it helps us establish the limits of soil stability under various conditions and contributes to informed decision-making in geotechnical engineering and construction projects.

Table 6.4: Comparison for a complete collapse

Most unfavourable (-52.3m to -62.3m NAP)				
Deformed mesh	**3m spacing [m]**	**4m spacing [m]**	**7m spacing [m]**	**9m spacing [m]**
Embedded piles 3D	0.06969	0.06897	0.06832	0.0669

6.5. Feasibility of the options

Tension piles spaced 4 meters apart effectively mitigate ground uplift. However, an issue arises: increasing the center-to-center distance does not reduce deformations substantially. As referenced in NEN9997, 2016, even a 1-centimeter deformation is deemed unacceptable; comparing it with the results, it can be seen that 6cm deformation would happen in each scenario.

Now, this approach might be suitable for a small area, but the Energy Storage Lake covers a vast space of 30 km^2. This would make the project extremely complex. Striking a balance between ensuring our structures' strength and the construction's practicality is crucial.

Taking these considerations, it becomes evident that relying solely on tension piles may not be a feasible solution for preventing the uplift of the Energy Storage Lake bed. To fulfil the goal of ensuring both technical excellence and practicality in the Energy Storage Lake, we must explore alternative strategies that strike the right balance between structural integrity and the challenges posed by actual construction.

7

Solutions for DELTA21

This chapter explores how findings from this master's thesis report can enhance DELTA 21 project. There are three main ways in which DELTA21 can benefit from these findings:

1. **Increasing the low water level:** The findings from the thesis report offer valuable insights into strategies or methods that can be employed to raise the low water level beyond the current threshold of -22.5m NAP. By understanding the soil characteristics in the area, DELTA21 can explore approaches to effectively manage the water level and potentially increase it to a higher level. This can potentially enhance energy storage capacity and improve overall water resource management.

2. **Decreasing the ESL depth:** The master's thesis report, particularly Chapter 4.4, indicates the possibility of reducing the Energy Storage Lake (ESL) depth to at least -25.6m NAP. This finding is significant for DELTA21 as it allows them to assess the feasibility and implications of decreasing the ESL depth. By considering the soil profile in detail, DELTA21 can optimize the design and operation of the Energy Storage Lake, leading to improved energy storage efficiency and other potential benefits.
   Cost Benefits: Reducing the ESL depth potentially brings economic advantages through lowered construction and maintenance costs. A shallower lake might demand less excavation and earthwork, reducing initial capital investment. Furthermore, optimizing the ESL depth based on soil characteristics can enhance energy storage efficiency. This optimization empowers DELTA21 to store and release energy, improving operational efficiency more effectively.
   Environmental Benefits: A well-considered ESL depth adjustment can minimise land disturbance, preserving natural habitats and ecosystems. This aligns with sustainable development goals and bolsters the project's environmental responsibility and reputation.

3. **Underwater concrete:** Underwater concrete presents a potential solution for reinforcing the Energy Storage Lake's foundation and raising water levels. However, its feasibility in this large-scale project should be carefully assessed due to specialized requirements and environmental considerations. Implementing underwater concrete may require comprehensive planning and evaluation.

During the master's thesis research, a new soil investigation was conducted better to understand the soil profile beneath the Energy Storage Lake. This investigation provides valuable information for DELTA21, enabling them to refine their geological and geotechnical models. By incorporating these findings, DELTA21 can make informed decisions regarding the Energy Storage Lake's design, construction, and long-term stability. Comprehensive soil investigations necessitate financial investment in equipment, personnel, and testing. Additionally, the research and analysis phase may extend the project timeline, potentially delaying the implementation of enhancements to DELTA21.

The incorporation of new soil investigation findings leads to the following:

Cost Benefits: Incorporating these findings helps avert potential design errors, such as underestimating soil stability or encountering unforeseen challenges during construction. A more accurate understanding of the soil profile streamlines engineering design and construction, thus contributing to cost savings.

Risk Reduction: Enhanced insight into the soil profile mitigates the risk of instability or subsidence, ensuring the long-term stability of the Energy Storage Lake. This risk reduction minimizes the potential for costly repairs or operational disruptions.

In summary, integrating the insights from the master's thesis report can benefit DELTA21 by potentially increasing the low water level, decreasing the ESL depth, and improving their understanding of the soil profile. These benefits can lead to enhanced water level management, increased energy storage capacity, improved energy storage efficiency, and more effective project planning and implementation. While there are associated costs with research, analysis, and implementation, the potential long-term gains in revenue, sustainability, and risk reduction outweigh the initial expenditures.

8
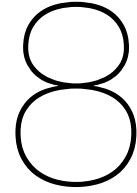
Discussion

In the course of conducting this research, several assumptions were made. To begin with, an assumption was made that the soil conditions under the ESL would resemble those in different distant locations, although these locations were more than 1500 meters away from the available data. Consequently, assuming continuity introduces a significant level of uncertainty. Another uncertainty related to this previous one is the soil parameters used for all the calculations. Again, this is assumed from far-away data locations.

Let's revisit the fundamental research questions that underpin this master's thesis. Beginning with the question: "Is there a clay layer under the Energy Storage Lake (Valmeer)?; If so, at what depth?" We currently lack definitive knowledge on this matter. The available soil data is insufficient to characterise the problem comprehensively. To facilitate progress, a substantial assumption has been employed to facilitate worst-case scenario analysis.

Transitioning to the subsequent question: "Can this clay layer and the sand layer(s) above it withstand the backpressure of the groundwater at the bottom of the clay layer? Is that resistance stable enough?; If not, what can be done to ensure safety?" This question proves to be difficult to answer, lacking a straightforward answer due to the array of assumptions made concerning the location of the clay layer. These varying assumptions yield divergent outcomes. In some scenarios, the clay layer exhibits stability under pressure, while in others, it demonstrates uplift values. The complexity arises from the inherent uncertainties associated with geotechnical analyses and soil behaviour. Factors such as soil composition, groundwater levels, and loading conditions can all influence the response of the clay layer.

Finally, we address the following question: "If the stability of the clay layer is not ensured, can tension piles be used to prevent uplift instability of the clay layer?" This study explores the potential of stress distribution facilitated by tension piles without a concrete floor. From the findings acquired with this research, the tension piles modelled exhibit substantial potential to enhance soil stability. However, the extent to which they effectively transfer stresses between one another, instead of merely supporting the structural load, remains unanswered.

Certain limitations are inherent in this study. For instance, while attempting to simulate a complete soil model collapse, there was an observed decrease in heave. However, an actual collapse of the soil model did not occur. This suggests that an uplift issue might not be prevalent in this location, at least not based on the available soil data. Another limitation is using one unique size of tension piles; not varying the diameter, length, and shape reduced the outcomes. The main limitation for micropiles is that as micropiles get longer, their load-carrying capacity will decrease. This is because longer micropiles may encounter greater frictional resistance along their length, reducing their capacity to support heavy loads.

<div style="text-align: right; font-size: 3em;">9</div>

Conclusions and recommendations

9.1. Conclusions

The conclusions drawn from the analysis using the Finite Element Method (FEM) in the context of the Energy Storage Lake (ESL) bed are crucial for understanding its stability and potential challenges. Here's an elaboration on the findings and their significance:

1. Embedded Piles for Stability: During the investigation of the main research question, two models were investigated. Embedded piles or volume piles. The results gained from that analysis were that the volume piles had the same order of magnitude as the embedded piles, being, for example, 0.03957m and 0.04026m, respectively, when the centre-to-centre distance is 2m. The analysis underscores embedded piles as a pragmatic approach to balancing accuracy and computational efficiency in ESL bed stability assessments and is thus used for the main analysis. While it may not replicate real-world scenarios perfectly, it offers valuable insights into how structures respond within such soil environments.

2. Sensitivity to Clay Layer Depth: The investigation examines the sensitivity of the ESL bed to varying clay layer depths using embedded piles with different centre-to-centre distances. It is clear that when the clay layer is located more superficial, the pressure needed to contrast the backpressure is higher than the one needed for a deeper clay layer. Maintaining a constant centre-to-centre distance of 4 meters consistently yields positive outcomes. While these findings may not offer a definitive solution, they do contribute to a reduction in soil displacements at that specific location.

3. Interchangeability of Piles: The study explores the interchangeability of volume and embedded piles, highlighting their comparable functionality and effectiveness. The analysis shows the behaviour and performance of central piles within the ESL, providing insights into dynamic forces and environmental factors affecting pile movement. Particularly, it emphasizes the significance of skin resistance in tension piles under tensile loading conditions.

4. Collapse Investigation: The research section dedicated to a complete collapse investigation reveals an inverse correlation between increasing centre-to-centre distances and de-escalating mesh deformations. However, it's observed that the deformations remain within a similar magnitude order as those with the 4m spacing. Even tho the surface deformations at the bottom of the ESL increase when the centre-to-centre distances increase. This suggests that the contribution of tension piles to soil stability may be more related to their weight than their spacing, though further research is needed to explore this phenomenon.

5. Optimal Spacing for Uplift Mitigation: The research concludes that an optimal centre-to-centre spacing of 4m effectively combats uplift in the ESL bed. Nonetheless, it is important to note that the research falls short of meeting the minimum acceptable requirement of 1 centimetre (according to the NEN9997, 2016) for deformations, as the deformations recorded during this study exceed 6 centimetres.

6. Complex Interplay of Soil Layers: The presence of the clay layer in this specific location gives rise to an impermeable layer that, when subjected to backpressure, could experience uplift if an insufficient pressure gradient exists above the clay layer. This phenomenon highlights the intricate interplay between soil layers and their response to varying pressures. The presence and depth of the impermeable clay layer directly impact the feasibility of the ESL project. Deeper clay layers (-66.4m to -75.9m NAP project specific) may offer advantages in terms of increased energy storage capacity, potentially making the project more economically viable. Deeper clay layers allow for the excavation of a deeper ESL bed, potentially increasing the project's energy storage capacity. Conversely, shallower clay layers (-52.3m to -62.3m NAP for this project) may limit the depth of the ESL and, consequently, its capacity. Illustrating this point is the maximum depth at which the ESL for this project would achieve equilibrium, measured at -25.7 meters NAP.

The failure mode that will dictate the 4m centre-to-centre is that when micropiles are installed closely together, the soil between them can experience displacement and redistribution as the micropiles settle under the influence of loads. This displacement can have a direct impact on the load-bearing capacity of each micropile within the group. Furthermore, the interaction between adjacent micropiles can result in uneven distribution of tension load among them, with one micropile potentially bearing more load while another carries less. This interaction effect becomes particularly pronounced when micropiles are closely spaced. All in all, the spacing between micropiles influences the overall stiffness of the micropile group, affecting settlement behaviour.

In conclusion, these findings provide critical insights into the stability and behaviour of the ESL bed. They offer valuable information for engineering decisions, emphasizing the importance of maintaining optimal spacing, considering the interchangeability of pile types, and recognizing the complex interplay between soil layers.

9.2. Recommendations

Further soil investigation is required to understand better the exact location of the impermeable layer within the ESL. Specifically, additional boreholes and Cone Penetration Tests (CPTs) should be conducted in the middle of the ESL. Furthermore, remote sensing techniques can assess the layer's continuity and verify the clay layer's positioning.

These investigations would provide valuable insights into the nature of the impermeable layer, allowing for a determination of whether it comprises a clay or water-resistant layer. However, it is important to note that these measures are beyond the scope of the current graduation project and will not be further explored or implemented in this study.

The presence of a clay layer in a specific location introduces an impermeable barrier that, when subjected to backpressure, may experience uplift if the pressure above the clay layer is insufficient. Therefore, it is essential to investigate various sea level water depths, as they directly influence the backpressure exerted beneath the clay layer.

While this project has given insight into the significance of the impermeable layer and its implications for the ESL performance, further research and field investigations are necessary to gather a more comprehensive understanding of the site conditions and behaviour of the impermeable layer.

References

Ansorena Ruiz, R. (2020). *Conceptual design of the valmeer's pump storage station of the delta21 plan* (Master's thesis). Technische Universiteit Delft.

Arias, P., Bellouin, N., Coppola, E., Jones, R., Krinner, G., Marotzke, J., Naik, V., Palmer, M., Plattner, G.-K., Rogelj, J., et al. (2021). Climate change 2021: The physical science basis. contribution of working group i to the sixth assessment report of the intergovernmental panel on climate change; technical summary.

CUR2001-4. (2011). *Ontwerpregels voor trekpalen*. Stichiting CUR.

European Commission and European Environment Agency. (2021). *The european climate adaptation platform climate-adapt*. Retrieved August 19, 2023, from https://climate-adapt.eea.europa.eu/en/countries-regions/countries/netherlands

Goel, S., & Patra, N. R. (2007). Prediction of load displacement response of single piles under uplift load. *Geotechnical and Geological Engineering*, *25*(1), 57.

Heibaum, M., & Herten, M. (2009). Geotechnical verifications using the finite-element method? *Bautechnik*, *86*(S1), 7–15.

Lavooij, H., Berle, L., Tonneijck, H., M.and De Boer, & Vrijling, H. (2018). Delta21 deelrapport waterveiligheid.

Meehl, G. A., Zwiers, F., Evans, J., Knutson, T., Mearns, L., & Whetton, P. (2000). Trends in extreme weather and climate events: Issues related to modeling extremes in projections of future climate change. *Bulletin of the American Meteorological Society*, *81*(3), 427–436.

NEN9997. (2016). *Geotechnical design of structures - part 1: General rules*. Royal Netherlands Standardization Institute.

report 236, C. (2017). *Micro piles*. Stichiting CUR.

Rijkswaterstaat. (2013a). *Delta works*. Retrieved June 6, 2021, from https://www.rijkswaterstaat.nl/en/water/water-safety/delta-works

Rijkswaterstaat. (2013b). *Maeslant barrier*. Retrieved June 6, 2021, from https://www.rijkswaterstaat.nl/en/about-us/gems-of-rijkswaterstaat/maeslant-barrier

Robertson, P. K., Campanella, R. G., Gillespie, D., & Greig, J. (updated by Robertson, 2010). Use of piezometer cone data. *Use of in situ tests in geotechnical engineering*, 1263 to 1280.

van Adrichem, S. (2021). *Influence of rapid drawdown on dike stability* (Master's thesis). Technische Universiteit Delft.

Versteeg, S. (2023). A design of the delta21 sea defence using the adaptive pathway approach.

Zegwaard, A., & Wester, P. (2014). Inside matters of facts: Re-opening dams and debates in the netherlands. *Water Alternatives*, *7*(3).

A
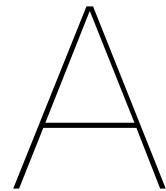
Soil investigation data

This appendix contains the Cone Penetration Tests (CPTs) employed to determine the relevant soil parameters for the Energy Storage Lake (ESL) site.

A.1. S36H0003300 soil data
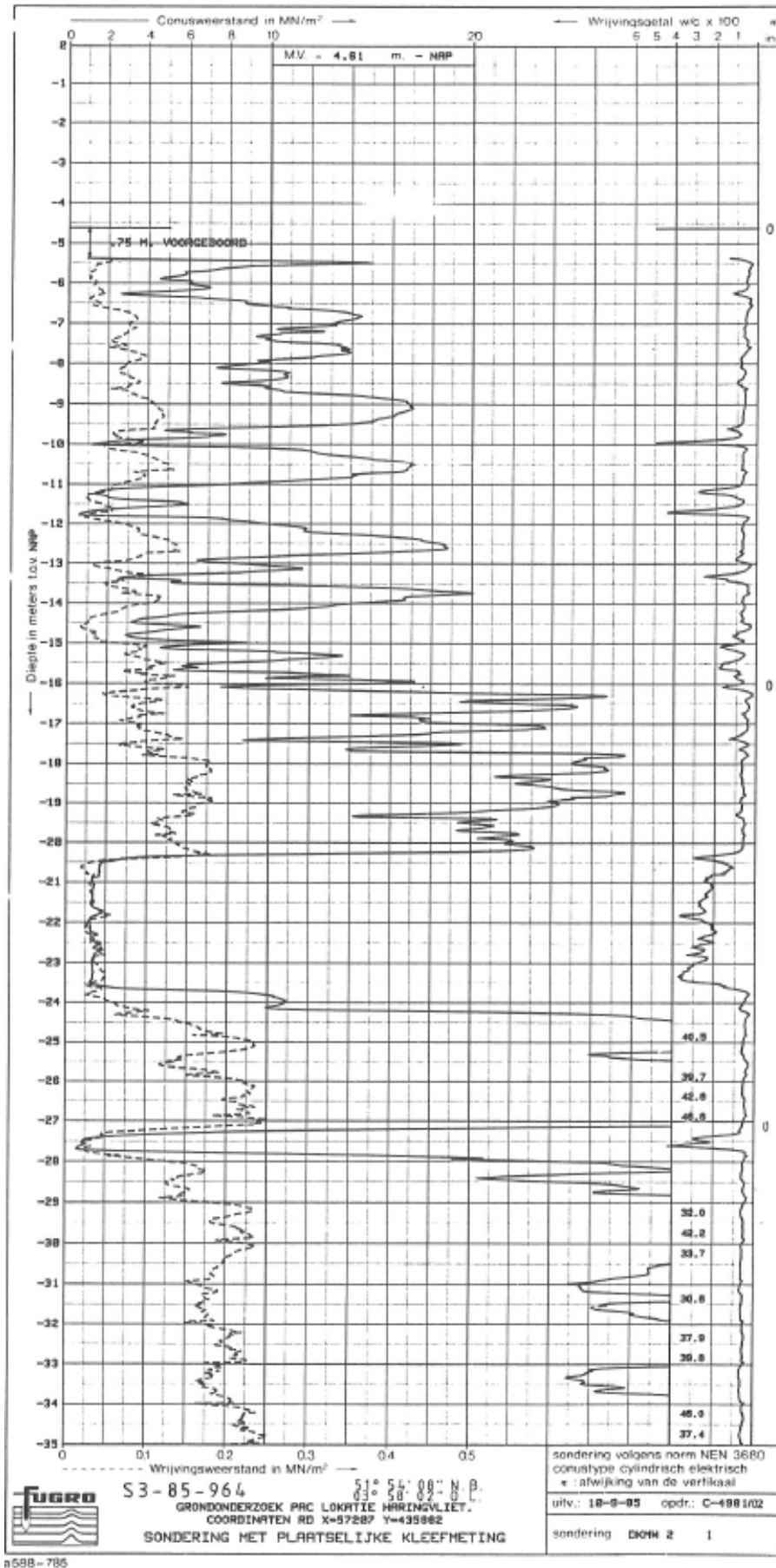
Figure A.1: S36H0003300 data (Source: DINOloket)
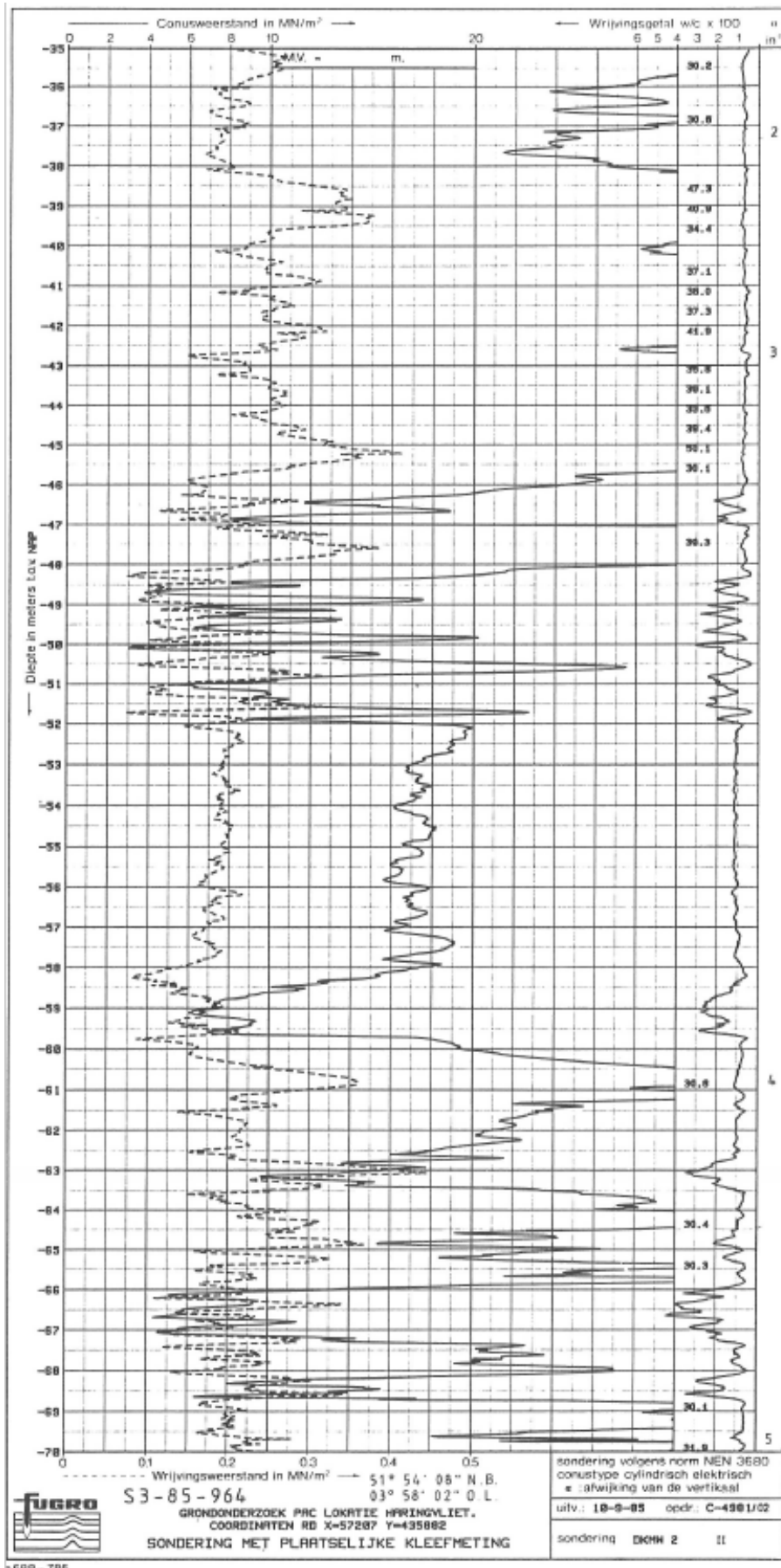
Figure A.2: S36H0003300 data (Source: DINOloket)

B

FEM parameters

B.1. Parameters used for the Clay layer:

Figure B.1: Soil parameters used in PLAXIS for the CLAY layer.

B.2. Parameters used for the Sand layer:

General Mechanical Groundwater Thermal Interfaces Initial

Property	Unit	Value
Material set		
Identification		Sand_19
Soil model		Hardening Soil ▼
Drainage type		Drained ▼
Colour		RGB 232, 226, 161
Comments		
Unit weights		
γ_{unsat}	kN/m³	18.00
γ_{sat}	kN/m³	19.00
Void ratio		
e_{init}		0.5000
n_{init}		0.3333
Rayleigh damping		
Input method		Direct ▼
Rayleigh α		0.000
Rayleigh β		0.000

General Mechanical **Groundwater** Thermal Interfaces Initial

Property	Unit	Value
Model		
Classification type		Standard ⌄
Soil class (Standard)		Medium ▼
Soil		
< 2 µm	%	19.00
2 µm - 50 µm	%	41.00
50 µm – 2 mm	%	40.00
Flow parameters		
Permeabilities		
Use defaults		☐
k_x	m/day	0.01673
k_y	m/day	0.01673
Void ratio dependency		☑
c_k		1000E12
Porosity		
n_{init}		0.3333
Unsaturated zone		
$-\psi_{unsat}$	m	10.00E3

General **Mechanical** Groundwater Thermal Interfaces Initial

Property	Unit	Value
Stiffness		
E_{50}^{ref}	kN/m²	40.00E3
E_{oed}^{ref}	kN/m²	40.00E3
E_{ur}^{ref}	kN/m²	160.0E3
v_{ur}		0.3000
Alternatives		
Use alternatives		☐
C_c		8.635E-3
C_s		3.466E-3
e_{init}		0.5000
Stress-dependency		
power (m)		0.5000
P_{ref}	kN/m²	100.0
Strength		
Shear		
c'_{ref}	kN/m²	1.000
φ' (phi)	°	32.50
ψ (psi)	°	2.500
Depth-dependency		
c'_{inc}	kN/m²/m	0.000
y_{ref}	m	0.000
Dilatancy cutoff		
Dilatancy-cutoff		☐
e_{min}		1.000E-9
e_{max}		999.0
Tension		
Tension cut-off		☐
Miscellaneous		
Use defaults		☐
K_0^{nc}		0.4627
R_f		0.9000
Excess pore pressure calcula		
Determination		v-undrained definition ▼
v_u definition method		Direct ▼
$v_{u,equivalent}$ (nu)		0.4950
Skempton B		0.9783
$K_{w,ref}/n$	kN/m²	6.000E6

Figure B.2: Soil parameters used in PLAXIS for the SAND layer.

B.3. Structure parameters used in PLAXIS 2D

B.3.1. Structure parameters used for embedded beams

Figure B.3: General parameters for embedded beams in PLAXIS 2D.

Figure B.4: Mechanical parameters for embedded beams in PLAXIS 2D.

B.4. Structure parameters used in PLAXIS 3D
B.4.1. Structure parameters used for embedded beams

Figure B.5: General parameters for embedded beams in PLAXIS 3D.

Figure B.6: Mechanical parameters for embedded beams in PLAXIS 3D.

B.4.2. Structure parameters used for volume piles

The structural parameters applied to the volume piles were configured to mirror those of the adjacent volume piles. These volume piles shared the same diameter as the embedded piles and featured interfaces along their shafts. In figure B.7 the volume piles configuration is shown.
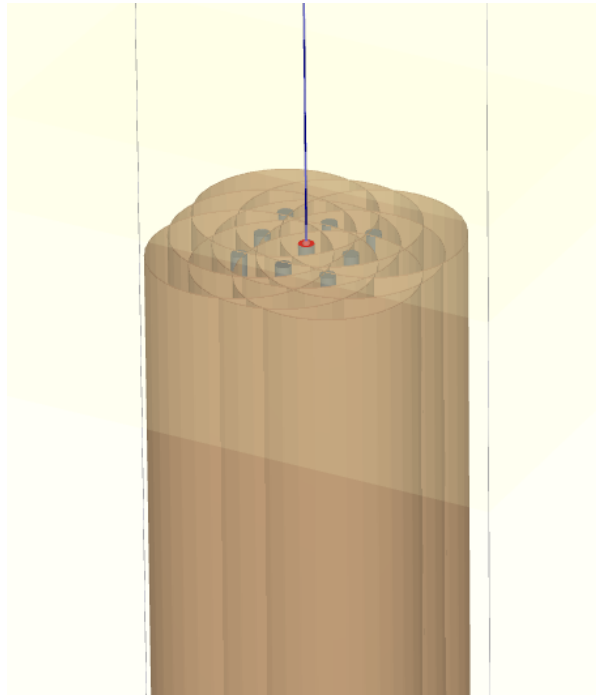
Figure B.7: Volume piles in PLAXIS 3D layout.

C
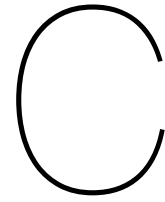
Tension piles investigation

Table C.1: center-to-center distance 1 m summary calculation.

R_t;shaft;d	R_t;kluid;d	G_paal;d	F_r;t;d	ppn(paal punt niveau)	shaft/kluid
[kN]	[kN]	[kN]	[kN]	[m NAP]	
0,0	0	0	0	-5,5	n/a
0,0	0	0	0	-6	n/a
0,0	0	0	0	-6,5	n/a
0,0	0	0	0	-7	n/a
0,0	0	0	0	-7,5	n/a
0,0	0	0	0	-8	n/a
0,0	0	0	0	-8,5	n/a
0,0	0	0	0	-9	n/a
0,0	0	0	0	-9,5	n/a
0,0	0	0	0	-10	n/a
0,0	0	0	0	-10,5	n/a
0,0	0	0	0	-11	n/a
0,0	0	0	0	-11,5	n/a
0,0	0	0	0	-12	n/a
0,0	0	0	0	-12,5	n/a
0,0	0	0	0	-13	n/a
0,0	0	0	0	-13,5	n/a
0,0	0	0	0	-14	n/a
0,0	0	0	0	-14,5	n/a
0,0	0	0	0	-15	n/a
0,0	0	0	0	-15,5	n/a
0,0	0	0	0	-16	n/a
0,0	0	0	0	-16,5	n/a
0,0	0	0	0	-17	n/a
0,0	0	0	0	-17,5	n/a
0,0	0	0	0	-18	n/a
0,0	0	0	0	-18,5	n/a
0,0	0	0	0	-19	n/a
0,0	0	0	0	-19,5	n/a
0,0	0	0	0	-20	n/a
0,0	0	0	0	-20,5	n/a
0,0	0	0	0	-21	n/a
0,0	0	0	0	-21,5	n/a

Table C.1 continued from previous page

R_t;shaft;d	R_t;kluid;d	G_paal;d	F_r;t;d	ppn (paal punt niveau)	shaft/kluid
0,0	0	0	0	-22	n/a
0,0	0	0	0	-22,5	n/a
0,0	0	0	0	-23	n/a
0,0	0	0	0	-23,5	n/a
0,0	0	0	0	-24	n/a
0,0	0	0	0	-24,5	n/a
0,0	0	0	0	-25	n/a
0,0	0	0	0	-25,5	n/a
0,0	0	0	0	-26	n/a
0,0	0	0	0	-26,5	n/a
0,0	0	0	0	-27	n/a
0,0	0	0	0	-27,5	n/a
0,0	1	1	1	-28	n/a
0,0	5	2	2	-28,5	n/a
0,0	9	3	3	-29	n/a
0,0	13	4	4	-29,5	n/a
0,0	17	5	5	-30	n/a
0,0	21	5	5	-30,5	n/a
0,0	25	6	6	-31	n/a
0,0	29	7	7	-31,5	n/a
0,0	33	8	8	-32	n/a
0,0	37	9	9	-32,5	n/a
0,0	41	10	10	-33	n/a
0,0	45	11	11	-33,5	n/a
0,0	49	12	12	-34	n/a
0,0	53	13	13	-34,5	n/a
0,0	56	14	14	-35	n/a
0,0	60	15	15	-35,5	n/a
0,0	64	16	16	-36	n/a
0,0	68	16	16	-36,5	n/a
0,0	72	17	17	-37	n/a
0,0	76	18	18	-37,5	n/a
0,0	80	19	19	-38	n/a
0,0	84	20	20	-38,5	n/a
0,0	88	21	21	-39	n/a
0,0	92	22	22	-39,5	n/a
0,0	96	23	23	-40	n/a
0,0	100	24	24	-40,5	n/a
0,0	104	25	25	-41	n/a
0,0	108	26	26	-41,5	n/a
0,0	112	27	27	-42	n/a
0,0	116	27	27	-42,5	n/a
0,0	120	28	28	-43	n/a
0,0	124	29	29	-43,5	n/a
0,0	128	30	30	-44	n/a
0,0	132	31	31	-44,5	n/a
0,0	136	32	32	-45	n/a
0,0	140	33	33	-45,5	n/a
0,0	144	34	34	-46	n/a
0,0	148	35	35	**-46,5**	n/a
0,0	151	36	36	**-47**	n/a
0,0	155	37	37	**-47,5**	n/a

Table C.1 continued from previous page

R_t;shaft;d	R_t;kluid;d	G_paal;d	F_r;t;d	ppn (paal punt niveau)	shaft/kluid
0,0	159	38	**38**	**-48**	n/a
0,0	162	38	**38**	**-48,5**	n/a
0,0	166	39	**39**	**-49**	n/a
0,0	169	40	**40**	**-49,5**	n/a
0,0	173	41	**41**	**-50**	n/a
0,0	176	42	**42**	**-50,5**	n/a
0,0	180	43	**43**	**-51**	n/a
0,0	184	44	**44**	**-51,5**	n/a
0,0	187	45	**45**	**-52**	n/a
89,0	191	46	**135**	**-52,5**	shaft
138,7	195	47	**185**	**-53**	shaft
173,5	199	48	**221**	**-53,5**	shaft
195,7	203	49	**244**	**-54**	shaft
208,2	207	49	**256**	**-54,5**	kluid
215,0	211	50	**261**	**-55**	kluid
219,6	215	51	**266**	**-55,5**	kluid
223,7	219	52	**271**	**-56**	kluid
227,7	223	53	**276**	**-56,5**	kluid
231,7	227	54	**281**	**-57**	kluid
235,7	231	55	**286**	**-57,5**	kluid
239,6	235	56	**290**	**-58**	kluid
243,7	239	57	**295**	**-58,5**	kluid
247,7	242	58	**300**	**-59**	kluid
251,6	246	59	**305**	**-59,5**	kluid
255,6	250	60	**310**	**-60**	kluid
259,6	254	60	**315**	**-60,5**	kluid
263,5	258	61	**320**	**-61**	kluid
267,5	262	62	**325**	**-61,5**	kluid
271,5	266	63	**330**	**-62**	kluid
275,5	270	64	**334**	**-62,5**	kluid
279,4	274	65	**339**	**-63**	kluid
283,4	278	66	**344**	**-63,5**	kluid
287,4	282	67	**349**	**-64**	kluid
291,3	286	68	**354**	**-64,5**	kluid
295,3	290	69	**359**	**-65**	kluid
299,3	294	70	**364**	**-65,5**	kluid
303,2	298	71	**369**	**-66**	kluid
307,2	302	71	**374**	**-66,5**	kluid
311,2	306	72	**378**	**-67**	kluid
315,1	310	73	**383**	**-67,5**	kluid
319,1	314	74	**388**	**-68**	kluid
323,1	318	75	**393**	**-68,5**	kluid
327,0	322	76	**398**	**-69**	kluid
331,0	326	77	**403**	**-69,5**	kluid
335,0	330	78	**408**	**-70**	kluid
338,4	334	79	**413**	**-70,5**	kluid
342,0	337	80	**417**	**-71**	kluid
345,6	341	81	**422**	**-71,5**	kluid
349,1	345	82	**426**	**-72**	kluid
352,7	348	82	**431**	**-72,5**	kluid
356,3	352	83	**435**	**-73**	kluid
359,9	355	84	**440**	**-73,5**	kluid

Table C.1 continued from previous page

R_t;shaft;d	R_t;kluid;d	G_paal;d	F_r;t;d	ppn (paal punt niveau)	shaft/kluid
363,4	359	85	**444**	**-74**	kluid
367,0	362	86	**449**	**-74,5**	kluid
370,6	366	87	**453**	**-75**	kluid
374,2	370	88	**458**	**-75,5**	kluid
377,7	373	89	**462**	**-76**	kluid
381,3	377	90	**467**	**-76,5**	kluid
384,9	380	91	**471**	**-77**	kluid
388,4	384	92	**475**	**-77,5**	kluid
392,0	387	93	**480**	**-78**	kluid
395,6	391	93	**484**	**-78,5**	kluid
399,2	395	94	**489**	**-79**	kluid
402,7	398	95	**493**	**-79,5**	kluid
406,3	402	96	**498**	**-80**	kluid
409,9	405	97	**502**	**-80,5**	kluid
413,5	409	98	**507**	**-81**	kluid
417,0	412	99	**511**	**-81,5**	kluid
420,6	416	100	**516**	**-82**	kluid
424,2	420	101	**520**	**-82,5**	kluid
427,7	423	102	**525**	**-83**	kluid
431,3	427	103	**529**	**-83,5**	kluid
434,9	430	104	**534**	**-84**	kluid

Table C.2: center-to-center distance 2 m summary calculation.

R_t;d	R_t;kluid;d	G_paal;d	F_r;t;d	ppn(paal punt niveau)	shaft/kluid
[kN]	[kN]	[kN]	[kN]	[m NAP]	
0,0	0	0	**0**	**-5,5**	n/a
0,0	0	0	**0**	**-6**	n/a
0,0	0	0	**0**	**-6,5**	n/a
0,0	0	0	**0**	**-7**	n/a
0,0	0	0	**0**	**-7,5**	n/a
0,0	0	0	**0**	**-8**	n/a
0,0	0	0	**0**	**-8,5**	n/a
0,0	0	0	**0**	**-9**	n/a
0,0	0	0	**0**	**-9,5**	n/a
0,0	0	0	**0**	**-10**	n/a
0,0	0	0	**0**	**-10,5**	n/a
0,0	0	0	**0**	**-11**	n/a
0,0	0	0	**0**	**-11,5**	n/a
0,0	0	0	**0**	**-12**	n/a
0,0	0	0	**0**	**-12,5**	n/a
0,0	0	0	**0**	**-13**	n/a
0,0	0	0	**0**	**-13,5**	n/a
0,0	0	0	**0**	**-14**	n/a
0,0	0	0	**0**	**-14,5**	n/a
0,0	0	0	**0**	**-15**	n/a
0,0	0	0	**0**	**-15,5**	n/a
0,0	0	0	**0**	**-16**	n/a
0,0	0	0	**0**	**-16,5**	n/a
0,0	0	0	**0**	**-17**	n/a
0,0	0	0	**0**	**-17,5**	n/a

Table C.2 continued from previous page

R_t;d	R_t;kluid;d	G_paal;d	F_r;t;d	ppn(paal punt niveau)	shaft/kluid
0,0	0	0	**0**	**-18**	n/a
0,0	0	0	**0**	**-18,5**	n/a
0,0	0	0	**0**	**-19**	n/a
0,0	0	0	**0**	**-19,5**	n/a
0,0	0	0	**0**	**-20**	n/a
0,0	0	0	**0**	**-20,5**	n/a
0,0	0	0	**0**	**-21**	n/a
0,0	0	0	**0**	**-21,5**	n/a
0,0	0	0	**0**	**-22**	n/a
0,0	0	0	**0**	**-22,5**	n/a
0,0	0	0	**0**	**-23**	n/a
0,0	0	0	**0**	**-23,5**	n/a
0,0	0	0	**0**	**-24**	n/a
0,0	0	0	**0**	**-24,5**	n/a
0,0	0	0	**0**	**-25**	n/a
0,0	0	0	**0**	**-25,5**	n/a
0,0	0	0	**0**	**-26**	n/a
0,0	0	0	**0**	**-26,5**	n/a
0,0	0	0	**0**	**-27**	n/a
0,0	0	0	**0**	**-27,5**	n/a
0,0	14	1	**1**	**-28**	n/a
0,0	32	2	**2**	**-28,5**	n/a
0,0	50	3	**3**	**-29**	n/a
0,0	67	4	**4**	**-29,5**	n/a
0,0	85	5	**5**	**-30**	n/a
0,0	103	5	**5**	**-30,5**	n/a
0,0	120	6	**6**	**-31**	n/a
0,0	138	7	**7**	**-31,5**	n/a
0,0	155	8	**8**	**-32**	n/a
0,0	173	9	**9**	**-32,5**	n/a
0,0	191	10	**10**	**-33**	n/a
0,0	208	11	**11**	**-33,5**	n/a
0,0	226	12	**12**	**-34**	n/a
0,0	243	13	**13**	**-34,5**	n/a
0,0	261	14	**14**	**-35**	n/a
0,0	279	15	**15**	**-35,5**	n/a
0,0	296	16	**16**	**-36**	n/a
0,0	314	16	**16**	**-36,5**	n/a
0,0	331	17	**17**	**-37**	n/a
0,0	349	18	**18**	**-37,5**	n/a
0,0	367	19	**19**	**-38**	n/a
0,0	384	20	**20**	**-38,5**	n/a
0,0	402	21	**21**	**-39**	n/a
0,0	420	22	**22**	**-39,5**	n/a
0,0	437	23	**23**	**-40**	n/a
0,0	455	24	**24**	**-40,5**	n/a
0,0	472	25	**25**	**-41**	n/a
0,0	490	26	**26**	**-41,5**	n/a
0,0	508	27	**27**	**-42**	n/a
0,0	525	27	**27**	**-42,5**	n/a
0,0	543	28	**28**	**-43**	n/a
0,0	560	29	**29**	**-43,5**	n/a

Table C.2 continued from previous page

R_t;d	R_t;kluid;d	G_paal;d	F_r;t;d	ppn(paal punt niveau)	shaft/kluid
0,0	578	30	**30**	**-44**	n/a
0,0	596	31	**31**	**-44,5**	n/a
0,0	613	32	**32**	**-45**	n/a
0,0	631	33	**33**	**-45,5**	n/a
0,0	648	34	**34**	**-46**	n/a
0,0	665	35	**35**	**-46,5**	n/a
0,0	680	36	**36**	**-47**	n/a
0,0	696	37	**37**	**-47,5**	n/a
0,0	712	38	**38**	**-48**	n/a
0,0	728	38	**38**	**-48,5**	n/a
0,0	744	39	**39**	**-49**	n/a
0,0	760	40	**40**	**-49,5**	n/a
0,0	776	41	**41**	**-50**	n/a
0,0	791	42	**42**	**-50,5**	n/a
0,0	807	43	**43**	**-51**	n/a
0,0	823	44	**44**	**-51,5**	n/a
0,0	839	45	**45**	**-52**	n/a
89,0	856	46	**135**	**-52,5**	shaft
169,5	874	47	**216**	**-53**	shaft
246,2	892	48	**294**	**-53,5**	shaft
319,1	909	49	**368**	**-54**	shaft
388,6	927	49	**438**	**-54,5**	shaft
454,5	944	50	**505**	**-55**	shaft
517,2	962	51	**568**	**-55,5**	shaft
576,6	980	52	**629**	**-56**	shaft
632,9	997	53	**686**	**-56,5**	shaft
686,2	1015	54	**740**	**-57**	shaft
736,6	1032	55	**792**	**-57,5**	shaft
784,3	1050	56	**840**	**-58**	shaft
835,2	1068	57	**892**	**-58,5**	shaft
882,6	1085	58	**940**	**-59**	shaft
926,6	1103	59	**985**	**-59,5**	shaft
967,5	1120	60	**1027**	**-60**	shaft
1005,6	1138	60	**1066**	**-60,5**	shaft
1041,0	1156	61	**1102**	**-61**	shaft
1073,9	1173	62	**1136**	**-61,5**	shaft
1104,7	1191	63	**1168**	**-62**	shaft
1133,4	1208	64	**1198**	**-62,5**	shaft
1160,5	1226	65	**1226**	**-63**	shaft
1185,9	1244	66	**1252**	**-63,5**	shaft
1210,0	1261	67	**1277**	**-64**	shaft
1233,0	1279	68	**1301**	**-64,5**	shaft
1254,9	1297	69	**1324**	**-65**	shaft
1276,0	1314	70	**1346**	**-65,5**	shaft
1296,4	1332	71	**1367**	**-66**	shaft
1316,2	1349	71	**1388**	**-66,5**	shaft
1335,5	1367	72	**1408**	**-67**	shaft
1354,5	1385	73	**1428**	**-67,5**	shaft
1373,0	1402	74	**1447**	**-68**	shaft
1391,4	1420	75	**1467**	**-68,5**	shaft
1409,5	1437	76	**1486**	**-69**	shaft
1427,4	1455	77	**1504**	**-69,5**	shaft

Table C.2 continued from previous page

R_t;d	R_t;kluid;d	G_paal;d	F_r;t;d	ppn(paal punt niveau)	shaft/kluid
1445,2	1473	78	**1523**	**-70**	shaft
1462,4	1489	79	**1541**	**-70,5**	shaft
1479,2	1505	80	**1559**	**-71**	shaft
1495,9	1520	81	**1576**	**-71,5**	shaft
1512,3	1536	82	**1594**	**-72**	shaft
1528,5	1552	82	**1611**	**-72,5**	shaft
1544,6	1568	83	**1628**	**-73**	shaft
1560,6	1584	84	**1645**	**-73,5**	shaft
1576,5	1600	85	**1662**	**-74**	shaft
1592,3	1616	86	**1678**	**-74,5**	shaft
1608,1	1631	87	**1695**	**-75**	shaft
1623,8	1647	88	**1712**	**-75,5**	shaft
1639,5	1663	89	**1728**	**-76**	shaft
1655,1	1679	90	**1745**	**-76,5**	shaft
1670,8	1695	91	**1761**	**-77**	shaft
1686,4	1711	92	**1778**	**-77,5**	shaft
1702,0	1727	93	**1795**	**-78**	shaft
1717,5	1742	93	**1811**	**-78,5**	shaft
1733,1	1758	94	**1827**	**-79**	shaft
1748,7	1774	95	**1844**	**-79,5**	shaft
1764,2	1790	96	**1860**	**-80**	shaft
1779,7	1806	97	**1877**	**-80,5**	shaft
1795,3	1822	98	**1893**	**-81**	shaft
1810,8	1837	99	**1910**	**-81,5**	shaft
1826,3	1853	100	**1926**	**-82**	shaft
1841,9	1869	101	**1943**	**-82,5**	shaft
1857,4	1885	102	**1959**	**-83**	shaft
1872,9	1901	103	**1976**	**-83,5**	shaft
1888,4	1917	104	**1992**	**-84**	shaft

Table C.3: center-to-center distance 3 m summary calculation.

R_t;d	R_t;kluid;d	G_paal;d	F_r;t;d	ppn(paal punt niveau)	shaft/kluid
[kN]	[kN]	[kN]	[kN]	[m NAP]	
0,0	0	0	**0**	**-5,5**	n/a
0,0	0	0	**0**	**-6**	n/a
0,0	0	0	**0**	**-6,5**	n/a
0,0	0	0	**0**	**-7**	n/a
0,0	0	0	**0**	**-7,5**	n/a
0,0	0	0	**0**	**-8**	n/a
0,0	0	0	**0**	**-8,5**	n/a
0,0	0	0	**0**	**-9**	n/a
0,0	0	0	**0**	**-9,5**	n/a
0,0	0	0	**0**	**-10**	n/a
0,0	0	0	**0**	**-10,5**	n/a
0,0	0	0	**0**	**-11**	n/a
0,0	0	0	**0**	**-11,5**	n/a
0,0	0	0	**0**	**-12**	n/a
0,0	0	0	**0**	**-12,5**	n/a
0,0	0	0	**0**	**-13**	n/a
0,0	0	0	**0**	**-13,5**	n/a

Table C.3 continued from previous page

R_t;d	R_t;kluid;d	G_paal;d	F_r;t;d	ppn(paal punt niveau)	shaft/kluid
0,0	0	0	0	-14	n/a
0,0	0	0	0	-14,5	n/a
0,0	0	0	0	-15	n/a
0,0	0	0	0	-15,5	n/a
0,0	0	0	0	-16	n/a
0,0	0	0	0	-16,5	n/a
0,0	0	0	0	-17	n/a
0,0	0	0	0	-17,5	n/a
0,0	0	0	0	-18	n/a
0,0	0	0	0	-18,5	n/a
0,0	0	0	0	-19	n/a
0,0	0	0	0	-19,5	n/a
0,0	0	0	0	-20	n/a
0,0	0	0	0	-20,5	n/a
0,0	0	0	0	-21	n/a
0,0	0	0	0	-21,5	n/a
0,0	0	0	0	-22	n/a
0,0	0	0	0	-22,5	n/a
0,0	0	0	0	-23	n/a
0,0	0	0	0	-23,5	n/a
0,0	0	0	0	-24	n/a
0,0	0	0	0	-24,5	n/a
0,0	0	0	0	-25	n/a
0,0	0	0	0	-25,5	n/a
0,0	0	0	0	-26	n/a
0,0	0	0	0	-26,5	n/a
0,0	0	0	0	-27	n/a
0,0	0	0	0	-27,5	n/a
0,0	37	1	1	-28	n/a
0,0	78	2	2	-28,5	n/a
0,0	118	3	3	-29	n/a
0,0	158	4	4	-29,5	n/a
0,0	199	5	5	-30	n/a
0,0	239	5	5	-30,5	n/a
0,0	279	6	6	-31	n/a
0,0	320	7	7	-31,5	n/a
0,0	360	8	8	-32	n/a
0,0	400	9	9	-32,5	n/a
0,0	441	10	10	-33	n/a
0,0	481	11	11	-33,5	n/a
0,0	521	12	12	-34	n/a
0,0	562	13	13	-34,5	n/a
0,0	602	14	14	-35	n/a
0,0	642	15	15	-35,5	n/a
0,0	683	16	16	-36	n/a
0,0	723	16	16	-36,5	n/a
0,0	763	17	17	-37	n/a
0,0	804	18	18	-37,5	n/a
0,0	844	19	19	-38	n/a
0,0	884	20	20	-38,5	n/a
0,0	925	21	21	-39	n/a
0,0	965	22	22	-39,5	n/a

Table C.3 continued from previous page

R_t;d	R_t;kluid;d	G_paal;d	F_r;t;d	ppn(paal punt niveau)	shaft/kluid
0,0	1005	23	23	-40	n/a
0,0	1046	24	24	-40,5	n/a
0,0	1086	25	25	-41	n/a
0,0	1126	26	26	-41,5	n/a
0,0	1167	27	27	-42	n/a
0,0	1207	27	27	-42,5	n/a
0,0	1247	28	28	-43	n/a
0,0	1288	29	29	-43,5	n/a
0,0	1328	30	30	-44	n/a
0,0	1368	31	31	-44,5	n/a
0,0	1409	32	32	-45	n/a
0,0	1449	33	33	-45,5	n/a
0,0	1489	34	34	-46	n/a
0,0	1526	35	35	-46,5	n/a
0,0	1562	36	36	-47	n/a
0,0	1599	37	37	-47,5	n/a
0,0	1635	38	38	-48	n/a
0,0	1671	38	38	-48,5	n/a
0,0	1707	39	39	-49	n/a
0,0	1744	40	40	-49,5	n/a
0,0	1780	41	41	-50	n/a
0,0	1816	42	42	-50,5	n/a
0,0	1853	43	43	-51	n/a
0,0	1889	44	44	-51,5	n/a
0,0	1925	45	45	-52	n/a
89,0	1965	46	135	-52,5	shaft
174,6	2006	47	221	-53	shaft
258,6	2046	48	306	-53,5	shaft
341,2	2086	49	390	-54	shaft
422,5	2127	49	472	-54,5	shaft
502,4	2167	50	553	-55	shaft
581,0	2207	51	632	-55,5	shaft
658,3	2248	52	711	-56	shaft
734,4	2288	53	788	-56,5	shaft
809,2	2328	54	863	-57	shaft
882,9	2369	55	938	-57,5	shaft
955,5	2409	56	1011	-58	shaft
1036,8	2449	57	1094	-58,5	shaft
1116,5	2490	58	1174	-59	shaft
1194,4	2530	59	1253	-59,5	shaft
1270,7	2570	60	1330	-60	shaft
1345,4	2611	60	1406	-60,5	shaft
1418,6	2651	61	1480	-61	shaft
1490,4	2691	62	1553	-61,5	shaft
1560,7	2732	63	1624	-62	shaft
1629,7	2772	64	1694	-62,5	shaft
1697,4	2812	65	1763	-63	shaft
1763,9	2853	66	1830	-63,5	shaft
1829,2	2893	67	1896	-64	shaft
1893,3	2933	68	1961	-64,5	shaft
1956,2	2974	69	2025	-65	shaft
2018,2	3014	70	2088	-65,5	shaft

Table C.3 continued from previous page

R_t;d	R_t;kluid;d	G_paal;d	F_r;t;d	ppn(paal punt niveau)	shaft/kluid
2079,1	3054	71	**2150**	**-66**	shaft
2139,0	3095	71	**2210**	**-66,5**	shaft
2197,9	3135	72	**2270**	**-67**	shaft
2256,0	3176	73	**2329**	**-67,5**	shaft
2313,1	3216	74	**2387**	**-68**	shaft
2369,5	3256	75	**2445**	**-68,5**	shaft
2425,0	3297	76	**2501**	**-69**	shaft
2479,7	3337	77	**2557**	**-69,5**	shaft
2533,7	3377	78	**2612**	**-70**	shaft
2586,8	3414	79	**2666**	**-70,5**	shaft
2639,2	3450	80	**2719**	**-71**	shaft
2690,8	3486	81	**2771**	**-71,5**	shaft
2741,7	3523	82	**2823**	**-72**	shaft
2791,9	3559	82	**2874**	**-72,5**	shaft
2841,4	3595	83	**2925**	**-73**	shaft
2890,2	3632	84	**2975**	**-73,5**	shaft
2938,5	3668	85	**3024**	**-74**	shaft
2986,1	3704	86	**3072**	**-74,5**	shaft
3033,2	3741	87	**3120**	**-75**	shaft
3079,7	3777	88	**3168**	**-75,5**	shaft
3125,7	3813	89	**3215**	**-76**	shaft
3171,2	3849	90	**3261**	**-76,5**	shaft
3216,2	3886	91	**3307**	**-77**	shaft
3260,7	3922	92	**3352**	**-77,5**	shaft
3304,8	3958	93	**3397**	**-78**	shaft
3348,4	3995	93	**3442**	**-78,5**	shaft
3391,6	4031	94	**3486**	**-79**	shaft
3434,4	4067	95	**3530**	**-79,5**	shaft
3476,8	4104	96	**3573**	**-80**	shaft
3518,8	4140	97	**3616**	**-80,5**	shaft
3560,5	4176	98	**3659**	**-81**	shaft
3601,9	4212	99	**3701**	**-81,5**	shaft
3642,9	4249	100	**3743**	**-82**	shaft
3683,6	4285	101	**3784**	**-82,5**	shaft
3724,0	4321	102	**3826**	**-83**	shaft
3764,1	4358	103	**3867**	**-83,5**	shaft
3803,9	4394	104	**3907**	**-84**	shaft

D
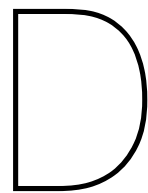
Preliminary PLAXIS model

D.1. No pile

Axisymmetric (2D model):
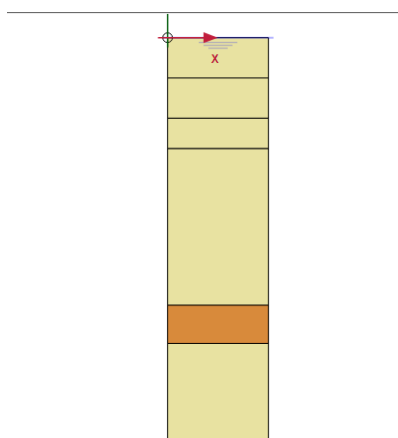
Figure D.1: In the following figure, it can be seen the default soil model used in PLAXIS 2D. Yellow being Sand and brown being Clay.
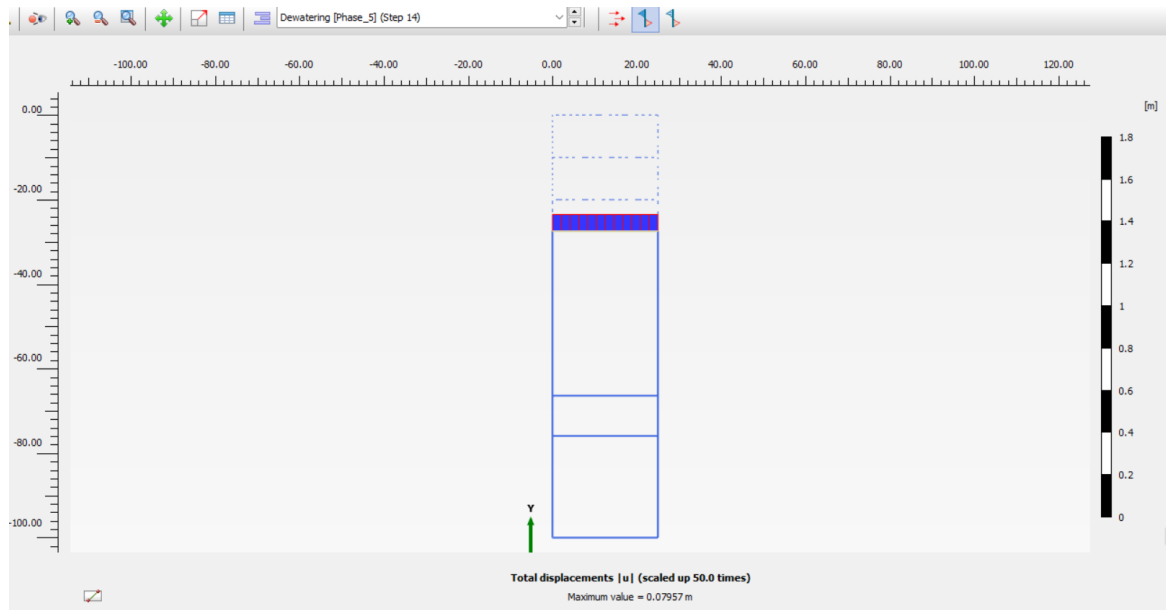
Figure D.2: In the following figure, it can be seen a cross-section at -27.51m NAP with the experienced total displacements. For the soil with no pile.

3D model:
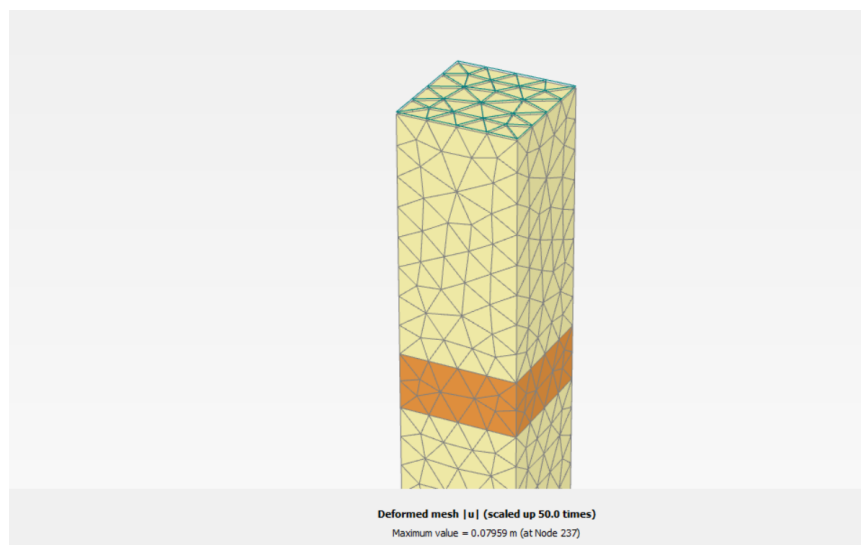
Figure D.3: In the following figure, it can be seen a cross-section at -27.51m NAP with the experienced total displacements. For the soil with no pile.

D.2. Single pile

Axisymmetric (2D model):
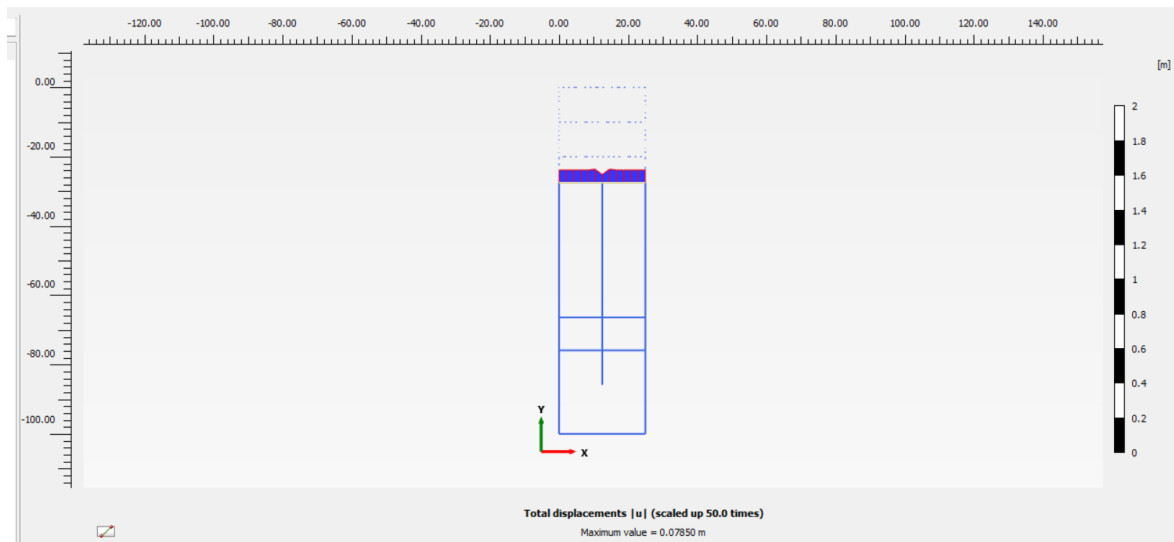
Figure D.4: In the following figure, it can be seen a cross-section at -27.51m NAP with the experienced total displacements. With one pile modelled.

Volume pile (3D model):
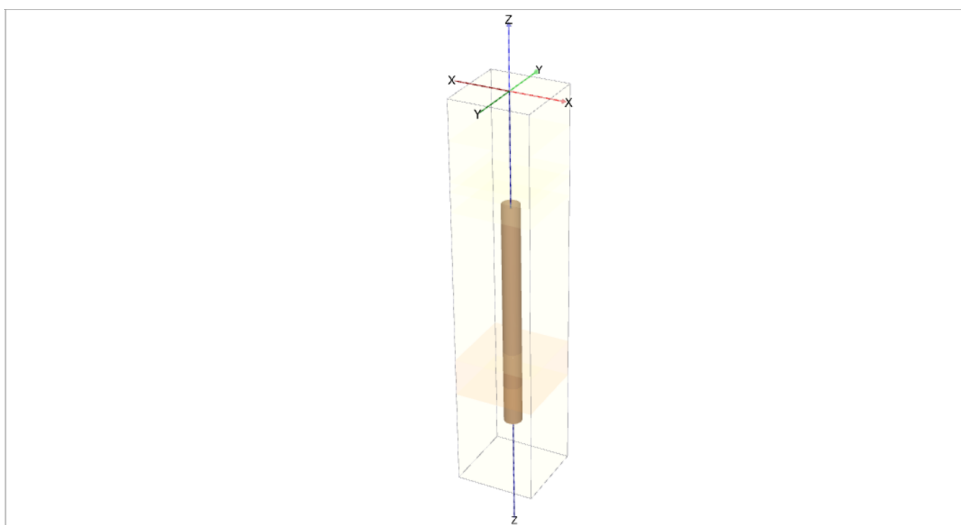
Figure D.5: In the following figure, the default soil model used in PLAXIS 3D can be seen. Yellow being Sand and brown being Clay.
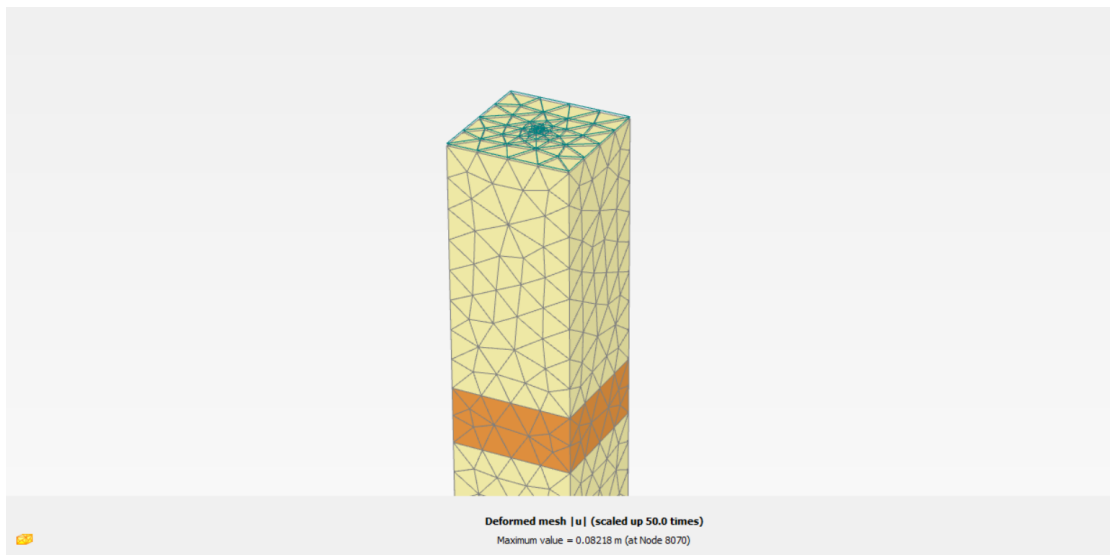
Figure D.6: In the following figure, a cross-section at -27.51m NAP with the experienced total displacements can be seen. With one volume pile modelled.

Embedded pile (3D model):
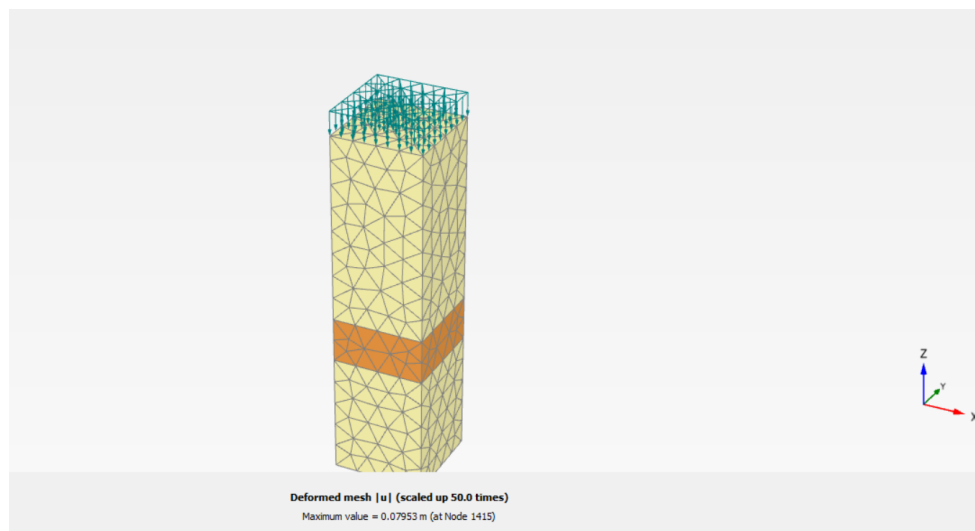
Figure D.7: In the following figure, a cross-section at -27.51m NAP with the experienced total displacements can be seen. With one embedded pile modelled.

D.3. 3 by 3 grid of piles

D.3.1. For 1m centre-to-centre (spacing is 2.5 times the diameter)

Volume pile (3D model):

Deformed mesh |u| (scaled up 50.0 times)
Maximum value = 0.08075 m (at Node 59263)
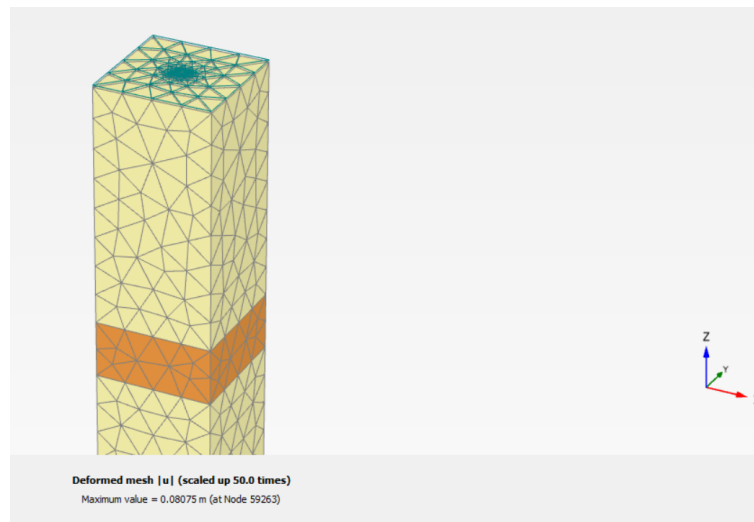
Figure D.8: In the following figure, a cross-section at -27.51m NAP with the experienced total displacements can be seen. With a 1m centre-to-centre volume pile grid modelled.

Embedded pile (3D model):

Deformed mesh |u| (scaled up 50.0 times)
Maximum value = 0.07582 m (at Node 345)
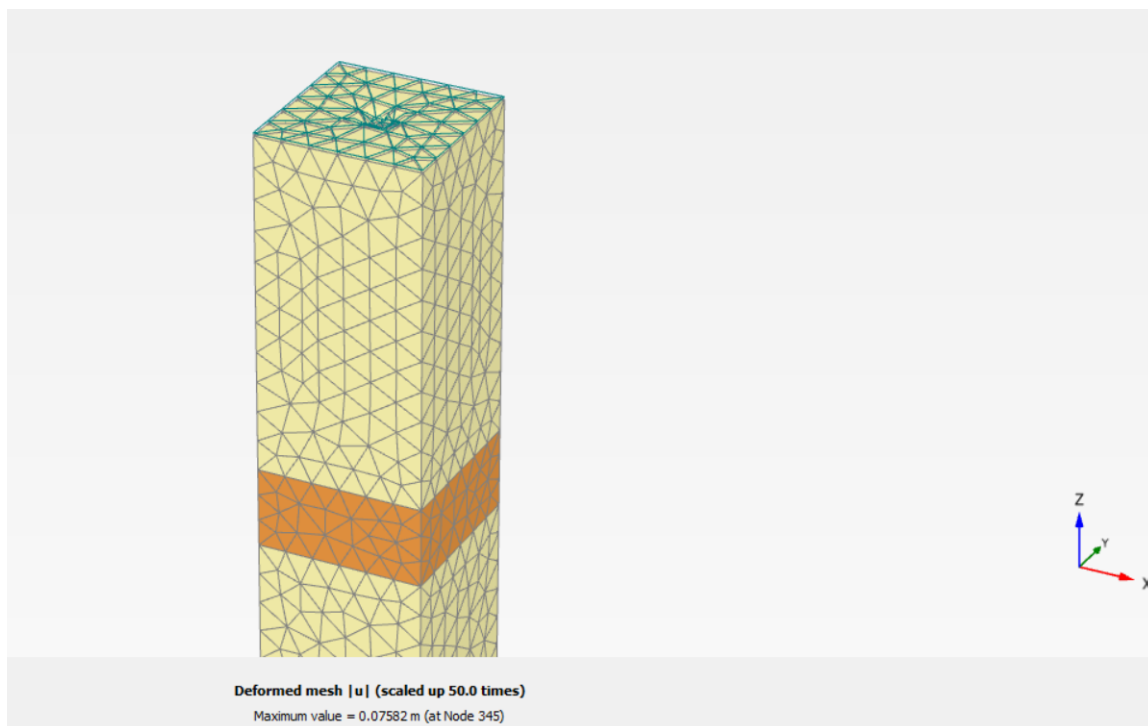
Figure D.9: In the following figure, a cross-section at -27.51m NAP with the experienced total displacements can be seen. With a 1m centre-to-centre embedded pile grid modelled.

D.3.2. For 1.2m centre-to-centre (spacing is three times the diameter)

Volume pile (3D model):
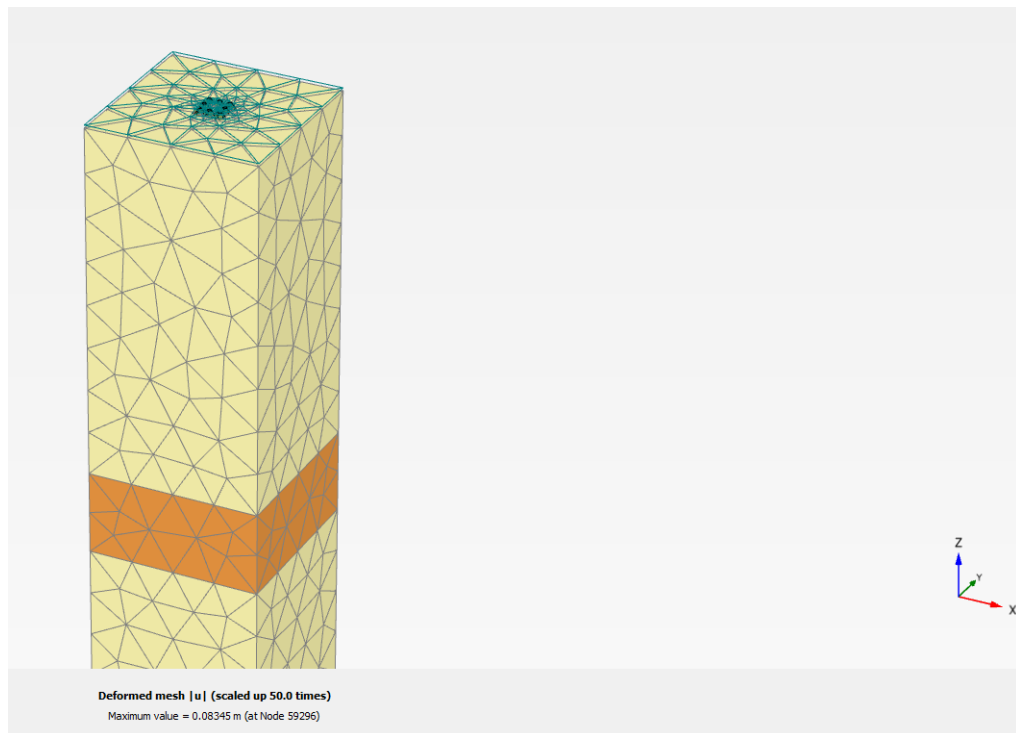
Figure D.10: In the following figure, a cross-section at -27.51m NAP with the experienced total displacements can be seen. With a 1,2m centre-to-centre volume pile grid modelled.

Embedded pile (3D model):
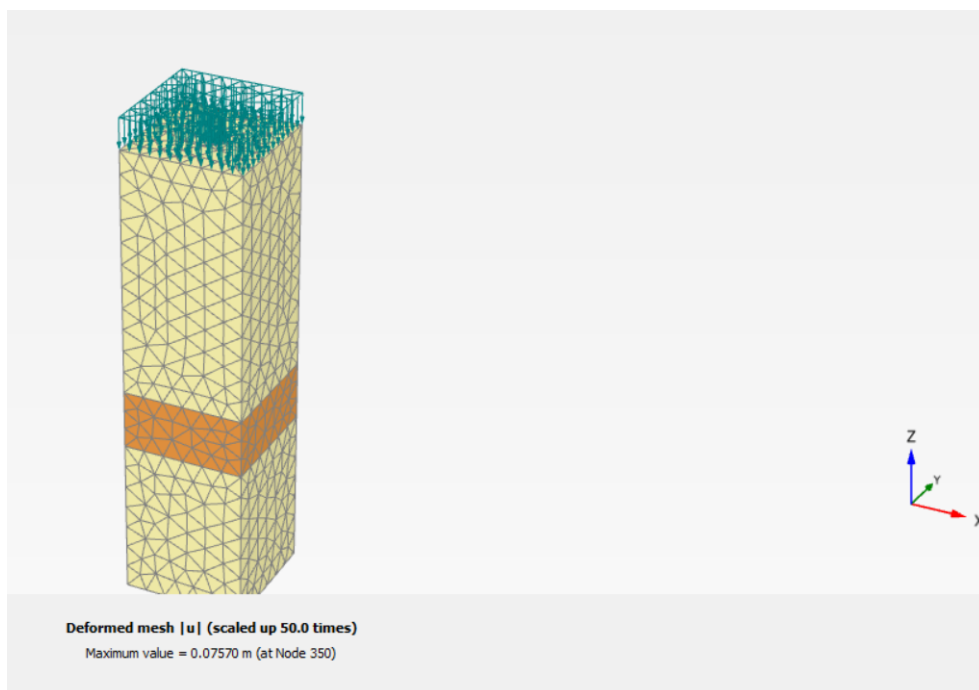
Figure D.11: In the following figure, a cross-section at -27.51m NAP with the experienced total displacements can be seen. With a 1,2m centre-to-centre embedded pile grid modelled.

D.3.3. For 2m centre-to-centre
Volume pile (3D model):

Deformed mesh |u| (scaled up 50.0 times)
Maximum value = 0.08193 m (at Node 60352)
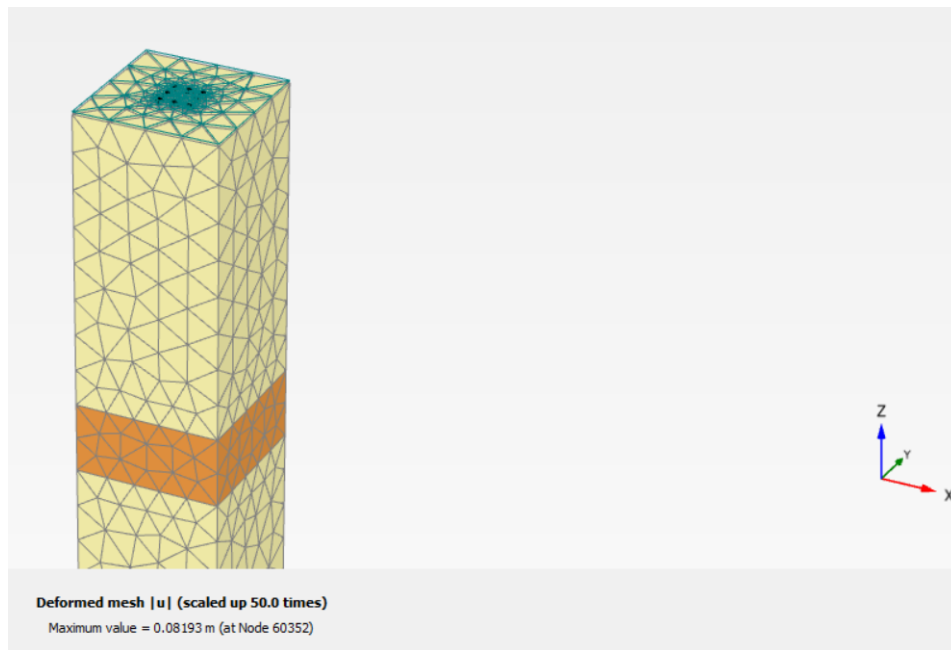
Figure D.12: In the following figure, a cross-section at -27.51m NAP with the experienced total displacements can be seen. With a 2m centre-to-centre volume pile grid modelled.

Embedded pile (3D model):

Deformed mesh |u| (scaled up 50.0 times)
Maximum value = 0.07567 m (at Node 2810)
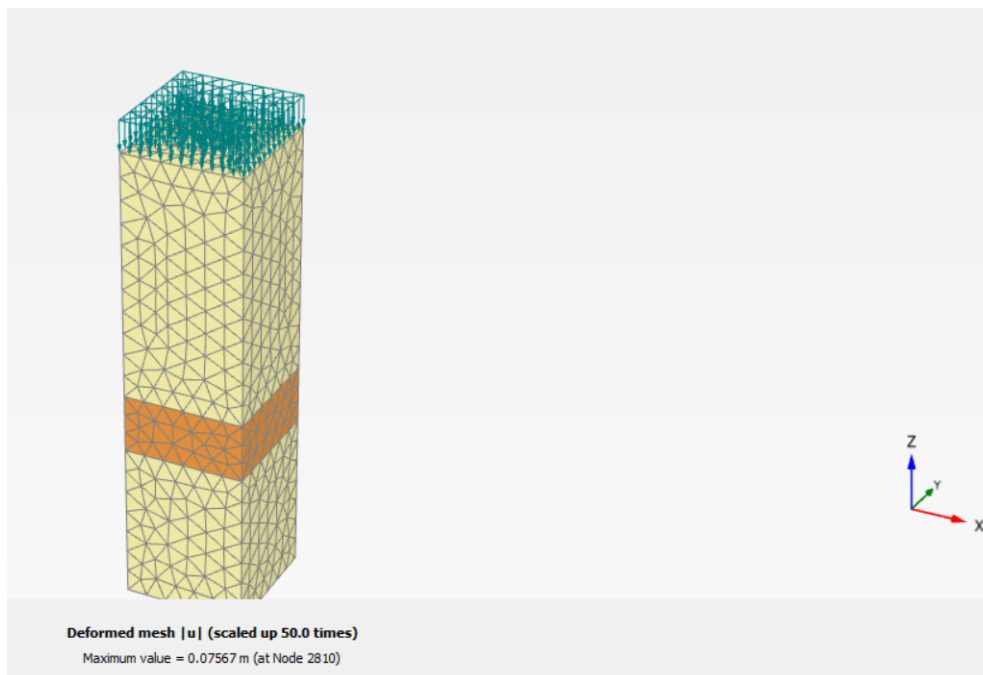
Figure D.13: In the following figure, a cross-section at -27.51m NAP with the experienced total displacements can be seen. With a 2m centre-to-centre embedded pile grid modelled.

D.3.4. For 3m centre-to-centre

Volume pile (3D model):
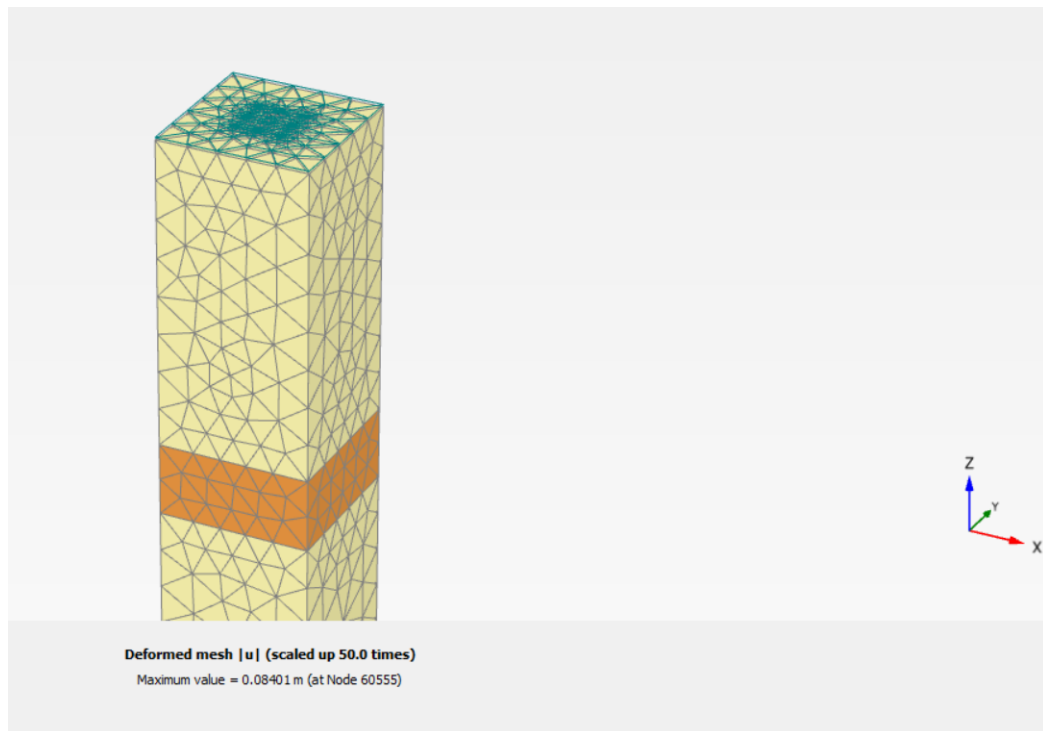
Figure D.14: In the following figure, a cross-section at -27.51m NAP with the experienced total displacements can be seen. With a 3m centre-to-centre volume pile grid modelled.

Embedded pile (3D model):
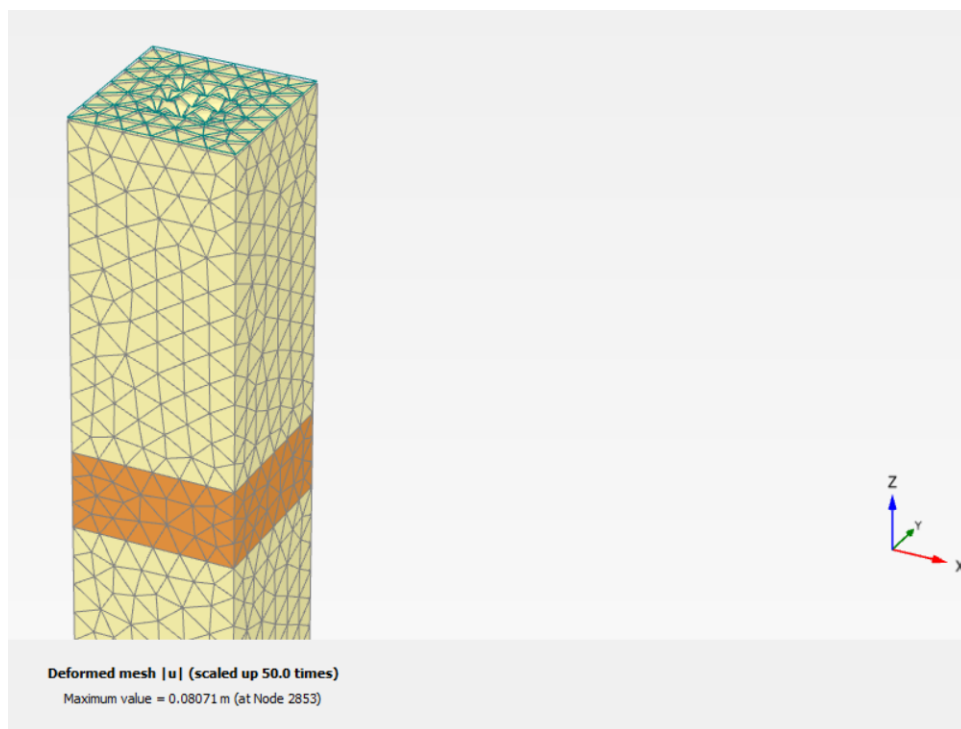
Figure D.15: In the following figure, it can be seen a cross-section at -27.51m NAP with the experienced total displacements. With a 3m centre-to-centre embedded pile grid modelled.

E
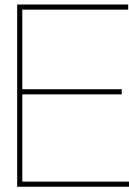
PLAXIS 3D models for different Clay Layer Depths

E.1. Clay layer at -61.3m to -71.3m NAP

E.1.1. For 1m centre-to-centre (spacing is 2.5 times the diameter)

Deformed mesh |u| (scaled up 50.0 times)
Maximum value = 0.08097 m (at Node 347)
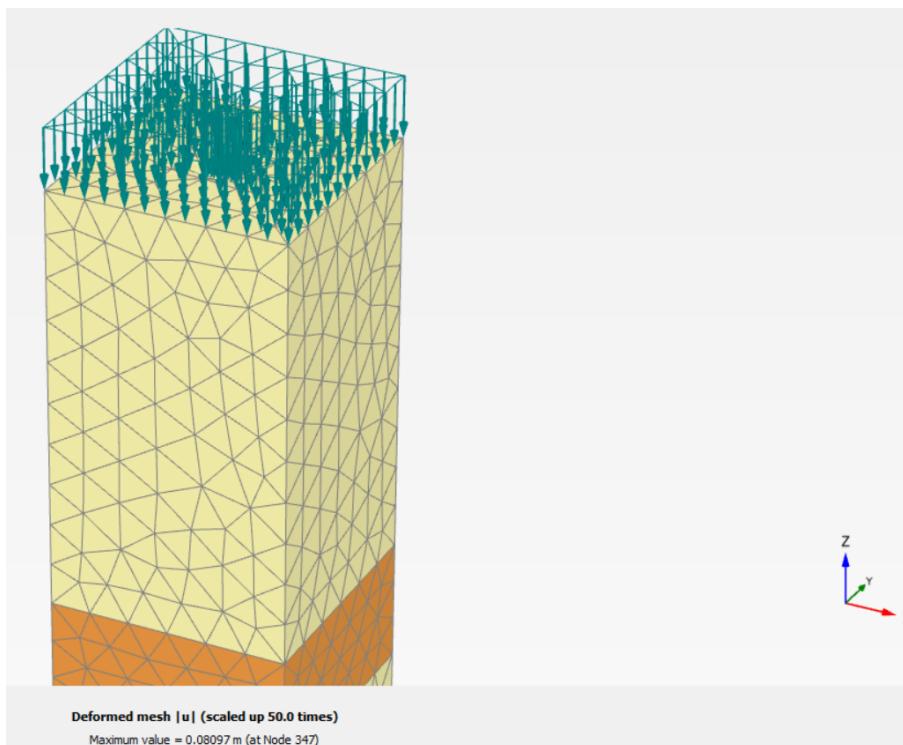
Figure E.1: In the following figure, a cross-section at -27.51m NAP with the experienced total displacements can be seen. With a 1m centre-to-centre embedded pile grid modelled.

E.1.2. For 1.2m centre-to-centre (spacing is three times the diameter)

Deformed mesh |u| (scaled up 50.0 times)
Maximum value = 0.08084 m (at Node 287)
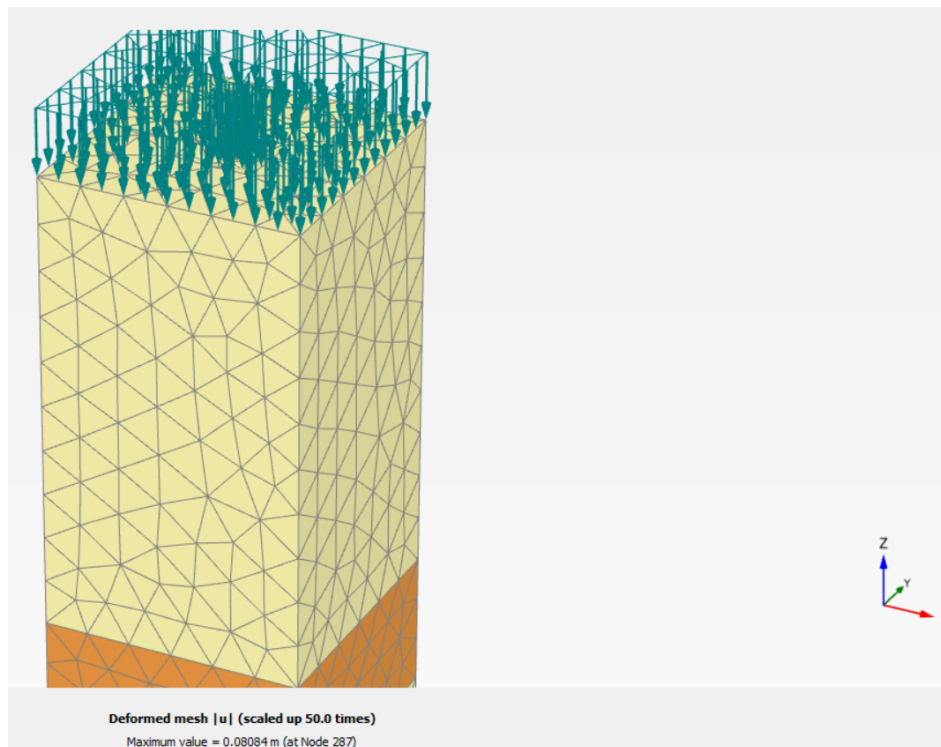
Figure E.2: In the following figure, a cross-section at -27.51m NAP with the experienced total displacements can be seen. With a 1,2m centre-to-centre embedded pile grid modelled.

E.1.3. For 2m centre-to-centre

Embedded pile (3D model):

Deformed mesh |u| (scaled up 50.0 times)
Maximum value = 0.08481 m (at Node 2842)
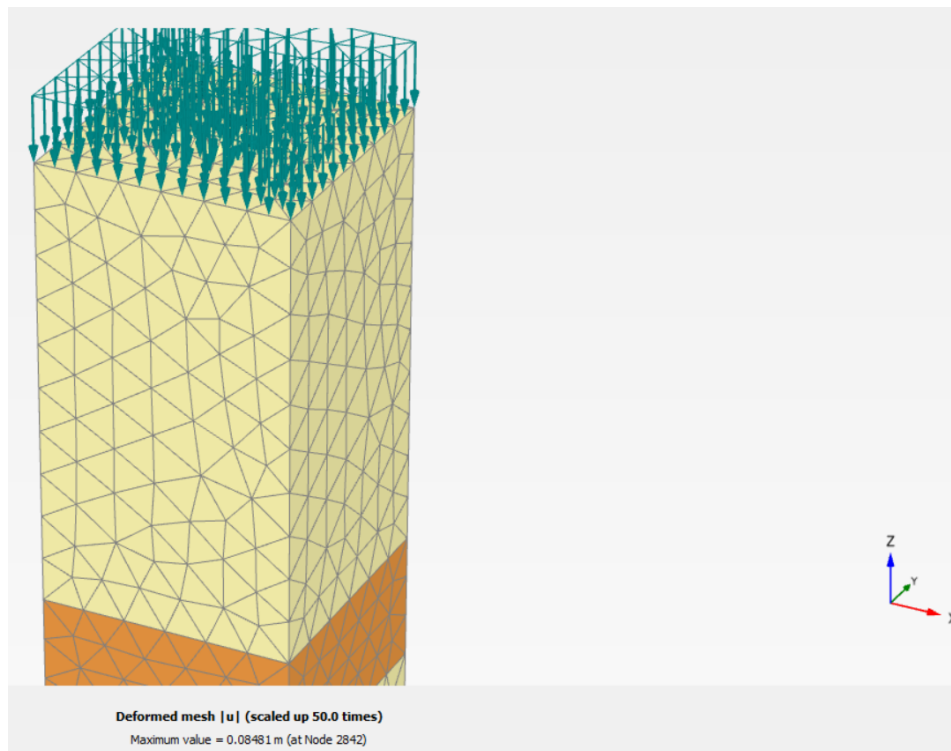
Figure E.3: In the following figure, a cross-section at -27.51m NAP with the experienced total displacements can be seen. With a 2m centre-to-centre embedded pile grid modelled.

E.1.4. For 3m centre-to-centre
Embedded pile (3D model):

Deformed mesh |u| (scaled up 50.0 times)
Maximum value = 0.08526 m (at Node 2931)
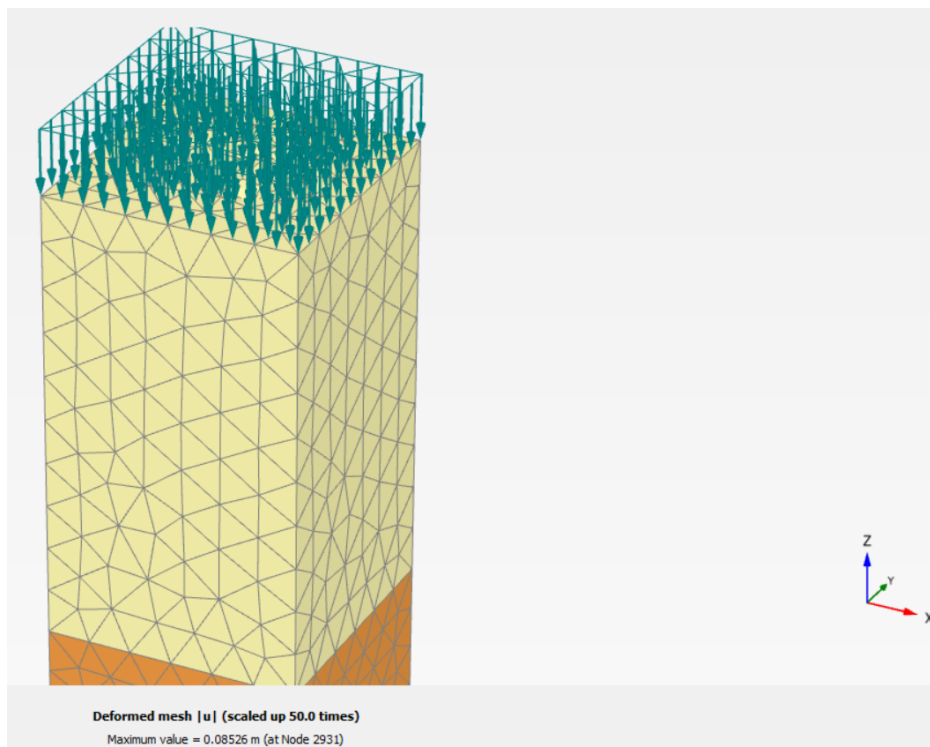
Figure E.4: In the following figure, a cross-section at -27.51m NAP with the experienced total displacements can be seen. With a 3m centre-to-centre embedded pile grid modelled.

E.2. Clay layer at -52.3m to -62.3m NAP

E.2.1. For 1m centre-to-centre (spacing is 2.5 times the diameter)

Deformed mesh |u| (scaled up 50.0 times)
Maximum value = 0.09395 m (at Node 2997)
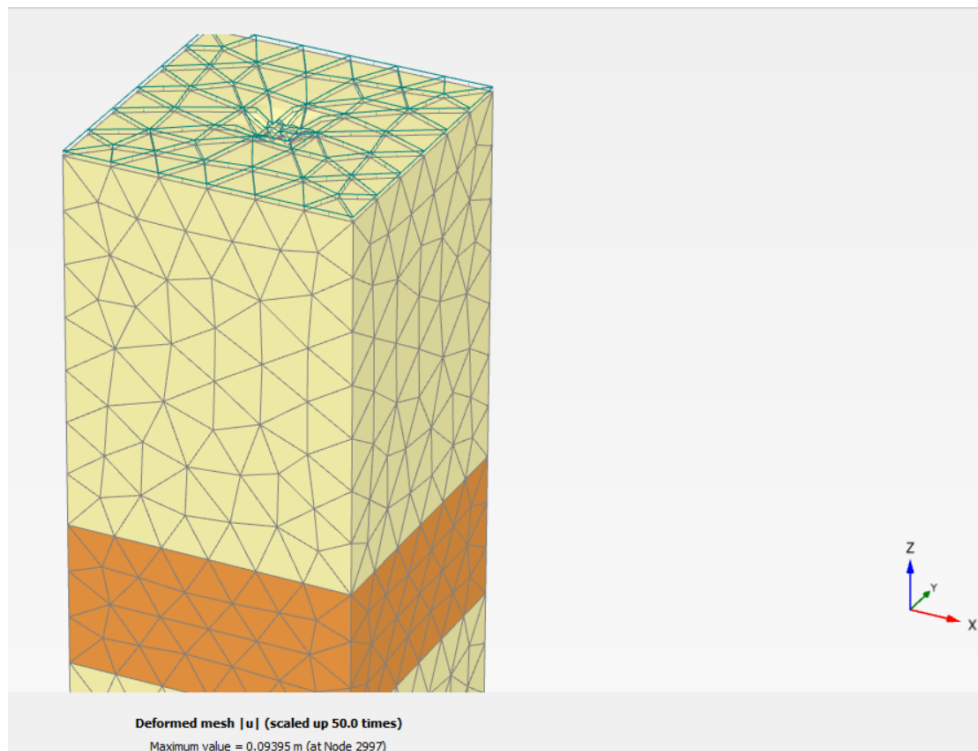
Figure E.5: In the following figure, a cross-section at -27.51m NAP with the experienced total displacements can be seen. With a 1m centre-to-centre embedded pile grid modelled.

E.2.2. For 1.2m centre-to-centre (spacing is three times the diameter)

Deformed mesh |u| (scaled up 50.0 times)
Maximum value = 0.09343 m (at Node 305)
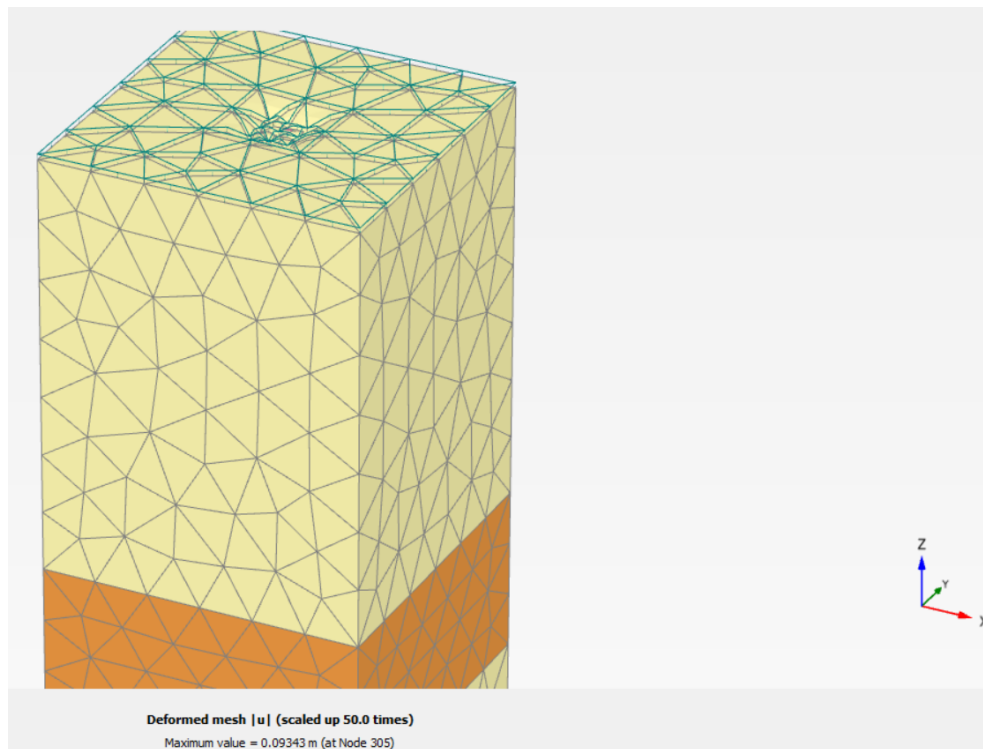
Figure E.6: In the following figure, a cross-section at -27.51m NAP with the experienced total displacements can be seen. With a 1,2m centre-to-centre embedded pile grid modelled.

E.2.3. For 2m centre-to-centre

Embedded pile (3D model):

Deformed mesh |u| (scaled up 50.0 times)
Maximum value = 0.09571 m (at Node 3043)
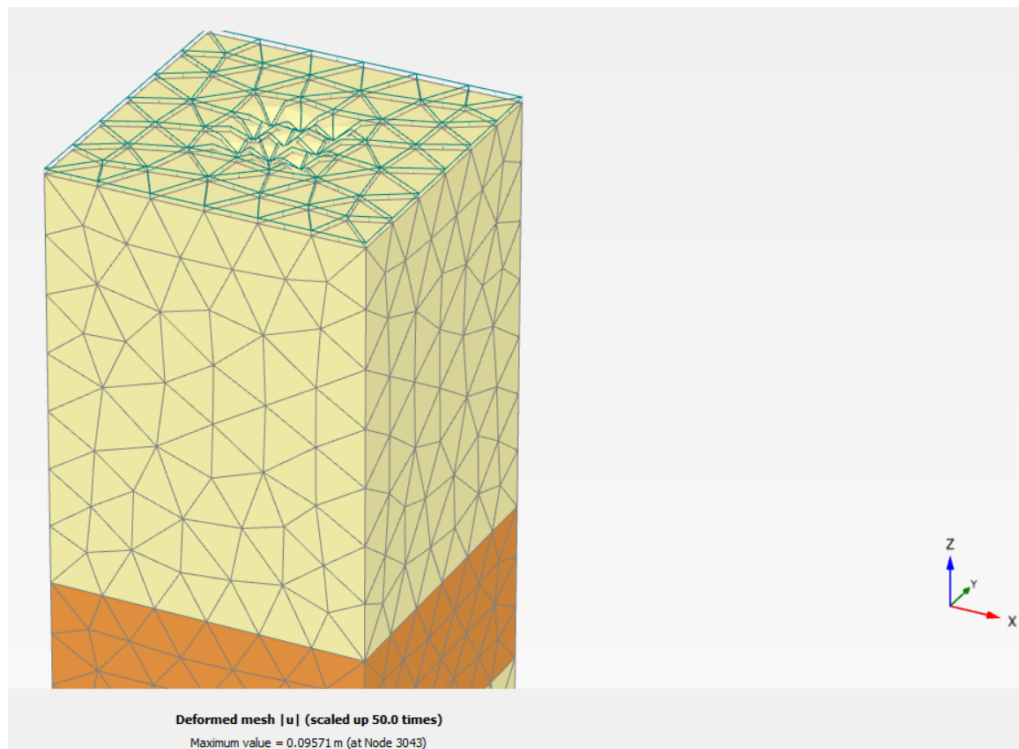
Figure E.7: In the following figure, a cross-section at -27.51m NAP with the experienced total displacements can be seen. With a 2m centre-to-centre embedded pile grid modelled.

E.2.4. For 3m centre-to-centre
Embedded pile (3D model):

Deformed mesh |u| (scaled up 50.0 times)
Maximum value = 0.09619 m (at Node 3104)
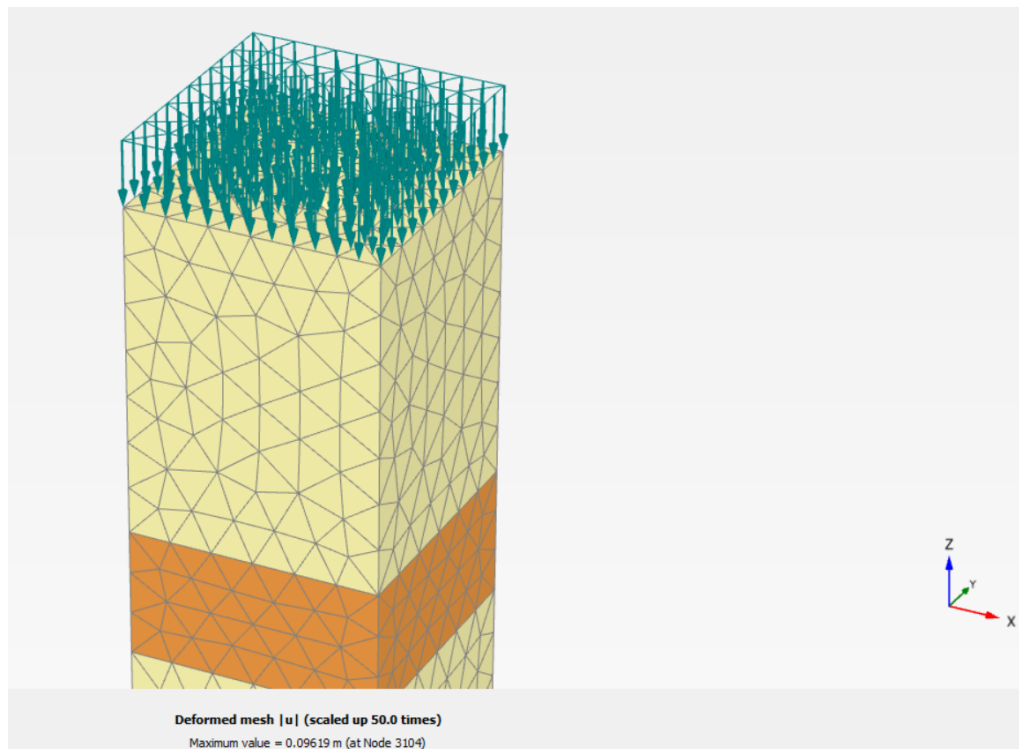
Figure E.8: In the following figure, a cross-section at -27.51m NAP with the experienced total displacements can be seen. With a 3m centre-to-centre embedded pile grid modelled.

E.2.5. For 4m centre-to-centre

Embedded pile (3D model):

Deformed mesh |u| (scaled up 50.0 times)
Maximum value = 0.09528 m (at Node 3100)
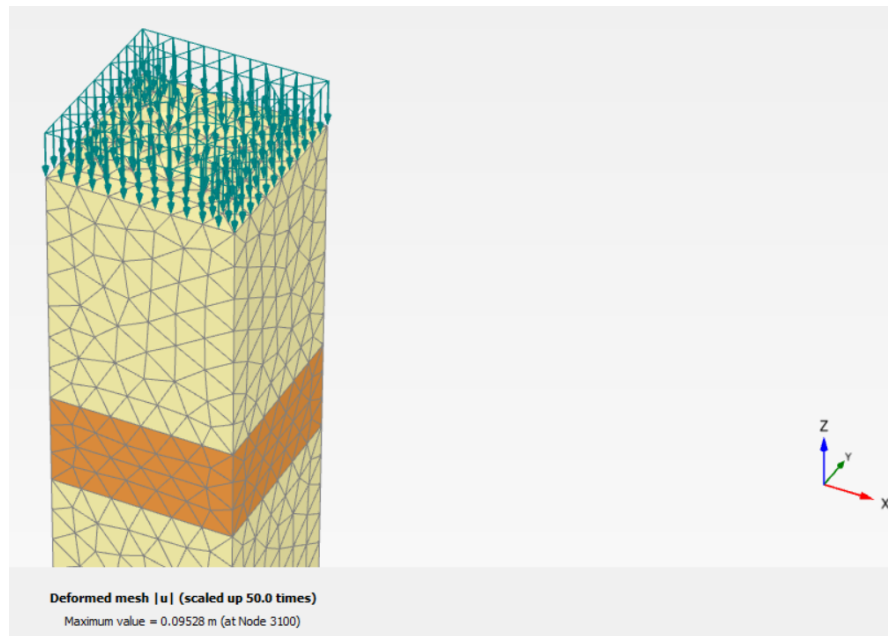
Figure E.9: In the following figure, a cross-section at -27.51m NAP with the experienced total displacements can be seen. With a 4m centre-to-centre embedded pile grid modelled.